



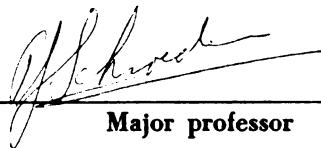
This is to certify that the
thesis entitled
ELECTRON TRANSPORT PROPERTIES OF METALLIC TIN
IN HIGH MAGNETIC FIELDS AND AT
LIQUID HELIUM TEMPERATURES

presented by

John Arthur Woollam

has been accepted towards fulfillment
of the requirements for

Ph.D. degree in Physics


Major professor

Date 26 January 1967

ABSTRACT

ELECTRON TRANSPORT PROPERTIES OF METALLIC TIN IN HIGH MAGNETIC FIELDS AND AT LIQUID HELIUM TEMPERATURES

by

John Arthur Woollam

The high field thermal magnetoresistance and de Haas-van Alphen type oscillations in the thermoelectric emf, are used to study the Fermi surface of tin.

It is demonstrated that the thermal magnetoresistance, using lock-in-amplifier techniques, has a much larger signal to noise ratio than conventional electrical magnetoresistance yet provides the same Fermi surface topology information.

The thermoelectric emf is shown to be especially sensitive to the quantization of energy levels. Quantum oscillations observed at 4.2°K, are as large as $4 \mu\text{V}/^\circ\text{K}$ at 1.2°K and 20 k gauss in metallic tin. These originate from the 3δ section of the Fermi surface, and their angular dependence is studied. Higher frequencies are also seen.

Oscillations from the 3δ section are observed in the thermal magnetoresistance, and superimposed on a strongly field dependent monotonic background.

In contrast with conventional Fermi surface investigation techniques, the thermal magnetoresistance, and the thermoelectric effects can be studied in one experiment. The possible effects of magnetic breakdown are observed simultaneously in both quantities.

ELECTRON TRANSPORT PROPERTIES OF METALLIC TIN
IN HIGH MAGNETIC FIELDS AND AT
LIQUID HELIUM TEMPERATURES

By

John Arthur Woollam

A THESIS

Submitted to
Michigan State University
in partial fulfillment of the requirements
for the degree of

DOCTOR OF PHILOSOPHY

Department of Physics and Astronomy

1967

20-40
6-20-71

Acknowledgments

I would like to thank my thesis advisor, Dr. Peter A. Schroeder, for his supervision, and especially for his help in the stereogram and data interpretation work.

The assistance and advice of Dr. Frank J. Blatt is gratefully acknowledged.

I am grateful to the National Science Foundation for financial support.

1
2
3

TABLE OF CONTENTS

- I. History of Quantum Effects

- II. The Theory of Quantum Effects
 - A. Quantization of Energy
 - B. The Degeneracy of the Levels
 - C. Oscillation in Free Energy
 - D. Oscillations in the Magnetization
 - E. Factors Effecting the Amplitude of the Oscillations
 - 1. Experimental
 - 2. The Effective Mass
 - 3. Temperature
 - 4. Collisions
 - 5. Electron Spin
 - F. Quantum Effects in Transport Phenomena

- III. Quantum Theories of Thermal Magnetoresistance and Thermoelectric Power
 - A. Quantum Theory of Thermal Magnetoresistance
 - B. The Horton Quantum Theory of Thermoelectric Power
 - C. The Zil'berman Quantum Theory of Thermoelectric Power
 - D. Absolute Magnitude of the Thermoelectric Oscillations

TABLE OF CONTENTS, Continued

- IV. High Field Thermal Magnetoresistance and Thermopower Tensors
 - A. History of the Thermal Magnetoresistance Tensor
 - B. Theory of the Thermal Magnetoresistance Tensor
 - C. The Effects of Magnetic Breakdown
 - D. Theory of the Thermoelectric Power Tensor
 - E. Kohler Corrections

- V. Experimental Apparatus and Measurement Techniques
 - A. Sample Preparation
 - B. The Apparatus
 - C. The Measurement of Voltages
 - D. Pole Pieces and Magnetic Field Homogeneity
 - E. Thermometry
 - F. Recording the Measurements
 - G. Field Modulation

- VI. Experimental Results
 - A. Quantum Oscillations in the Thermoelectric Emf and Thermal Magnetoresistance
 - B. Quantum Oscillations in the Thermoelectric Emf when Rotating at Constant Field Strength
 - C. Origins of the Oscillations and the F-S of Tin
 - D. Thermal Magnetoresistance in Rotation

TABLE OF CONTENTS, Continued

- VI. Experimental Results, continued
 - E. Field Dependent Structure in Magneto-
resistance
 - F. Correlation of Oscillation Amplitudes
with the Field Dependent Peaks in
Magnetoresistance

List of Figures

<u>Figure</u>	<u>Page</u>	<u>Description</u>
1	9	Cylinders of energy states
2	12	Oscillations in δn , ΔU , and δM
3	33	Zinc $W(H)$ and $\rho(H)$
4	35	Chart of field dependence $S(H)$, $\rho(H)$
5	42	Undulating cylinders type open orbit
6	43	Effect of open orbits on high field $S(H)$
7	43	Effect of open orbits on high field $S(H)$
8	48	Sample axes and coordinate system
9	49	General view of apparatus
10	50	Sample holder
11	55	Marginal oscillator
12	58	Field homogeneity plot
13	60	Block diagram of measuring equipment
14	66	Constant ΔT circuit
15	67	Differentiator circuit
16	72	Bessel functions
17	73	Roots of bessel functions
18	75	Oscillations in thermoelectric emf $4.2^\circ K$
19	76	Integers vrs $1/H$ at peaks
20	78	Simultaneous plot of $W(H)$ and $S(H)$ oscillations
21	80	Higher frequencies in emf oscillations
22	81	Angular dependence of periods
23	83	S oscillations in 180° rotation $H=21$ k gauss
24	84	S oscillations in slow rotation. Higher freqs.
25	86	$\sec\theta$ at peaks vrs integers

List of Figures (Continued)

<u>Figure</u>	<u>Page</u>	<u>Description</u>
26	87	Summary of W(H) and S(H) frequency data
27	90	Free electron Fermi surface of tin
28	92	Cross section of β δ section of F-S. Weisz
29	93	W(H) 21 K gauss 360 rotation
30	95	Stereogram of open orbits in tin
31	96	4(a) section of F-S. Supports aperiodic open orbits
32	97	Types of orbits
33	99	W(H) in rotation for various H's
34	100	Same as figure 33, crystal tilted
35	101	Electrical ρ (H) in rotation for various H's
36	102	Magnetic breakdown orbits. Young
37	103	Magnetic breakdown orbits. Young. Weisz
38	105	Inner section stereogram. Our data
39	107	Correlation of high field W(H) and S(H) oscillation amplitudes over wide range of angles. Shows angles of low oscillation amplitudes.
40	115	Intermediate superconducting magnetic state
41	119	Temperature measuring bridge
42	120	Automatic angle recording device
43	121	Pressure regulator
44	122	Carbon resistor calibration

11

Appendix

<u>Page</u>	<u>Description</u>
114	Intermediate superconducting magnetic state
116	a-c wheatstone bridge output correction
118	Magnet sweep control
119	a-c wheatstone bridge circuit diagram
120	Circuit diagram of automatic angle recording device
121	Helium bath pressure regulator
122	Carbon resistor calibration

elec
tion
orel

where
are t
mass

Under
exper
is an
with a
showe
be os
expli
streng
effect
introc
mass.
work w

I History of Quantum Effects

At low temperatures and in pure metals and semi metals, electron mean free paths become long. Under these conditions electrons in high magnetic fields can execute many cyclotron orbits before being scattered. Thus,

$$\omega \tau \gg 1 \tag{1}$$

where $\omega = \frac{eH}{m^*}$ is the cyclotron frequency and τ is the average time between electron collisions. m^* is the effective mass defined by:

$$m_{ij}^* = \frac{\hbar^2}{\frac{d^2 E}{dk_i dk_j}} \tag{2}$$

Under the conditions of equation (1) de Haas and van Alphen experimentally discovered that the magnetic susceptibility is an oscillatory function of the magnetic field strength with a frequency proportional to $\frac{1}{H}$.⁽¹⁾ In 1933 Peierls showed that the magnetization of a free electron gas should be oscillatory in $\frac{1}{H}$.⁽²⁾ Soon after that, Landau found an explicit form of the magnetization as a function of field strength⁽³⁾ and Shoenberg and Landau⁽⁴⁾ recognized the effect of the periodic field of the crystal lattice by introducing a generally anisotropic effective electron mass. Meanwhile, much experimental de Haas - van Alphen work was underway⁽⁵⁾ on the multivalent metals.



—
r
v
s
na
la
of
o
w
E
r
to
to
E
an
th
Va
Ha
We
ab
Wh
bro

In 1953 Onsager applied the Bohr-Sommerfeld quantization rule⁽⁶⁾:

$$\int (\bar{p} - \frac{e}{c} \bar{A}) \cdot d\bar{r} = (\lambda + \frac{1}{2}) h \quad (3)$$

where \bar{p} is the usual momentum and \bar{A} the magnetic vector potential. (3) is the condition for the quantization of magnetic flux in units of hc/e , and shows that the oscillatory diamagnetism reflects specific geometrical features of the Fermi surface. The λ^{th} maxima in magnetization counted from $\frac{1}{H} = 0$ occurs when

$$\lambda + \frac{1}{2} = \frac{hc}{e} A \frac{1}{H} \quad (4)$$

where A is an extremal area of intersection between the Fermi surface (F-S) and the family of planes, $\bar{p} \cdot \bar{H} = \text{constant}$. Lifshitz and Kosevich⁽⁷⁾ expanded these ideas, and a rigorous treatment will be given in the section on the theory of the oscillations.

A large amount of both experimental and theoretical Fermi surface work was done in the 1950's. Lifshitz, Azbel and Kaganov⁽⁸⁾ were able to give explicit expressions for the galvanomagnetic tensor in high magnetic fields for various Fermi surface conditions. Magnetoresistance and Hall effect thus became effective tools. Azbel and Kaner⁽⁹⁾ were the first to theoretically consider the resonant absorption at the surface of a single metallic crystal when the field was in the plane of the metal. These cyclotron resonance experiments are useful in determining

effect

for t

and

period

focus

range

reach

second

sensit

a very

A

nicely

took e

the wo

and go

deserve

rather

disturb

A

and a r

by D. S

million

1991, 19

the als

to calc

effective masses at different points on the F-S.

Cohen, Harrison, and Harrison⁽¹⁰⁾ developed a theory for the attenuation of sound by electrons in a metal, showing the attenuation periodic in $\frac{1}{H}$ and the resultant period proportional to the extremal wave vector \underline{k} . Acoustic attenuation exhibits both this "geometrical resonance", and de Haas - van Alphen type oscillations, so measurements can give both a calipered dimension and a cross sectional area of the F-S. In addition, the attenuation is sensitive to open orbit directions, so the method can be a very effective technique for studying F-S's.

Accounts of the work done in the 1950's are very nicely given in The Fermi Surface⁽¹¹⁾ which is the only book explicitly about Fermi surfaces. A good portion of the work reported is on the noble metals, copper, silver, and gold. Until then, quantum effects had not been observed in these metals, since they are monovalent and have rather large sections of F-S. Work on zinc, aluminum, bismuth, lead and tin are also reported.

A good recent summary of the de Haas - van Alphen effect and a review of quantum effects in studying F-S's is given by D. Shoenberg in LT9⁽¹²⁾. This presents a complete bibliography of experimental work done before September of 1964, giving 141 references. Band structure calculations are also summarized by V. Heine and he lists 55 references to calculations on specific materials.

van
eff
for
lat
all
and
lou
rel
tio
and
osc
Ste
the
net
but
tit
nea
def
pos
the
noe
nit
ele
aut
dir
pre
dir

In view of the rather rapid advance of de Haas - van Alphen, magnetoacoustic attenuation, Shubnikov - de Haas effects, etc., it is not surprising that people might look for quantum oscillations in the transport properties. Oscillations periodic in $\frac{1}{H}$ have now been seen in practically all observable properties. A good deal of this effort was, and is still being done by the low temperature group at Louisiana State University⁽¹³⁻¹⁶⁾ where they attempt to relate both bulk and oscillatory phenomena using the relations resulting from definitions of transport coefficients and the Onsager relations⁽¹⁷⁾. However, the first quantum oscillations in the thermoelectric power were seen by M. C. Steel and J. Babiskin⁽¹⁸⁾ in the semi metal, Bi. Since then, Grenier, et al⁽¹³⁾ saw oscillations in another semi metal, Sb. They postulate observing oscillations in zinc but cannot tell if this is due to oscillations in the quantities used to calculate the thermopower from their measured properties⁽¹⁴⁾. The isothermal thermopower is defined as $S = \frac{d(\text{emf})}{dT}$. Our observations in tin have both positive and negative emfs and since dT can't be negative, the oscillations are undisputably oscillations in the thermoelectric power. We believe that this is the first definite observation of quantum oscillations in the thermoelectric power of a pure metal. Furthermore, the above authors looked only with the magnetic field along symmetry directions of the crystal. We have observed how the frequency changes for the field in various non-symmetry directions, and have



ob
of
we
(S
is
eff
eff
in
ily
dy
tan
The
Bo
and
for
mag
br
dis
Ho
the
ere
deta

observed the oscillations in continuous rotation at fixed field.

Quantum oscillations in the thermal magnetoresistance were seen in several metals by Grenier, et al⁽¹³⁻¹⁶⁾. (See also LT9 reference 12, p. 802)

Theoretically, quantization of transport phenomena is far less understood than is the de Haas - van Alphen effect, fundamentally because the de Haas - van Alphen effect is due to the diamagnetism of conduction electrons in thermodynamic equilibrium. Transport phenomena necessarily involve electron scattering and non-equilibrium thermodynamics.

The Zil'berman⁽¹⁹⁾ thermopower theory uses the Boltzmann transport equation to treat the lack of equilibrium. The effects of quantizing magnetic fields on the classical Boltzmann equation were not treated. The Kalashnikov⁽²⁰⁾ and Horton⁽²¹⁾ thermopower theories use the density matrix formalism to account for the quantization imposed by the magnetic field. However, these theories use the equilibrium equation of motion for the density matrix. For a discussion of this limitation see the paper by Adams and Holstein⁽²²⁾.

Thomas will soon publish: "Magnetic Corrections to the Boltzmann Equation" in the Physical Review⁽²³⁾. However, no thermopower calculations were made.

The existing theories will be discussed in greater detail later.

II The Theory of Quantum Effects

A. Quantization of Energy^(24,25)

Consider a free electron in a uniform magnetic field parallel to the z axis. Use the magnetic vector potential in the Landau gauge

$$\bar{A} = (0, Hx, 0) \quad (5)$$

The appropriate momentum conjugate to \bar{r} , when a magnetic field is present is

$$\bar{p} = m\bar{v} + e\bar{A} \quad (6)$$

The Hamiltonian is then

$$H = \frac{1}{2m} (\bar{p} - e\bar{A})^2 \quad (7)$$

The Schrodinger equation becomes

$$\frac{\hbar^2}{2m} \nabla^2 \psi - \frac{ieHx\hbar}{m} \frac{\partial \psi}{\partial y} - \frac{e^2 H^2}{2m} x^2 \psi + E\psi = 0 \quad (8)$$

Now let

$$\psi = \psi(x) e^{i(k_y y + k_z z)} \quad (9)$$

(9) in (8) gives

$$\frac{\hbar^2}{2m} \nabla^2 \psi(x) - \left\{ \frac{(\hbar k_y - eHx)^2}{2m} - \left(E - \frac{\hbar^2 k_z^2}{2m} \right) \right\} \psi(x) = 0 \quad (10)$$

11

En

ce

W

En

(E

don

W

ed

th

co

co

to

This is the equation for the harmonic oscillator in $\psi(x)$ centered on x_0 , where

$$x_0 = \frac{\hbar k_y}{eH} \quad (11)$$

with a natural frequency of

$$\omega = \frac{eH}{m} \quad (12)$$

The quantum mechanical treatment of the harmonic oscillator (H.O.) problem is given in many texts⁽²⁶⁾ so we can write down the eigenfunctions and eigenvalues as

$$\psi = e^{i(k_y y + k_z z)} \times \text{H.O. wave functions of } (x-x_0) \quad (13)$$

$$E = \frac{\hbar^2 k_z^2}{2m} + \left(\lambda + \frac{1}{2}\right) \hbar \omega \quad (14)$$

where ω is given by (12).

Zil'berman⁽¹⁹⁾ solved the Schrodinger equation for the eigenvalues and eigenfunctions allowing for the presence of the periodic lattice potential and found the solutions could still be written in the form of (13) and (14).

Onsager⁽⁶⁾ applied the Bohr-Sommerfeld quantization condition

$$\int \bar{p} \cdot d\bar{q} = \left(\lambda + \frac{1}{2}\right) h \quad (15)$$

to get

$$A = \left(\lambda + \frac{1}{2}\right) \frac{2\pi eH}{\hbar} \quad (16)$$

who

law

are

tax

the

on

the

E. M.

who

Equ

The

The

so

The

where A is the cross sectional area in k space perpendicular to the field direction. Equation (16) relates the area to the energy given in equation (14) and will be important in the explicit expressions for the quantum oscillations.

Equations (14) and (16) show that there is quantization in the x - y plane in k space and electrons condense onto cylinders centered along the z axis as shown in figure 1.

B. The Degeneracy of the Levels

x_0 must fall within the specimen so

$$-\frac{1}{2} L_x < x_0 < \frac{1}{2} L_x \quad (17)$$

where the electron is contained within a box L_x, L_y, L_z .

Equation (11) then says that

$$-\frac{1}{2} \frac{eHL_x}{\hbar} < k_y < \frac{1}{2} \frac{eH}{\hbar} L_x \quad (18)$$

The number of allowed values of k_y is thus

$$L_x L_y \frac{eH}{2\pi\hbar} = \text{degeneracy for fixed } k_z \quad (18)$$

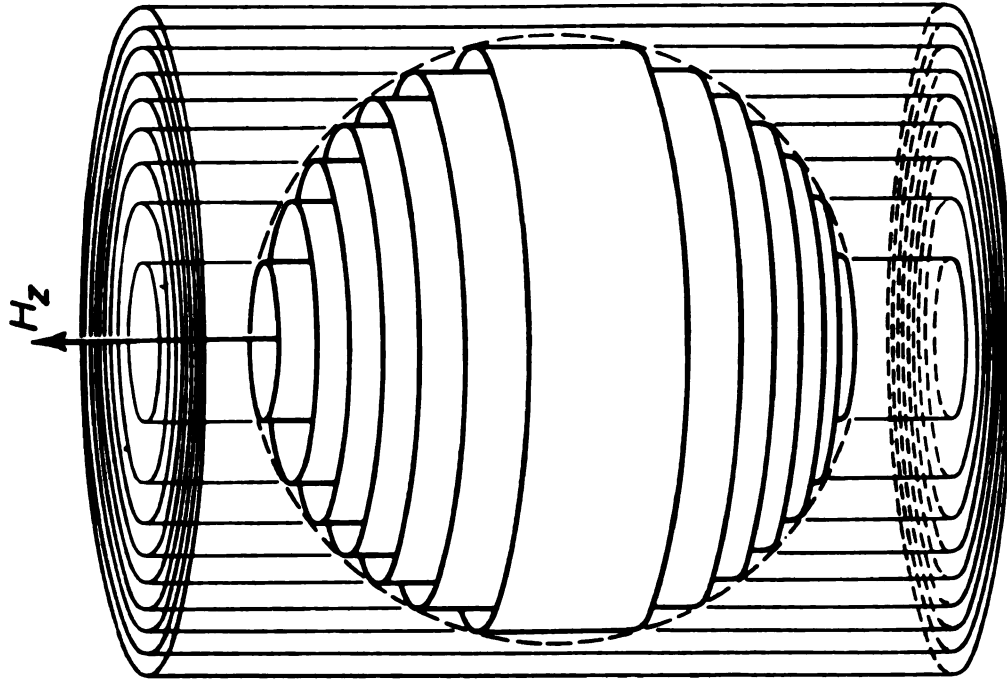
The energy between states of neighboring n values is $\hbar\omega$

so the number of states per unit energy range is

$$L_x L_y \frac{m}{2\pi\hbar^2} = \text{density of states} \quad (20)$$

This is the same as the density of states in zero magnetic

Figure 1



The quantization of the energy spectrum in the xy -plane into discrete cylindrical surfaces in k -space under the influence of an applied magnetic field H_z (after Chambers, 1956).

Reference 27

1

field so the average density of states is unaffected by the field. The field condenses many states into highly degenerate cylinders as pictured in Figure 1.

Now consider a slab in k space perpendicular to the field direction, of thickness δk_z . The number of allowed values of k_z in δk_z is $\frac{L_z}{2\pi} \delta k_z$ and the number of allowed values of k_y for fixed k_z is given by (19). Thus the total number of states for a fixed λ in the slice δk_z is the product or

$$\begin{aligned} \text{degeneracy} &= L_x L_y L_z \frac{e \delta k_z}{4\pi^2 \hbar} H & (21) \\ &\equiv L_x L_y L_z \xi H \end{aligned}$$

which defines the degeneracy per unit volume for the λ^{th} level as

$$\text{degeneracy/vol} = \xi H \quad (22)$$

where

$$\xi = \frac{e \delta k_z}{4\pi^2 \hbar} \quad (23)$$

C. Oscillation in Free Energy

Assume that the electron gas is at absolute zero temperature. The Fermi energy can be shown to be nearly constant as the field varies.

All the λ levels in the slice δk_z are filled when

$$E'_F \equiv E_F - \frac{\hbar^2 k_z^2}{2m} > \left(\lambda + \frac{1}{2}\right) \hbar \omega \quad (24)$$

PLATE 100

and all levels above λ' are empty. If there are δn electrons per unit volume in the slice δk_z then

$$\delta n = \lambda' \xi H + \xi H \quad (25)$$

since from (22) ξH is the degeneracy/unit volume of the λ' th level and $\lambda = 0$ is a filled level.

$$\delta n = (\lambda' + 1) \xi H \quad (26)$$

Thus δn increases linearly with H until λ' coincides with the fermi level. Then all electrons on the λ' th level empty out. When this occurs,

$$(\lambda' + \frac{1}{2}) \hbar \omega = E'_F \quad (27)$$

and since λ' is usually very large compared to $\frac{1}{2}$,

$$\lambda' = \frac{mE'_F}{\hbar e} \frac{1}{H} \quad (28)$$

Thus δn is a periodic function of $\frac{1}{H}$ with period

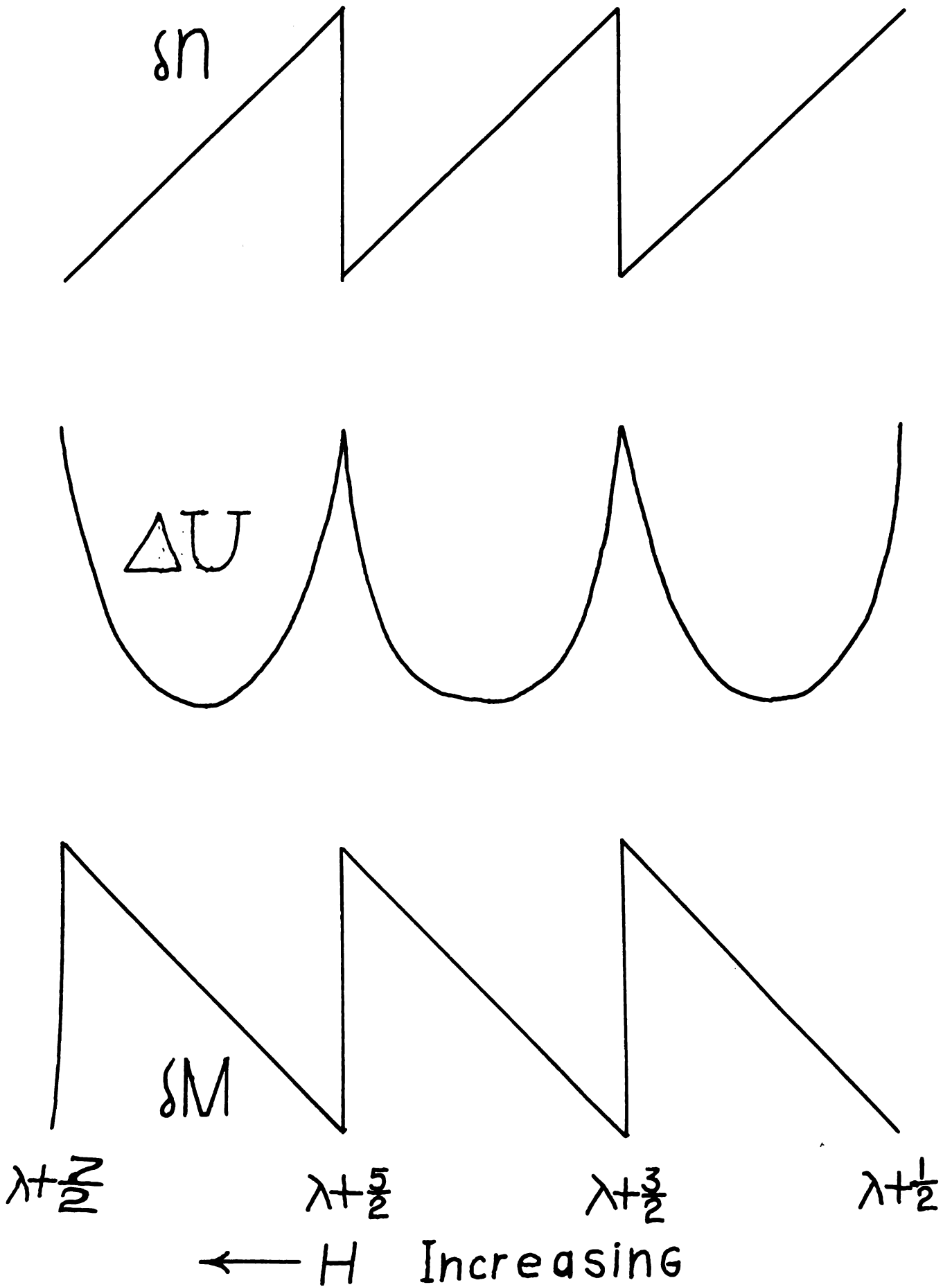
$$P = \frac{\hbar e}{mE'_F} \quad (29)$$

so the population oscillates about δn_0 with amplitude $\frac{1}{2}\xi H$. This is shown in Figure 2.

The energy in δk_z is

$$\delta U_0 = \xi H \hbar \omega \sum^{\lambda'} (\lambda + \frac{1}{2}) + \delta n_0 \frac{\hbar^2 k_z^2}{2m} \quad (30)$$

Figure 2



Evaluating the sum and using (26) gives

$$\delta U_0 = \frac{1}{2} \frac{\hbar\omega}{\xi H} \delta n_0^2 + \frac{\delta n_0 k_z^2 \hbar^2}{2m} \quad (31)$$

For a slightly different value of H but with the same λ'

$$\delta U = \frac{1}{2} \frac{\hbar\omega}{\xi H} \delta n^2 + \frac{\delta n k_z^2 \hbar^2}{2m} + (\delta n_0 - \delta n) E_F \quad (32)$$

Call the difference between (31) and (32) ΔU . Then using (26) and (27) get

$$\Delta U = \frac{1}{2} \frac{e\hbar}{m\xi} \left[\delta n - \delta n_0 \right]^2 \quad (33)$$

which is the change in energy of the whole Fermi surface due to the slice δk_z . It is also a periodic function of $\frac{1}{H}$ with the same period as the number of electrons per unit volume in the slice δk_z , as given in (29). This variation is shown in Figure 2.

Since the total number of particles in the system remains constant, the canonical ensemble is appropriate and ΔU is then the free energy per unit volume. Any other physical quantity can be calculated from it provided it is an equilibrium property.

D. Oscillations in the Magnetization

For the thermodynamic system considered

$$\delta M = \frac{\partial \Delta U}{\partial H} \quad (34)$$

and

This

tion

The

Plan

SM 1

give

band

when

Now

and

$$\delta M = - \frac{e\hbar}{m\xi} (\delta n - \delta n_0) \frac{\partial \delta n}{\partial H} \quad (35)$$

This neglects the effects of scattering from lattice vibrations; that is, the sample is at absolute zero.

$$\frac{d\delta n}{dH} = (\lambda' + 1)\xi \approx (\lambda' + \frac{1}{2})\xi = \frac{\xi E_F'}{\hbar\omega} \quad (36)$$

$$\delta M = \frac{-E_F'}{H} (\delta n - \delta n_0) \quad (37)$$

The variation of δM , ΔU and δn with field is shown in Figure 2. $\delta n - \delta n_0$ varies between $\pm \frac{1}{2}\xi H$ so the range of δM is $\mp \frac{1}{2}\xi E_F'$. Thus δM is periodic in $\frac{1}{H}$ with a period given by (29). Being a periodic function it can be expanded in a Fourier series.

$$\delta M = \sum_{p=1}^{\infty} \delta k_z A_p \sin p_x \quad (38)$$

where x is dictated by the periodicity as

$$x = 2\pi \frac{mE_F'}{e\hbar H} \quad -\pi < x < \pi \quad (39)$$

Now

$$\int_{-\pi}^{\pi} \delta M \sin p_x dx = \delta k_z \sum_p A_p \int_{-\pi}^{\pi} \sin^2 p_x dx \quad (40)$$

which

Now s

M =

but

the in

for k₂

a Pres

M =

Now f

so

Thus,

which gives A_p as

$$A_p = (-1)^p \frac{e\hbar E_F'}{4\pi^3 p} \quad (41)$$

Now sum (38) over all possible k_z to get

$$M = \frac{e\hbar}{4\pi^3} \sum_p \frac{(-1)^p}{p} \int_{-k_F}^{k_F} dk_z \cdot E_F' \sin \left[\frac{p_2 \pi m}{e\hbar H} \left(E_F - \frac{\hbar^2 k_z^2}{2m} \right) \right] \quad (42)$$

but

$$\frac{e\hbar H}{m} \ll E_F \quad \text{in most metals, so} \quad (43)$$

the integrand oscillates rapidly as a function of k_z except for $k_z \approx 0$. When $k_z = 0$ (24) gives $E_F' = E_F$ and (42) becomes a Fresnel integral and has the value

$$M = \frac{E_F e\hbar}{4\pi^3} \left(\frac{e\hbar H}{2} \right)^{\frac{1}{2}} \sum_p \frac{(-1)^p}{p^{\frac{3}{2}}} \sin \left(\frac{2\pi p m E_F}{e\hbar H} - \frac{\pi}{4} \right) \quad (44)$$

Now for $k_z = 0$ (16) and (14) give

$$\frac{2\pi p m E_F}{e\hbar H} = \frac{p\hbar A}{eH} \quad (45)$$

so

$$M = \frac{E_F e\hbar}{4\pi^3} \left(\frac{e\hbar H}{2} \right)^{\frac{1}{2}} \sum_p \frac{(-1)^p}{p^{\frac{3}{2}}} \sin \left(\frac{p\hbar A}{eH} - \frac{\pi}{4} \right) \quad (46)$$

Thus, the period of the oscillation gives a direct measure

of the cross sectional area of the Fermi surface in a plane perpendicular to the field. This area is measured at a stationary section, in this case $k_z = 0$, that is, a maximum or minimum in the area. The period of the oscillations is

$$P = \frac{2\pi e}{\hbar A} \quad (47)$$

E. Factors Effecting the Amplitude of the Oscillations.

1. Experimental

If the peaks are separated by ΔH then the field must be uniform over the sample to within at least this amount. The sample must be an ordered lattice free from impurities so that many cyclotron orbits can be completed. For reasons apparent below, the temperature must usually be below 4.2° Kelvin.

2. The Effective Mass

The effective mass defined by equation (2) must be small. The smaller this is, the greater the oscillation amplitude. The $\beta\delta$ section of the fermi surface of tin, for example, has a ratio of effective mass to real mass of .09. In some materials this is as small as .003. The effective mass is directly proportional to the radius of curvature of the fermi surface at an extremum.

3. Temperature

At temperatures above absolute zero the states near

the Fe

empty

pared

Dingle

market

plied

where

miss

lower

solda

domin

4. c

must

tron

5. 1

disc

freq

fact

the Fermi level will be partially populated instead of empty or full. The thermal energy kT must be small compared to the separation between Landau levels $\hbar\omega$.

Dingle⁽²⁸⁾ makes a complete analysis of the effect on the magnetization oscillations and finds the amplitude multiplied by

$$L_p = \frac{x_p}{\sinh x_p} \quad (48)$$

where

$$x_p = 2\pi^2 p \frac{kT}{\hbar\omega} \quad (49)$$

This factor damps higher harmonics to a greater degree than lower harmonics. Therefore, the oscillations appear sinusoidal rather than spike shaped since the fundamental is dominant.

4. Collisions

If $\bar{\tau}$ is the average time between collisions then this must be long compared with the time to complete one cyclotron orbit. Collisions introduce an amplitude factor of

$$\exp \frac{2\pi}{\omega\bar{\tau}} \quad (50)$$

5. Electron Spin

The effect of spin is to double all the levels so far discussed. The new set of levels contributes the same frequency but the effect is to introduce an amplitude factor

$$\cos (p\pi g m^*/m) \quad (51)$$

where

(45).

F. Qua

get th

ar

where

densit

$\frac{1}{h}$ with

Pundat

gives

ties.

mal a

will

becau

field

of st

be ar

tiora

(52)

where p is the order of the harmonic in the sum in equation (45). g is a "spin splitting factor".

F. Quantum Effects in Transport Phenomena

Pippard⁽²⁴⁾ extends the theory presented above to get the expression

$$\text{amplitude } N_0 = H^2 \left(\frac{d \ln A}{dE} \right)^2 \text{ amplitude } \frac{dM}{dH} \quad (52)$$

where N_0 is the density of states. This shows that the density of states is an oscillatory function periodic in $\frac{1}{H}$ with the same period as the magnetization oscillations. Fundamentally, it is the oscillatory density of states which gives rise to the oscillations in all the observed quantities. In (52) the term $\frac{d \ln A}{dE}$ is evaluated at the extremal area of the F-S. (52) also shows that higher harmonics will be emphasized in the density of states oscillations because of the derivative of magnetization with respect to field.

Dingle⁽²⁸⁾ makes a direct calculation of the density of states by a different method which again shows it to be an oscillatory function of $\frac{1}{H}$.

If the average time between collisions (τ) is proportional to the reciprocal of the density of states, then (52) becomes

$$\frac{\text{amplitude } \tau}{\tau} = \frac{H^2}{N_0} \left(\frac{d \ln A}{dE} \right)^2 \text{ amplitude } \frac{dM}{dH} \quad (53)$$

It i
ther
cond
on r

Bolt:

Using

Thus
power
tory
tion
cond
sect
not
expr
tia
dit

In simplified models of the electrical conductivity

$$\sigma = \frac{ne^2\tau}{m^*} \quad (54)$$

It is later shown that the electronic contribution to the thermal conductivity is proportional to the electrical conductivity. Thus the thermal conductivity also depends on τ .

The diffusion thermopower as calculated from the Boltzman equation is

$$S = \frac{\pi^2 k^2 T}{3e} \left(\frac{\partial \ln \sigma(E)}{\partial E} \right)_{E = E_F} \quad (55)$$

Using (54) this gives

$$S \sim \frac{1}{\tau} \frac{\partial \tau}{\partial E} \Big|_{E_F} \quad (56)$$

Thus, both the thermal conductivity and the thermoelectric power depend on τ . (53) then shows that they are oscillatory functions of $\frac{1}{H}$ with the same period as the magnetization oscillations. The oscillatory thermopower, thermal conductivity, and magnetization should yield the same cross sectional areas of the F-S.

The above is a very approximate argument and should not give the correct oscillation amplitudes. Proper expressions are found by including quantization in the initial calculations, rather than substituting a quantum condition into an equation derived not assuming quantization.

Hortob.

by Ad

insit

trans

oscil

not p

A. Quan

cient

tion f

equat

These

When

most

domin

under

theor

theor

vity

the e

just

III Quantum Theories of Thermal Magnetoresistance and Thermoelectric Power

In this section we quote some of the results of Horton's Ph.D. thesis⁽²¹⁾, but rely on the calculations by Adams and Holstein⁽²²⁾, and Zil'berman⁽¹⁹⁾ for physical insight into the origin of the quantum oscillations in transport. The Kalashnikov⁽²⁰⁾ theory of thermopower oscillations, based on the Adams and Holstein paper, is not presented.

A. Quantum Theory of Thermal Magnetoresistance

Horton⁽²¹⁾ calculates all of the transport coefficients in the quantum oscillation region and gets an equation for the oscillatory thermal conductivity \tilde{K} and an equation for the oscillatory electrical conductivity $\tilde{\sigma}$. These equations show that the Wiedemann-Franz law is valid when scattering is by impurities. Near 1° Kelvin where most of our experiments were done, impurities are the dominant scattering sources.

The theory of Adams and Holstein⁽²²⁾ gives a better understanding of the physics involved than does the Horton theory. We, therefore, present the Adams and Holstein theory for quantum oscillations in the electrical conductivity and use the Wiedemann-Franz law to relate these to the electronic part of the thermal conductivity. This is justified within the limits of the Horton theory:

$$\tilde{K}_{ik} = \frac{1}{3} \frac{\pi^2 k^2}{e^2} T \tilde{\sigma}_{ik} \quad (57)$$

vanom

use th

for th

The on

brium

should

it is

T

Adams

a term

mechar

which

the co

oscill

is a

one.

of the

stein

the c

occur

not f

Adams and Holstein⁽²²⁾ calculate the transverse galvanomagnetic effects for the case of weak scattering. They use the density matrix formalism and arrive at an expression for the electrical conductivity in quantizing magnetic fields. The only limitation of this theory is that it uses equilibrium quantum thermodynamics, whereas transport theory should treat the lack of equilibrium. Its virtue is that it is a quantum mechanical treatment.

The equation for the electrical conductivity found by Adams and Holstein is a product of an oscillatory part and a term containing the scattering. Seven types of scattering mechanisms are considered and it is the scattering terms which determine the magnitude and temperature dependence of the conductivity. The oscillatory part arises from the oscillatory density of states which they find is

$$n(E) = 2 (2\pi)^{-2} \sum_{\lambda=0}^{\lambda'} \frac{1}{\lambda + \delta} \quad (58)$$

δ is a function of field and has values between zero and one. Whenever a Landau level passes through an extremum of the F-S, $\delta = 0$ and (58) diverges. Since Adams and Holstein find the transverse conductivity to be

$$\sigma_{xx} = \text{constant} \times n(E) \quad (59)$$

the conductivity diverges also. The infinite conductivity occurring periodic in $\frac{1}{H}$ would be observable if it were not for the fact that the Landau levels are broadened by

collisions.

Adams and Holstein make a Fourier expansion of (58) and (59) since $n(E)$ and σ_{xx} are periodic functions. They also calculate the effect of collisions, and the effect of thermal broadening. The result is

$$\sigma_{xx} \sim \sum_{p=0}^{\lambda'} \exp\left(-\frac{2\pi p}{\omega\tau}\right) \left[\frac{2\pi^2 p k T / \hbar \omega}{\sinh \frac{2\pi p k T}{\hbar \omega}} \right] \cos\left(\frac{2\pi p}{PH} - \frac{\pi}{2}\right) \quad (60)$$

where τ is the average time between collisions. The exponential term thus accounts for the effect of collisions, the bracketed term for the effect of thermal broadening. These are the same temperature and collision corrections which appear in the equation for the oscillatory magnetization (48-50).

Thus the electronic part of the thermal conductivity and, therefore, its inverse the thermal magnetoresistance, are oscillatory functions of $\frac{1}{H}$. The periodicity P , of these oscillations is the same as the magnetization oscillations (47) and they determine the same cross sectional areas of the Fermi surface.

B. The Horton Quantum Theory of Thermoelectric Power

Horton⁽²¹⁾ uses the density matrix formalism and assumes scattering by impurities only. His final expression is in explicit form and includes the higher harmonics:

S ~

where

This

be pr

ics i

coeff

F_p i

8.6

(61)

S

$$\begin{aligned}
S \sim 1 - \frac{15}{8\pi^2} \frac{2}{kT} \left(\frac{\hbar\omega}{E_F} \right)^{\frac{1}{2}} \sum_p \frac{(-1)^p}{p} A_3 \sin\left(\frac{2\pi p}{PH} - \frac{\pi}{4}\right) \\
+ \frac{45}{8\pi^2} \frac{2}{E_F} \frac{\hbar\omega}{2} \sum_p \frac{(-1)^p}{p} A_4 \cos\left(\frac{2\pi p}{PH} - \frac{\pi}{4}\right)
\end{aligned} \tag{61}$$

where

$$\begin{aligned}
A_3 &= -2\pi e^{-\gamma}(1-\gamma) \\
A_4 &= \pi^2 e^{-\gamma} (2-\gamma) \\
\gamma &= \frac{2\pi^2 kT}{\hbar\omega}
\end{aligned} \tag{62}$$

This agrees within a constant, to Zilberman's theory⁽¹⁹⁾ to be presented. However, Zilberman drops all higher harmonics in (61).

The ratio of the coefficient of the sin terms to the coefficient of the cos terms is

$$\frac{2E_F}{3\pi kT} \tag{63}$$

E_F is usually a few electron volts and kT at 1° Kelvin is 8.6×10^{-5} e.v. so the ratio in (63) is roughly 10^4 and (61) becomes

$$S \sim 1 + \frac{15}{4\pi} \frac{2}{kT} \frac{\hbar\omega}{E_F} \sum_p \frac{(-1)^p}{p} e^{-\gamma}(1-\gamma) \sin\left(\frac{2\pi p}{PH} - \frac{\pi}{4}\right) \tag{64}$$

It is
of the
multi
proba
This,
termin
Zilbe

C. The Z

value
field
tiall
the p
 $k_1 n$
diff
poter
sin t
ages
at y
alon
acros

It is difficult to make a calculation of absolute magnitude of the oscillations from Horton's theory because the term multiplying the bracket in (64) depends on the transition probability between initial and final scattering states. This, in turn, depends on the matrix elements of the scattering potential. However, an estimate will be made from Zilberman's final equation.

C. The Zilberman Quantum Theory of Thermoelectric Power

Zilberman⁽¹⁹⁾ calculates the eigenfunctions and eigenvalues of the Hamiltonian for an electron in the periodic field of the lattice. The energy eigenvalues are essentially the same as for the electron when not considering the presence of the lattice (13,14). The eigenfunctions

$$\psi_{k_1 n k_3} = \text{const.} \times \sin\left[\frac{\pi}{a}(x+y+z)\right] \exp\{i(k_1 x + k_3 z)\} \phi_n(y-y_0) \quad (65)$$

differ from the eigenfunctions found with no lattice potential present (13,14), only by the presence of the sin term. When calculating matrix elements the sin averages to $\frac{1}{2}$ since it is a rapidly oscillating function.

Zilberman next calculates the current through a plane at $y = 0$ where H is in the z direction and the current is along y . This current J_y equals the number of transfers across the plane per second times the electronic charge.

$$J_y = c$$

$$\left\{ \begin{matrix} f_1 \\ f_2 \end{matrix} \right. (E_r)$$

Here V

produc

defect

to the

states

scatte

contai

for th

and su

the +j

2

funct.

and f

f

f

f

where

where

where

where

where

$$J_y = \text{constant} \times \int_{k_1} \int_{x_1} \int_{n,m} \int_{k_2 x_3} |V_{k_1 n k_3; x_1 m x_3}|^2 \delta(E_{k_1 n k_3} - E_{x_1 m x_3}) \quad (66)$$

$$\left\{ f_{k_1}(E_{n k_3}) [1 - f_{x_1}(E_{m x_3})] - f_{x_1}(E_{m x_3}) [1 - f_{k_1}(E_{n k_3})] \right\} dk, dx, dk_3 dx_3$$

Here $V_{k_1 n k_3; x_1 m x_3}$ is the matrix element of the perturbation produced by elastic scattering by impurities and lattice defects. The square of the matrix element is proportional to the transition probability between the initial and final states. The term $\delta(E_{k_1 n k_3} - E_{x_1 m x_3})$ accounts for elastic scattering, that is, conservation of energy. The term containing the distribution functions gives the probability for the initial state to be full and the final state empty and subtracts the contribution from the -y direction from the +y direction contribution.

Zilberman then assumes the change in the distribution function comes both from the presence of an electric field and from a temperature gradient:

$$f_{x_1} = f_{k_1} + (x_1 - k_1) \frac{\hbar c}{eH} \left[\frac{\partial T}{\partial y} \frac{\partial f_{k_1}}{\partial T} + \frac{\partial E_0}{\partial y} \frac{\partial f_{k_1}}{\partial E} \right] \quad (67)$$

where E_0 is the Fermi energy. The scattering potential is

$$V = V_0 \sum_p \delta(\bar{r} - \bar{p}) \quad (68)$$

where the sum p is over lattice impurity sites. The matrix

element
then e
Poisson
harmon
oscill
of the
show o
agreen

$$J_y = \frac{\Gamma}{H} + k^2 T \frac{\lambda}{\epsilon}$$

where
The t
 $J_y = c$
er =

where

$$\frac{\partial E_0}{\partial y}$$

elements of (68) are then calculated using (65), and (66) is then evaluated. The calculation is simplified by using the Poisson summation formula⁽²¹⁾. This introduces sums over harmonics of cosine terms and is the origin of the quantum oscillatory effects. The oscillatory effects arise because of the sum over quantum levels h and m in (66). The results show quantum oscillations in the electrical conductivity in agreement with the theory of Adams and Holstein:

$$\begin{aligned}
 J_y = \frac{m^4 c}{H^2} (eF + \frac{\partial E_0}{\partial y}) & \left[\frac{8}{3} E_0^2 + .3 \hbar \omega E_0 - \frac{80\pi^2}{3} \frac{kT E_0^{\frac{3}{2}}}{(\hbar \omega)^{\frac{1}{2}}} e^{-\gamma} \cos\left(\frac{2\pi}{PH} - \frac{\pi}{4}\right) \right] \\
 + k^2 T \frac{\partial T}{\partial y} & \left[\frac{16\pi^2}{9} E_0 + \frac{\pi^2}{10} \hbar \omega - \frac{20\pi}{3} \frac{(\hbar \omega)^{\frac{1}{2}}}{kT} E_0^{\frac{3}{2}} e^{-\gamma(1-\gamma)} \sin\left(\frac{2\pi}{PH} - \frac{\pi}{4}\right) \right] \quad (69)
 \end{aligned}$$

where $\gamma = 2\pi^2 \frac{kT}{\hbar \omega}$ and F is the electric field.

The thermoelectric emf oscillations are found by letting $J_y = 0$ in (69), and dropping small terms. The result is

$$\begin{aligned}
 eF = - \frac{\partial E_0}{\partial y} - \frac{2}{3} \frac{\partial T}{\partial y} \frac{\pi^2 k^2 T}{E_0} & \left[1 - \frac{9}{160} \frac{\hbar \omega}{E_0} + \frac{15(\hbar \omega E_0)^{\frac{1}{2}}}{4\pi kT} e^{-\gamma(1-\gamma)} \right. \\
 & \left. \times \sin\left(\frac{2\pi}{PH} - \frac{\pi}{4}\right) \right] \quad (70)
 \end{aligned}$$

where

$$\frac{\partial E_0}{\partial y} = k \frac{\partial T}{\partial y} \left[- \frac{\pi^2}{6} \frac{kT}{E_0} + \frac{3}{\pi^2} (1-\gamma) \frac{\hbar \omega}{4\pi E_0} e^{-\gamma} \sin\left(\frac{2\pi}{PH} - \frac{\pi}{4}\right) \right] \quad (71)$$

(70) differs from Zilberman's final equation by the factor

$\frac{22}{kT}$.

as well

Because

simple

eP

which

lation

oscill

cross-

tion a

D. Absolute

no

kT

E₀

This

γ =

$\pi^2 k^2 T$. However, the factor $\pi^2 k^2 T$ is necessary dimensionally as well as being a direct result of letting $J_y = 0$ in (69). Because of this, (70) and (71) have common terms and a more simple relation results than was given by Zilberman:

$$eF = -\frac{2}{3} \frac{\partial T}{\partial y} \frac{\pi^2 k^2 T}{E_0} \left[\frac{3}{4} - \frac{9}{160} \frac{\hbar\omega}{E_0} + \frac{18(\hbar\omega E_0)^{\frac{1}{2}}}{4\pi kT} e^{-\gamma(1-\gamma)} \right. \\ \left. \times \sin\left(\frac{2\pi}{PH} - \frac{\pi}{4}\right) \right] \quad (72)$$

which predicts the same period P (47) and phase of oscillations $-\frac{\pi}{4}$ as the Horton⁽²¹⁾ theory (64). Thus, quantum oscillations in the thermoelectric power yield the same cross-sectional areas of the Fermi surface as the magnetization and thermal magnetoresistance oscillations yield.

D. Absolute Magnitude of the Thermoelectric Oscillations

To estimate the oscillation amplitude we use

$$\hbar\omega = 1.4 \times 10^{-2} \text{ e.v. at 21 k gauss for an effective mass} \\ \text{of } .09 m_0 \text{ appropriate for the } 3\delta \\ \text{orbit of Tin.} \quad (73)$$

$$kT = 1.1 \times 10^{-4} \text{ e.v. at } 1.2^\circ \text{ Kelvin} \quad (74)$$

$$E_0 = 5 \text{ e.v.} \quad (75)$$

This makes

$$\gamma = .16 \text{ and } e^{-\gamma} = .85 \quad (76)$$

In (72

other

S =

where

Zilber

altitude

the ma

and e

and 3.

since

trical

temper

oscill

ductin

latic

1.2°

will

and c

This

tions

only

poten

In (72) the term containing the sin is much larger than the other two terms in the bracket and (72) becomes

$$S = \frac{12\pi k}{e} \left(\frac{\hbar\omega}{E_0} \right)^{\frac{1}{2}} e^{-\gamma(1-\gamma)} \sin\left(\frac{2\pi}{PH} - \frac{\pi}{4}\right) \quad (77)$$

where S is the absolute thermoelectric power. Neither Zilberman nor Horton consider the factors effecting the amplitude of the oscillations as was considered in II,E for the magnetization oscillations. However, the experimental and effective mass factors will be the same. (See II E, 1. and 3.) Most likely the spin factor (51) will be the same, since this effects only the Landau level structure.

Adams and Holstein found that the oscillations in electrical conductivity (60) were damped by the same (48,49,50) temperature and collision factors as the magnetization oscillations were damped. It is difficult to justify introducing identical factors for the thermoelectric power oscillations. However, when (48) is evaluated at 21 k gauss and 1.2° Kelvin it effects the amplitude by less than 2% so (77) will be evaluated not considering the effects of temperature and collisions.

$$S \sim .4\text{uV}/^\circ\text{K} \sin\left(\frac{2\pi}{PH} - \frac{\pi}{4}\right) \quad (78)$$

This is a factor of 10 smaller than the observed oscillations. This is not too surprising since Zilberman considered only one type of scattering mechanism and the scattering potential (68) is probably much too simplified.

It is interesting that (77) predicts the oscillation amplitude to be independent of temperature. Higher temperatures will, however, broaden the Landau levels and reduce the oscillation amplitude.

IV
E

A. Hist

resid

Chan

and

theo

inde

by ge

quant

This

tool

paper

Chan

exper

W. K.

when

curr

Thus

IV High Field Thermal Magnetoresistance and Thermopower Tensors

A. History of the Thermal Magnetoresistance Tensor

The significance of high field electrical magnetoresistance was first pointed out by Kohler⁽²⁹⁾ and by Chambers⁽³⁰⁾. It was Lifshitz, Azbel and Kaganov (LAK), and Lifshitz and Peschanskii⁽³¹⁾ who essentially put the theory in final form. They showed that the behavior was independent of the collision process, being governed only by geometrical features of the F-S. They also assumed that quantization due to the magnetic field was not significant. This makes high field magnetoresistance a very effective tool for studying F-S topology.

An extensive reference to theoretical and experimental papers through 1960 is given in The Fermi Surface by Chambers⁽¹¹⁾. Fawcett reviewed both the theoretical and experimental results through April of 1964⁽³²⁾.

The thermal magnetoresistance tensor is defined as $W_{ik}(\bar{H})$ from:⁽³³⁾

$$\frac{\partial T}{\partial x_i} = - \pi_{ik} j_k - W_{ik} Q_k \quad (79)$$

where Q_{ik} is the heat flux vector, and j_k is the electrical current vector, which is zero in our experiments.

Thus,

$$\frac{\partial T}{\partial x_i} = - W_{ik} Q_k \quad (80)$$

If a
only

If t
y di

For c

whic
field

ret
that

nate
the

is c
ters

F-S
res

If Q_k has components along the sample axis (y direction) only, then

$$\begin{pmatrix} \frac{\partial T}{\partial x} \\ \frac{\partial T}{\partial y} \\ \frac{\partial T}{\partial z} \end{pmatrix} = - \begin{pmatrix} W_{xy} Q_y \\ W_{yy} Q_y \\ W_{zy} Q_y \end{pmatrix} \quad (81)$$

If the only temperature difference measured is along the y direction, then

$$\frac{\partial T}{\partial y} = - W_{yy} Q_y \quad (82)$$

For constant power and sample length, this gives

$$\Delta T(\bar{H}) \sim W_{yy}(\bar{H}) \quad (83)$$

which is used to experimentally plot W as a function of field strength and direction.

The thermal magnetoresistance, $W(\bar{H})$, was treated theoretically by Azbel, Kaganov and Lifshitz⁽³⁴⁾. They showed that for low temperatures, where impurity scattering dominates, the Wiedemann-Franz law (57) is obeyed. Therefore, the electronic part of the thermal magnetoresistance tensor is completely analogous to the electrical magnetoresistance tensor. The thermal magnetoresistance will supply the same F-S topology information as does the electrical magnetoresistance.

tax

195

but

der

rat

rea

as d

stud

to i

was s

In Co

tion.

it ma

tropy

fixed

sista

the L

as a f

in Fla

T

indium

They d

fields

The first experimental work on thermal magnetoresistance at 4.2° Kelvin was by Shalyt⁽³⁵⁾ in 1944 on Bi. In 1950 Hulm⁽³⁶⁾ studied single crystals of tin to 1500 gauss, but did not rotate at fixed fields, and his work was incidental to the study of superconductivity. His samples were rather impure so that 1500 gauss was not large enough to reach the conditions of reference (31):

$$\omega\tau \gg 1 \quad (84)$$

as defined by (1). In 1953 Mendelissohn and Rosenberg⁽³⁷⁾ studied Zn, Cd, Sn and Tl as a function of field strength to 18.5 k gauss, but for some reason only the zinc crystal was studied for the field along more than one direction. In Cd, Sn, and Tl they don't even specify the field direction. Since the tin sample was only 99.996% pure, perhaps it made little difference what the field direction was.

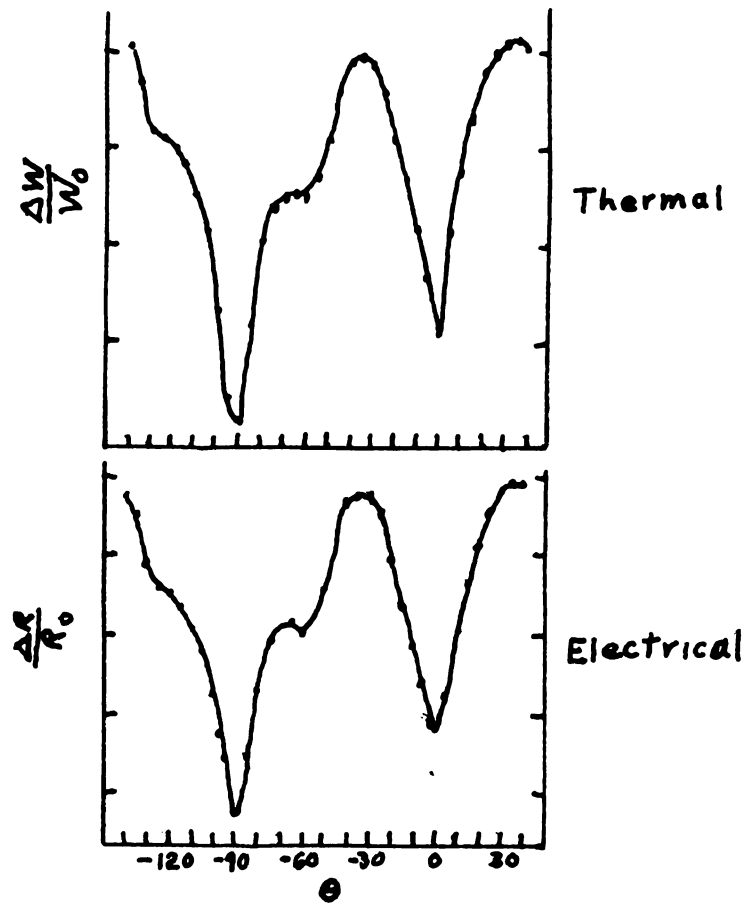
P. B. Alers⁽³⁸⁾ was the first to observe the anisotropy of the thermal magnetoresistance by rotating at fixed field. By also measuring the electrical magnetoresistance of zinc he was able to observe the behavior of the Lorentz ratio (see equation 57)

$$L(H) = \frac{1}{3} \frac{\pi^2 k^2}{e^2} \quad (85)$$

as a function of field and angle. His results are shown in Figure 3.

The Lorentz ratio of single crystals of lead and indium in transverse fields was studied by Challis, et al.⁽³⁹⁾ They did both rotations and field sweeps at 2° Kelvin in fields up to 20 k gauss. Although they find a 35%

Figure 3



Zinc 3.5°K 12.3 kGauss

variatio

p(H) by

is not s

The work

will yie

electric

Az

Wiedeman

ficients

scatteri

valid fo

and comp

thermal a

gradient

to a mag

We

has been

crystals

electric

demonstr

of tin.

fulness

Longo, S

variation in $\frac{L(H)}{L(H=0)}$ in rotation, the $W(H)$ varies by 500% and $p(H)$ by 65%. With the large variation in each quantity it is not surprising that their ratio is not quite constant. (12)

The work demonstrates that the thermal magnetoresistance will yield the same information about the F-S as does the electrical magnetoresistance.

Azbel, Kaganov, and Lifshitz⁽³⁴⁾ also predict the Wiedemann-Franz law to relate the Hall and Righi-Leduc coefficients. This is true only in the low temperature, impurity scattering region for compensated metals, but is generally valid for uncompensated metals. A metal is uncompensated if

$$n_A = n_h - n_e \neq 0 \quad (86)$$

and compensated if $n_A = 0$. The Righi-Leduc effect is the thermal analogy to the Hall effect. A transverse temperature gradient is measured when heat flows in a sample transverse to a magnetic field.

We conclude this section by stating that very little has been done on the thermal magnetoresistance in single crystals, and that it shows promise as an alternative to the electrical magnetoresistance for studying F-S's. We have demonstrated its effectiveness in a reasonably pure sample of tin. It would be interesting to further check its usefulness by looking at one of the AuSn or AuAl₂ crystals of Longo, Sellmyer, and Schroeder⁽⁴⁰⁾.

B. Theory of the Thermal Magnetoresistance Tensor

The Azbel, Kaganov, and Lifshitz⁽³⁴⁾ theory shows that the Wiedemann-Franz law is valid at low temperatures. The thermal magnetoresistance is completely analogous to the electrical magnetoresistance. Therefore, we need only consider the electrical magnetoresistance which was extensively studied by LAK⁽³¹⁾. Good treatments of the theory are presented by Ziman⁽⁴¹⁾, Chambers⁽⁴²⁾ and Sellmyer⁽⁴³⁾ and need not be presented here. Fawcett⁽⁴⁴⁾ summarizes the results as shown in Figure 4.

Figure 4

Type of orbit and state of compensation	Magneto-resistance	Thermopower
I. All closed and uncompensated $n_e \neq n_h$	$\sim H^0$ (saturates)	H^0
II. All closed and compensated $n_e = n_h$	$\sim H^2$ (quadratic)	H^1
III. Open in one direction	$\sim H^2 \cos^2 \alpha$	H^0
IV. Open in two directions	$\sim H^0$ (saturates)	H^0
V. Singular field-direction	$\sim H^0$ (saturates)	H^0

\vec{J} , or in our case \vec{q} , is in the plane perpendicular to \vec{H} making an angle α with the open orbit direction.

Tin is a compensated metal having orbits open in one direction, and orbits open in two directions, so II, III, and IV would apply. (possibly also V) To demonstrate the origin of the field dependencies listed in the chart,

consider the tensor for III.

$$\rho_{ij} = \begin{pmatrix} \sim H^2 & \sim H & \sim H \\ \sim H & \sim H^0 & \sim H^0 \\ \sim H & \sim H^0 & \sim H^0 \end{pmatrix} \quad (87)$$

The magnetic field is in the z direction and perpendicular to the sample axis. The open orbit is along the x-axis. Thus, if the open orbit is along the sample axis, the magneto resistance $\frac{\Delta\rho}{\rho}$ measured would be proportional to H^2 . If the open direction is perpendicular to the sample length, the magnetoresistance saturates. For open orbit directions making an angle α with the sample axis a similarity transformation of (87) is made to rotate the open direction into the sample direction. This is the origin of the $\cos^2\alpha$ term in III.

C. The Effects of Magnetic Breakdown

Blount⁽⁴⁵⁾ found that when high magnetic fields are present in metals having relatively small energy gaps, there is a finite probability for electrons to jump the gap and follow new orbits. This is called magnetic breakdown⁽⁴⁶⁻⁴⁹⁾ and the effect was seen in several metals with hexagonal close-packed structure⁽⁵⁰⁻⁵⁸⁾.

Blount found the probability of breakdown to be

$$P = \exp\left(-\frac{H_0}{H}\right) \quad (88)$$

where

$$H_0 = \frac{K\Delta^2 mc}{E_F e} \quad (89)$$

where Δ is the energy gap, E_F is the Fermi energy and K is a constant approximately equal to 1.

Magnetic breakdown can have a pronounced effect on the magnetoresistance. Complete breakdown has the effect of eliminating Bragg reflection. Open orbits on the F-S can become closed orbits and closed orbits can become open. Suppose the angle α in Figure 4 III is near $\frac{\pi}{2}$. The open orbit will cause saturation of the magnetoresistance. If magnetic breakdown is present this open orbit can become closed at higher magnetic fields. The magnetoresistance would become quadratic in H .

Magnetic breakdown has a pronounced effect on quantum oscillations also. The oscillations must originate from closed orbits on the F-S. If these closed orbits become open because of magnetic breakdown there can be no oscillations. Since the breakdown probability (88) does not vary sharply with field there is usually a mixture of open and closed orbits. The effect is to severely damp the oscillations but not completely eliminate them. Because of (88) they are more heavily damped at higher fields where breakdown is more complete.

Magnetic breakdown in tin will be discussed in a later section.

3. Theory of

Az
theory t
Thomson
(BGN), f
electric
cients.

The
vector i
their so

J_i

q_i

where E_k
the Onsa
coeffici
relation

a_i

d_i

b_i

Rather t

D. Theory of the Thermoelectric Power Tensor

Azbel, Kaganov and Lifshitz⁽³⁴⁾ extended the LAK⁽³¹⁾ theory to include the heat conductivity tensor and the Thomson coefficient. Bychkov, Gurevich and Nedlin⁽⁵⁹⁾, (BGN), further considered the theory to include the thermoelectric power, peltier coefficient and the Thomson coefficients.

The heat current vector is \bar{q} , and the electric current vector is \bar{J} . In general, \bar{J} and \bar{q} are defined in terms of their sources as

$$\mathbf{J}_i = \frac{a_{ik}}{T} E_k + b_{ik} \frac{\partial}{\partial x_k} \frac{1}{T} \quad (90)$$

$$\mathbf{q}_i = \frac{c_{ik}}{T} E_k + d_{ik} \frac{\partial}{\partial x_k} \frac{1}{T} \quad (91)$$

where E_k and $\frac{\partial}{\partial x_k} \frac{1}{T}$ are the generalized forces required in the Onsager⁽¹⁷⁾ relations. Thus, in a magnetic field the coefficients are functions of H and the Onsager symmetry relations hold:

$$a_{ik}(H) = a_{ki}(-H) \quad (92)$$

$$d_{ik}(H) = d_{ki}(-H) \quad (93)$$

$$b_{ik}(H) = c_{ki}(-H) \quad (94)$$

Rather than use (90) and (91), new coefficients can be

define

where C
the hea
tensor,

The
the rela
and (9)

Re

and new

Using (

defined such that:

$$E_i = \sigma_{ik}^{-1} j_k + \alpha_{ik} \frac{\partial T}{\partial x_k} \quad (95)$$

$$q_i = \beta_{ik} j_k - K_{ik} \frac{\partial T}{\partial x_k} \quad (96)$$

where σ_{ik} is the electrical conductivity tensor, K_{ik} is the heat conductivity tensor, α_{ik} is the thermal emf tensor, and β_{ik} is the Peltier coefficient.

The equations relating a_{ik} , b_{ik} , c_{ik} and d_{ik} determine the relations between σ_{ik} , K_{ik} , α_{ik} and β_{ik} given in (95) and (96).

Rewriting equation (95) gives

$$\sigma_{ik} = \frac{a_{ik}}{T} \text{ and } \alpha_{ik} = \frac{b_{lk} a_{il}^{-1}}{T} \quad (97)$$

and rewriting equation (96) gives

$$\beta_{ik} = c_{il} a_{lk}^{-1} \text{ and } K_{ik} = \frac{(d_{ik} - c_{il} a_{lm}^{-1} b_{mk})}{T^2} \quad (98)$$

Using (92), (93) and (94) the following relations hold:

$$\sigma_{ik}(H) = \sigma_{ki}(-H) \quad (99)$$

$$K_{ik}(H) = K_{ki}(-H) \quad (100)$$

$$T\alpha_{ik}(H) = \beta_{ki}(-H) \quad (101)$$

Notice

is als

T

must b

a_{ik} mu

a_{ik} are

there n

calcula

Th

various

for the

coeffic

c_{ik} and

then gi

The

are:

for clos

of elect

Notice that if β_{ki} is known as a function of H that α_{ik} is also known as a function of H from (101)

To calculate β_{ik} equation (98) says that c_{ik} and a_{ik} must be known. If we calculated α_{ik} directly then b_{ik} and a_{ik} must be known. From (90) and (91) notice that c_{ik} and a_{ik} are found when only E is present, whereas to find b_{ik} there must be a temperature gradient present. Thus β_{ik} is calculated, and from this α_{ik} found.

The expression for a_{ik} was worked out in detail for various F-S geometries by LAK and Lifshitz and Peschanski⁽³¹⁾ for the electrical conductivity. BGN⁽⁵⁹⁾ calculate the c_{ik} coefficients using the method of LAK, et al. Thus, knowing c_{ik} and a_{ik} (98) and matrix multiplication give β_{ik} . (101) then gives α_{ik} .

These tensors for the high field thermoelectric power are:

$$\alpha_{ik} = \frac{1}{T} \begin{pmatrix} v_{xx} & v_{yx}(-\gamma_0) & v_{zx} \\ -\gamma_0 v_{xy} & v_{yy} & v_{zy} \\ -\gamma_0 v_{xz} & -\gamma_0 v_{yz} & v_{zz} \end{pmatrix} \quad (102)$$

for closed F-S's with $n_A \neq 0$ that is, with unequal numbers of electrons and holes. Here γ_0 is defined by

$$\gamma_0 = \frac{m}{e\tau} \frac{1}{H} \quad (103)$$

and v_x

v_y and

The di

Boltzma

c is de

If $\frac{dr}{dE} \Big|_E$

If $n_e =$
holes, t

and

and v_{ij} are independent of field to first order. v_{xx} and v_{yy} are defined by

$$v_{xx} = v_{yy} = \frac{\pi^2 k^2 T^2}{3e} \frac{d}{dE} \ln(n_e - n_h) \quad (104)$$

The diffusion thermoelectric power calculated from the Boltzman equation is

$$S = \frac{\pi^2 k^2 T}{3e} \left. \frac{d \ln \sigma}{dE} \right|_{E_F} \quad (105)$$

σ is defined from simple theory⁽⁴¹⁾ as

$$\sigma = \frac{ne^2 \tau}{m} \quad (106)$$

If $\left. \frac{d\tau}{dE} \right|_{E_F} = 0$ then (105) becomes

$$S = \frac{\pi^2 k^2 T}{3e} \left. \frac{d \ln n}{dE} \right|_{E_F} \quad (107)$$

If n_e = the number of electrons and n_h = the number of holes, then (107) is

$$S = \frac{\pi^2 k^2 T}{3e} \left. \frac{d \ln (n_e - n_h)}{dE} \right|_{E_F} \quad (108)$$

and

$$v_{xx} = v_{yy} = ST \quad (109)$$

α_{ik} is therefore the thermoelectric power tensor in high magnetic fields.

The diagonal coefficients in (102) are independent of γ_0 and therefore independent of magnetic field strength. This applies only when there are no open orbits and $n_A \neq 0$.

For a compensated metal $n_A = 0$ and BGN get

$$\alpha_{ik} = \frac{1}{T} \begin{pmatrix} -\gamma_0^{-1} v_{xx} & -\gamma_0^{-1} v_{yx} & -\gamma_0^{-1} v_{zx} \\ -\gamma_0^{-1} v_{xy} & -\gamma_0^{-1} v_{yy} & -\gamma_0^{-1} v_{zy} \\ v_{xz} & v_{yz} & v_{zz} \end{pmatrix} \quad (110)$$

The x and y diagonal terms are linear in magnetic field, whereas the diagonal terms in electrical and thermal magnetoresistance are quadratic in field. In (110) z is again the direction of magnetic field so the transverse magneto thermopower is determined by either the xx or yy terms.

BGN treat the same three (III, IV, V in Figure 4) types of open orbits as LAK did. As an example of orbits open in one direction BGN take the "corrugated cylinder":

Figure 5



Again

when

perp

The

H ar

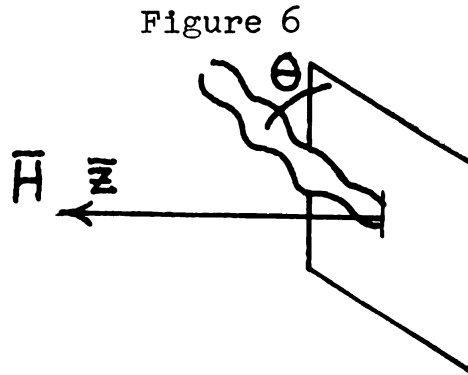
The

\bar{x} d

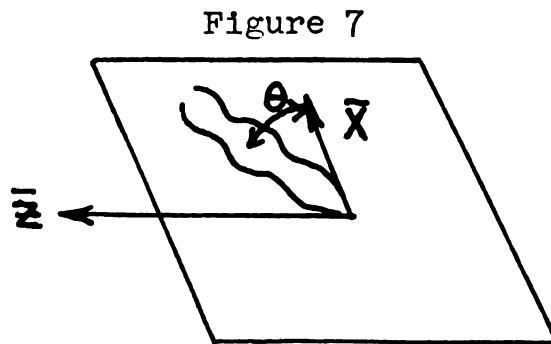
Again take \bar{H} as along the z direction, and define

$$\eta = \frac{\gamma_0}{\sin \theta} \quad (111)$$

where θ is the angle between the cylinder axis and the plane perpendicular to the field direction as shown in Figure 6:



The x axis is taken as in the plane, passing through both H and the cylinder axis as shown in Figure 7:



Therefore θ is the angle between the cylinder axis and the \bar{x} direction.

and with
that -
of v_0 ,

To
dicular

In
case the

along the
open dir

A rotati
dependen

For

not the
identical

independ
orbit of

necessar
case II

BGN get the following thermoelectric power tensor:

$$\alpha_{ik} = \frac{1}{T} \begin{pmatrix} v_{xx}(-\eta) & -\gamma_0^{-1} v_{yx}(-\eta) & -\gamma_0^{-1} v_{zx}(-\eta) \\ -\gamma_0 v_{xy}(-\eta) & v_{yy}(-\eta) & v_{zy}(-\eta) \\ -\gamma_0 v_{xz}(-\eta) & v_{yz}(-\eta) & v_{zz}(-\eta) \end{pmatrix} \quad (112)$$

and when $\eta \rightarrow \infty$ v_{ik} becomes a constant. From (111) we see that $\eta \rightarrow \infty$ when Θ is near 0 or π independent of the value of γ_0 , since γ_0 is always finite.

Thus, the thermopower saturates (H^0) when \bar{H} is perpendicular to this type of open orbit direction.

In (87) the xx and yy terms were H^2 and H^0 . In that case the open orbit was along x. If the open orbit was along the sample axis direction, H^2 was observed. If the open direction was perpendicular to this, H^0 was observed. A rotation of the coordinate system gave an $H^2 \cos^2 \alpha$ dependence as summarized in III of Figure 5.

For the thermoelectric power tensor the situation is not the same. Notice that the xx and yy terms in (112) are identical. Saturation would be observed as long as $\Theta \cong 0, \pi$ independent of the angle the sample made with the open orbit direction. No rotation of the coordinate system is necessary. Therefore, no $\cos^2 \alpha$ term is present as in case III for the magnetoresistance.

For the two other types of orbits (IV and V in Figure 4) BGN get

$$\alpha_{ik} = \frac{1}{T} \begin{pmatrix} v_{xx} & -- & -- \\ -- & v_{yy} & -- \\ -- & -- & v_{zz} \end{pmatrix} \quad (113)$$

where the v_{ii} are constants at high fields, and saturation results. The magneto thermoelectric power tensors are summarized in Figure 4.

E. Kohler Corrections

In an actual crystal a crystallographic axis of high symmetry is not always along the sample axis and the tensoral relations defined above have to be modified. Kohler⁽⁶⁰⁾ discusses this in detail. He shows that the thermopower is

$$E_{\phi} = E_{||} \cos^2 \phi + E_{\perp} \sin^2 \phi + \frac{\left(\frac{\lambda_{\perp}}{\lambda_{||}} - 1 \right) (E_{||} - E_{\perp})}{\sin^2 \phi + \frac{\lambda_{\perp}}{\lambda_{||}} \cos^2 \phi} \sin^2 \phi \cos^2 \phi$$

where || and \perp mean parallel and \perp to the [110] axis ϕ is the angle between the sample axis and [110] axis. The crystal used for our experiments had the [110] axis 11° from the sample axis and the Kohler corrections are negligible

since:

$$\cos 11^\circ = .982 \quad \cos^2 11^\circ = .963$$

$$\sin 11^\circ = .191 \quad \sin^2 11^\circ = .036$$

So even if $E_{||} = \frac{1}{2} E_{\perp}$ the measured E_{ϕ} is within 7% of

$$E_{\phi} = E_{||}$$

V. Experimental Apparatus and Measurement Techniques

A. Sample Preparation

In an attempt to obtain a sample with a major symmetry axis oriented along the sample axis, seven samples were grown. They were in the shape of a long cylinder and were grown in a Bridgeman furnace⁽⁶¹⁾. The first sample (SnI) was grown in a graphite crucible from 99.9999% pure tin and resulted in a resistance ratio

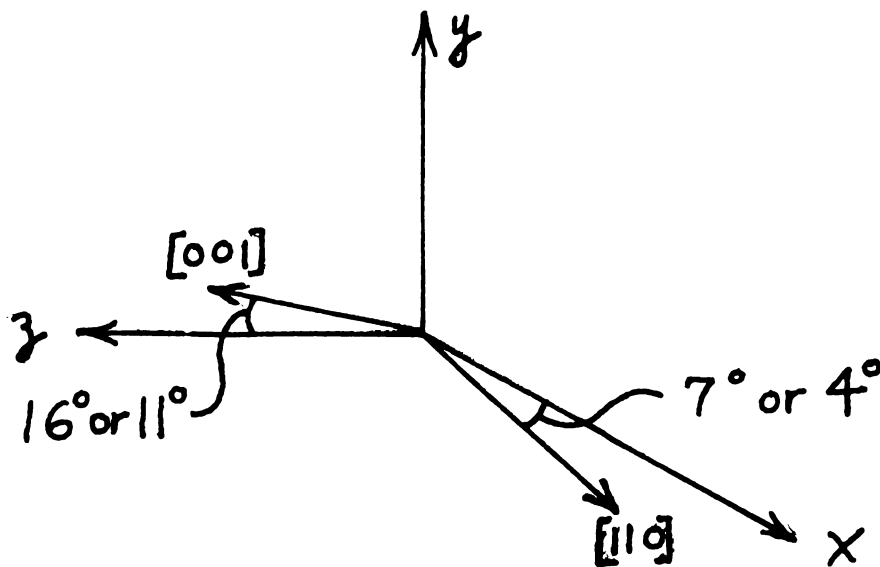
$$\frac{\rho_{300}}{\rho_{4.2}} = 31,000 \quad (115)$$

The sample had a two fold axis 52° off the sample axis. Therefore, little work was done on it and the results not analyzed. The remaining samples were grown in glass tubes internally tapered by pulling them slowly out of hydrofluoric acid. The tapering allowed the finished crystal to be easily removed from the tube. The tin was etched with two parts glycerin to one part HNO_3 , and washed in distilled water. Tin has a very low vapor pressure, and the glass and tin were extensively outgassed.

The crystal selected for most of the experiments (SnII) had a resistance ratio of 30,000. The [001] axis was 79° from the sample axis and the [110] axis was 86° from the sample axis. The sample was mounted vertically for the August through September data. On October 7th it was mounted so that [001] was 16° , and the [110] was 7° from the horizontal plane. \bar{H} was rotated in the horizontal

plane. The geometry is shown in figure 8.

Figure 8



\vec{H} is in the x-z plane

B. The Apparatus

The apparatus was designed to place the long cylindrical sample transverse to a uniform magnetic field. It was also necessary to have the sample in vacuum and to have one end of it in thermal contact with the liquid helium bath. A general view of the apparatus is shown in figure 9, and in figure 10 the details of the mounting of the sample in the vacuum can is shown.

The cross hatched part in figure 10 was made of copper because of its high thermal conductivity. This, along with the fact that liquid helium could enter the inner helium container to which the crystal was directly attached, assured that the end of the sample was close to bath temperature. The long section between the

Figure 9

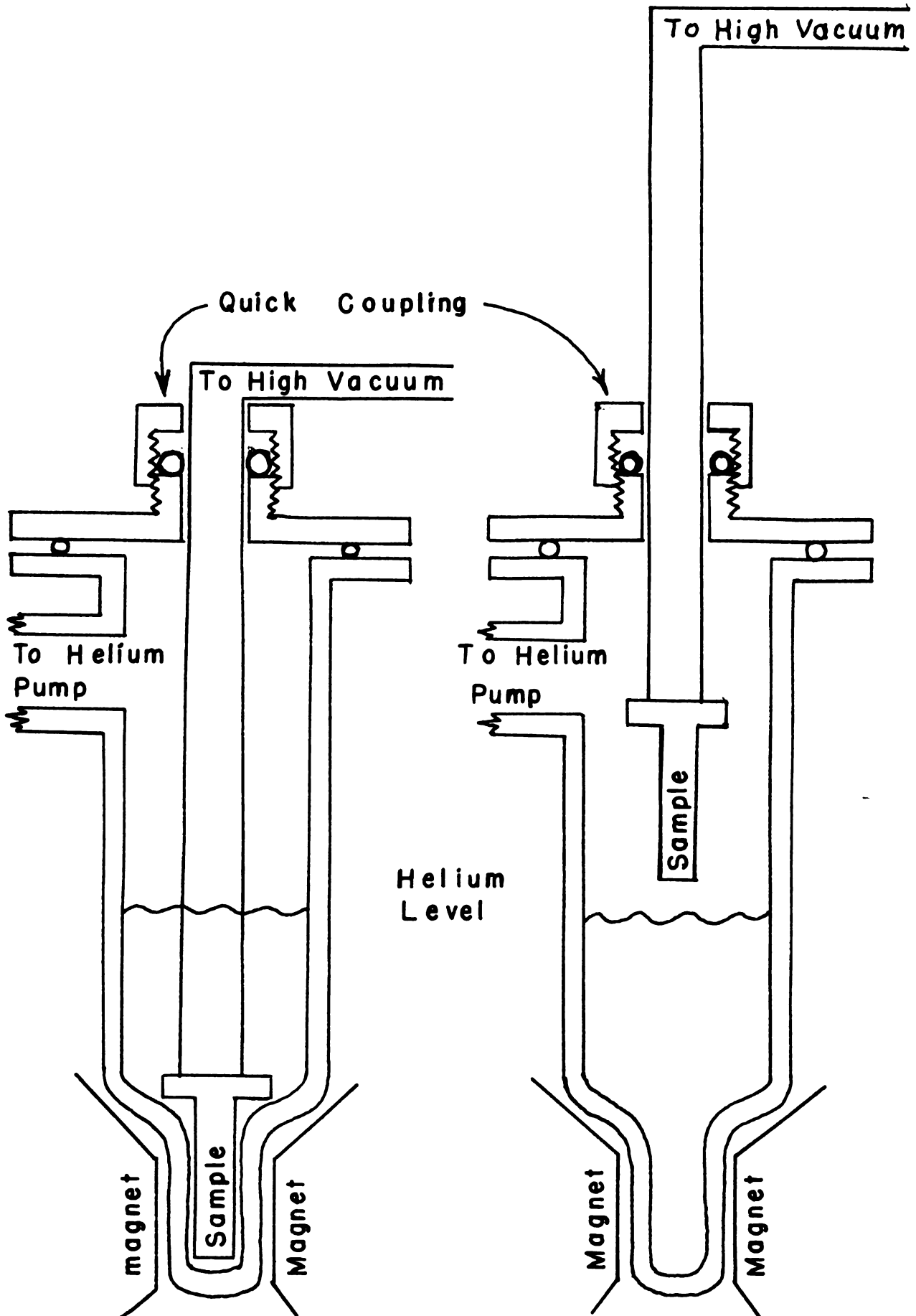
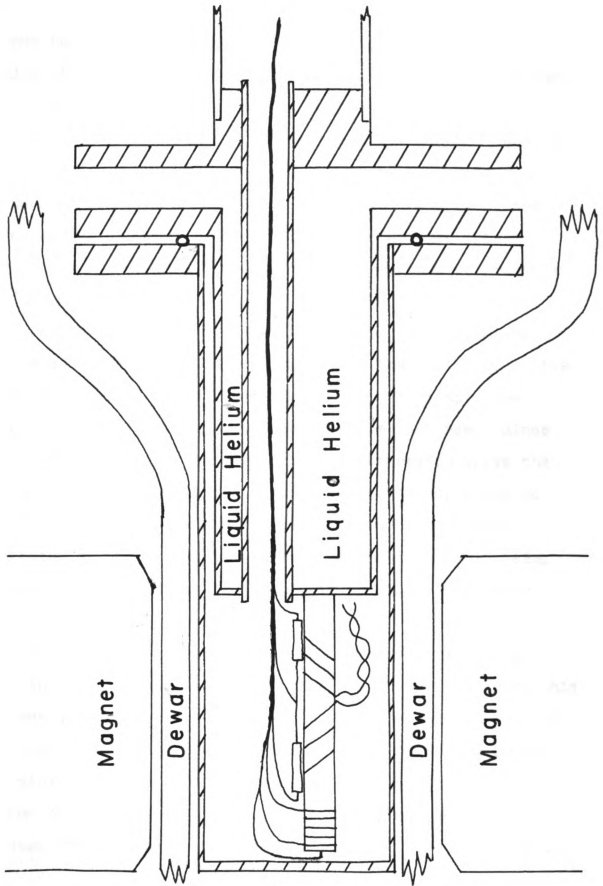


Figure 10



copper holder and outside of the dewar was made of thin walled stainless steel to reduce the heat flow to the helium.

The region around the sample was maintained at high vacuum by pumping through the long stainless support tube as shown in figure 9. An oil diffusion pump, backed by a mechanical pump, kept the vacuum at 2×10^{-5} mm Hg. as measured at room temperature near the diffusion pump intake. The region surrounding the sample was cryopumped to probably 10^{-6} mm Hg.

One of the most useful features of the apparatus was the veeco "quick" coupling which allowed the entire apparatus to be raised or lowered. See figure 9. The sample was thus centered in the magnetic field before each run. Since the "quick" coupling was a vacuum seal the region above the helium bath could be pumped to 0.13 mm Hg, corresponding to 1.008° Kelvin. The ultimate vacuum varied between runs depending on whether another dewar was simultaneously being pumped. The lowest possible temperature was never higher than 1.40° Kelvin.

The "quick" coupling was useful in case of a vacuum leak in the apparatus after the transfer of helium. When this happened, the apparatus was removed, and the leak fixed. It was then placed back over the dewar in the raised position and slowly lowered through the coupling, back into the bottom of the dewar. It could be lowered in about twenty minutes with a loss of less than a liter of helium. Lowering

the apparatus through the quick coupling meant that no "snow" collected inside the dewar. See figure 9 .

Temperatures intermediate between 4.2°K and 1.0°K were reached and maintained, to within 2×10^{-3} $^{\circ}\text{Kelvin}$, by pumping on the helium bath and maintaining a constant pressure above the helium with a regulator described in the appendix.

C. The Measurement of Voltages

The voltages were measured continuously as a function of field strength, and orientation at fixed field. The $\frac{d\phi}{dt}$ voltage pickup in the loop formed by the two lead wires was kept to a minimum by non-inductively twisting the wires. An increasing field out of the paper induces a current in each tiny loop, and each loop cancels the effect of its neighbor. The tightly wound leads present a very small area to the changing field. Being tightly wound, the two wires were in good thermal contact with each other at all points along the wires.

The emf leads were made of NbZr wire which remains superconducting in the presence of our maximum field of 21.5 Kgauss. They were spot welded to the sample to eliminate thermoelectric voltages generated by solder connections.

The NbZr wires were prepared by repeatedly coating them with Ge 7031 varnish which was thinned 4:1 with 50-50 alcohol:toluene. The wires were then baked for

for eight hours at 45°C . The resulting insulation was better than 20 Meg ohms after twisting the wires together.

The leads were wound around the sample. The sample and each lead formed non-inductive loops even though the sample was a "straight" wire. The sections of lead wire wound around the sample were in good thermal contact with it. The NbZr was therefore well below its 11°Kelvin transition temperature.

As a consequence of the winding procedure the $\frac{d\phi}{dt}$ pickup voltage was very small. When the field changed at the rate of 1 Kgauss per second the pickup was $\sim 1 \mu\text{V}$. Since sweep rates were generally less than 300 gauss per minute or 5 gauss per second, the pickup was about 5×10^{-9} volts. This is comparable to the amplitude of the smallest oscillations observed and was therefore acceptable. With even more care, for example more windings around the sample, this could probably be reduced to 10^{-9} volts.

NbZr was chosen for lead wires, because it remains superconducting in high magnetic fields. The thermopower of a superconductor is zero. Therefore, it was hoped that the measured thermopowers were due to the tin alone.

M. C. Steele, and J. de Launay⁽⁶²⁾ showed that a thermoelectric potential exists between a superconductor and the same metal in the normal state. They found the empirical relation:

$$E = E_0 \left(1 - \frac{T}{T_c} \right)^2$$

with

$$E_0 \sim 10^{-7} \text{ volts}$$

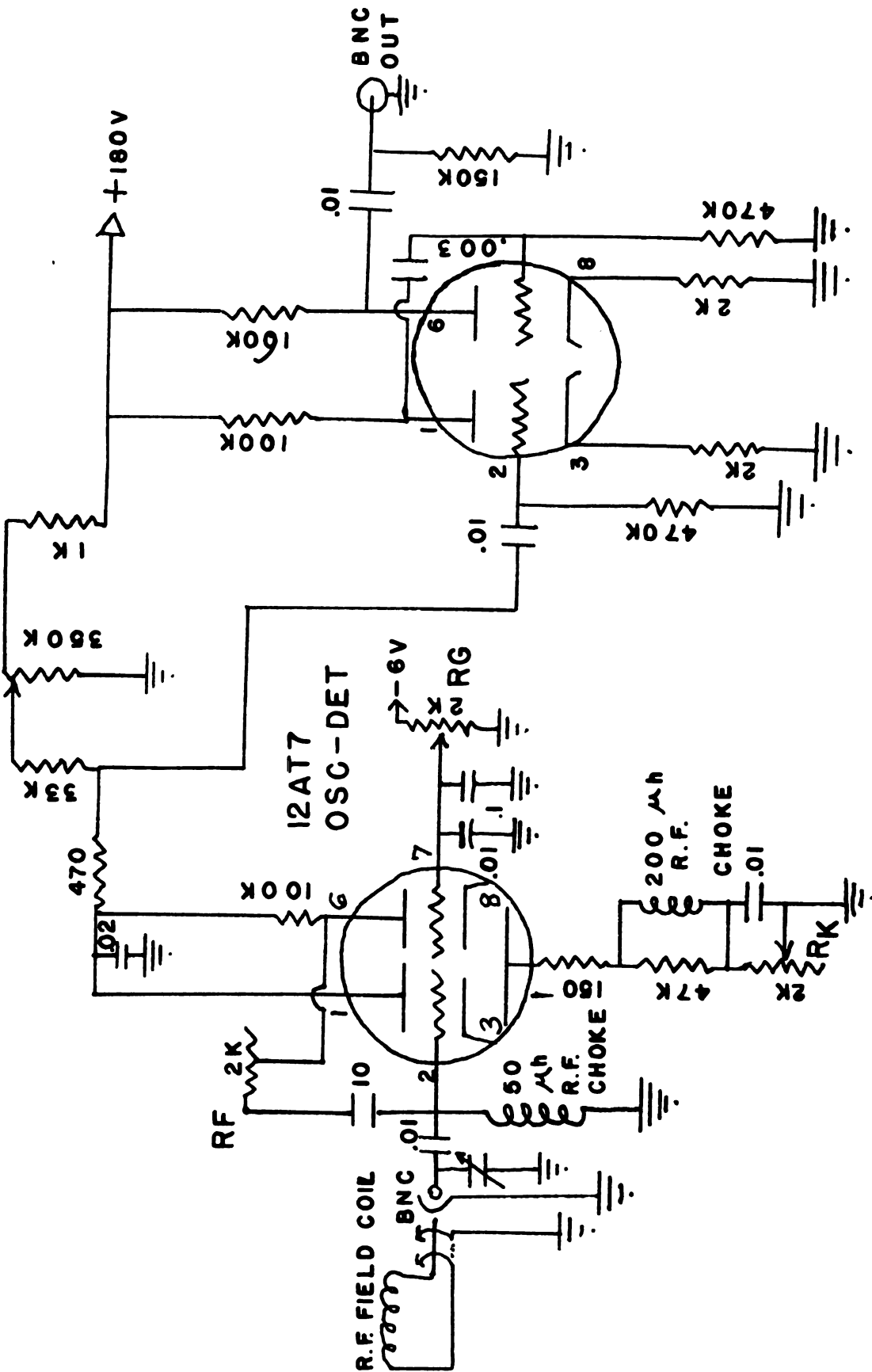
Thus, at 1°K, E could be $\sim 10^{-7}$ volts. With the well twisted wires, in good thermal contact, they would both go normal at the same place. The $\sim 10^{-7}$ volts generated in each lead tended to cancel each other. Voltages measured when no temperature gradient was across the sample, were about 10^{-6} volts. Part of this came from the incompletely cancelled $\sim 10^{-7}$ volts in each lead. Another possible source of this voltage was the thermoelectric emf generated in the normal part of the wire. When a large temperature difference (up to 300° Kelvin) existed across the wire of inhomogeneous composition, emfs were developed.

D. Pole Pieces and Magnetic Field Homogeneity

The pole faces for the Harvey Wells magnet had a 6" diameter and a $2 \frac{13}{16}$ " gap. They were aligned parallel to each other using an NMR probe. Alignment bolts were changed to make the NMR signal sharpest. The marginal oscillator used is shown in figure 11. A 60 cycle modulation coil was used along with a proton (water) resonance source.

New pole faces were designed and built from 1010 steel. These had a 4" diameter and a $1 \frac{3}{16}$ " gap. This gap allowed two $\frac{1}{16}$ " aluminum sheets to be inserted in back of the pole faces. This insured that the pole faces could be removed in the future. A spectro chemical analysis of the

Figure 11



1010 steel showed:

- .12% carbon
- .35% manganese
- ≤ .01% phosphorus
- .025% sulphur
- .33% silicon

Analysis was done by Allis-Chalmers research laboratories. The saturation magnetization was 21.0 kgauss. Using experimental data from Magnion Corporation the maximum field was estimated at 30 kgauss. The Olofsson Corporation of Lansing ground the faces of each pole piece parallel to within $\frac{4}{10,000}$ inches. They were ground flat with the same accuracy.

The 30 kgauss pole faces were designed for use with the Hoffman model HLMR-11 dewar. Unfortunately, the dewar would hold helium for only two hours after consuming seven liters of helium. Pumped to 1^oK it would probably last less than an hour. The dewar was leak tested and no leaks were discovered. It was concluded that contact was present across a vacuum jacket.

The 30 kgauss system mentioned above has great potential for a number of experiments. Higher frequencies in the thermopower quantum oscillations would be resolved. Combined with the field modulation technique (to be described) it would greatly increase the effectiveness of the oscillation studies.

The present experiments were done using the 6" diameter

pole faces with 3" gap, with a glass dewar. The field strength as a function of distance from the pole face center is shown in figure 12. Data were taken with a Rawson rotating coil gauss meter. These plots were important because the field must be uniform over the dimensions of the sample. If the field at one point on the sample differs from that at another by more than the separation between two oscillation peaks, the oscillations cannot be observed. (63) The separation between peaks is given by

$$H^2 P \quad (116)$$

where P is the period of the oscillations. Figure 12 shows that the field at 20k gauss varies less than 40 gauss over 1 inch. Thus $1.0 \times 10^{-7} \text{ g}^{-1}$ is the smallest period observable. At 18 k gauss this is $\sim 7 \times 10^{-8} \text{ g}^{-1}$ over 1 inch. For tin the dominant period along [001] axis was $\sim 5.7 \times 10^{-7} \text{ g}^{-1}$ and was easily resolvable with emf probes about one inch apart. Oscillations of period $2.5 \times 10^{-7} \text{ g}^{-1}$ were observed. To observe even higher frequency oscillations the probes must be placed closer than 1 inch apart to get better homogeneity over the sample.

E. Thermometry

Temperature gradients across the sample were measured using an a-c wheatstone bridge and carbon resistors as temperature sensors (64). The relative geometry is shown in

Figure 12

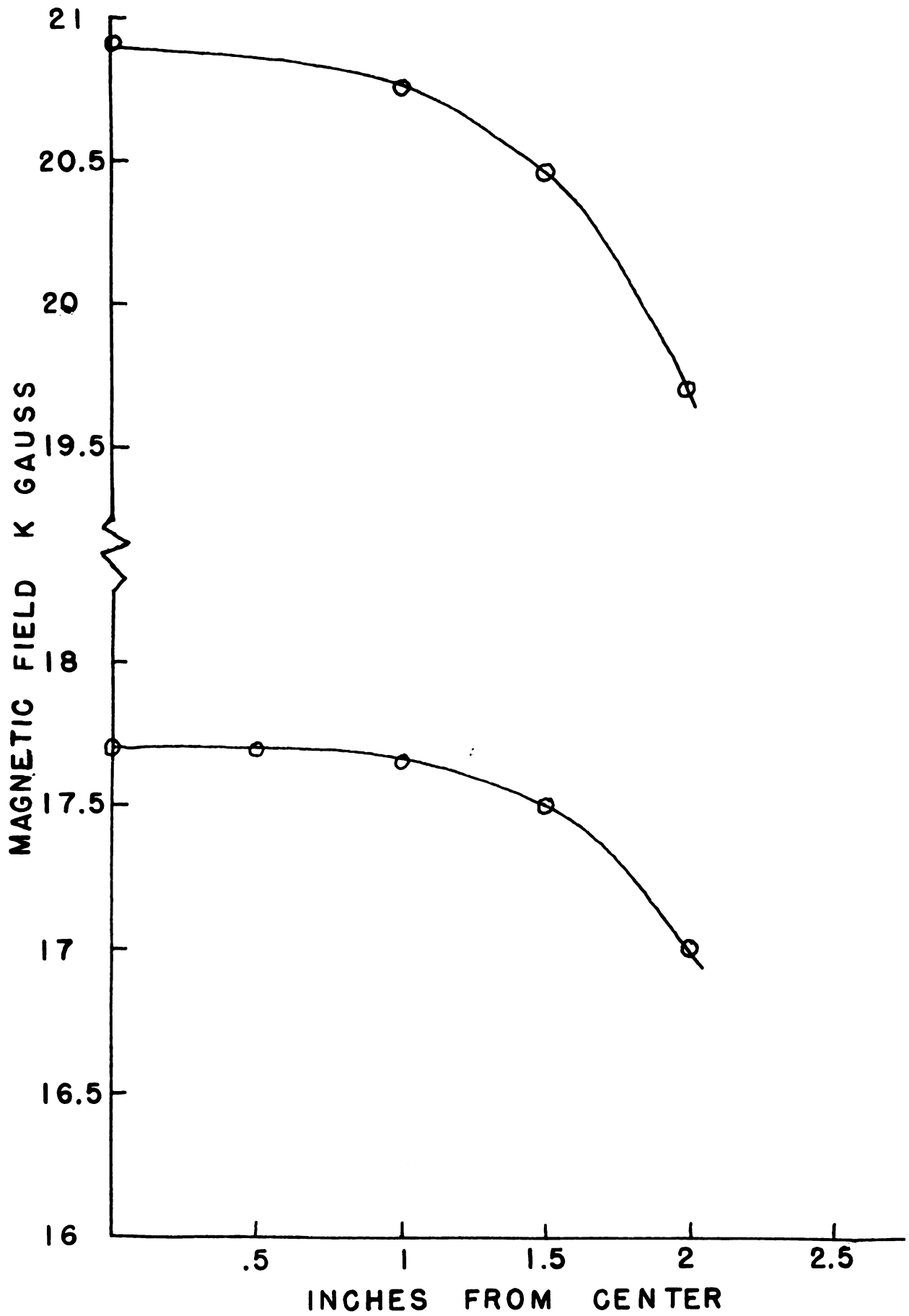
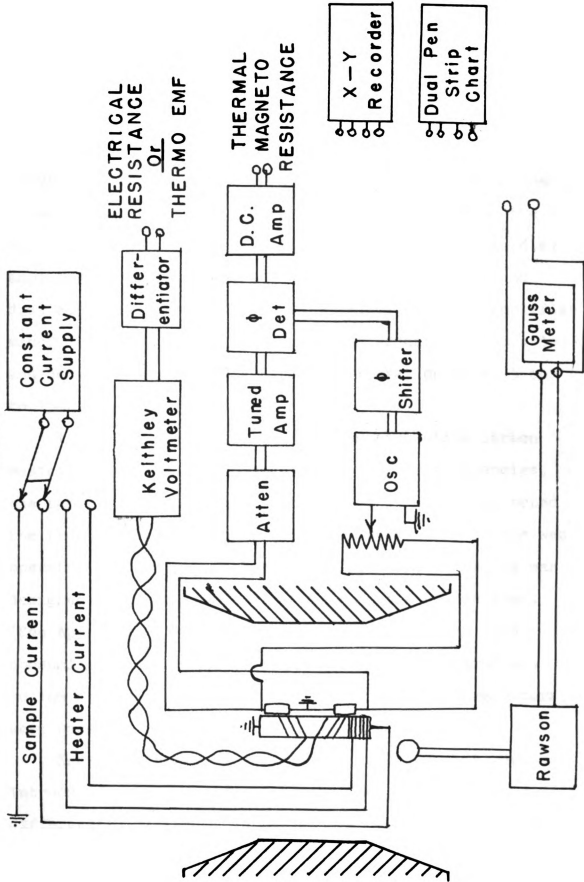


figure 13. The resistors were mounted directly over the emf leads and the heater was wound with manganin $33\Omega/\text{foot}$ alloy wire. In order to make magnetic fields produced by current in the heater negligible, six feet of wire was wound clockwise and the remaining six feet counterclockwise. The leads to the carbon resistors were Evenohm No. 36 wires⁽⁶⁵⁾. Evenohm has the feature of changing resistance by less than 1% in going from room temperature to 4.2° Kelvin. The resistors were mounted over insulating cigarette paper using GE 7031 varnish.

It was important to keep the insulation between leads, and between leads and ground, very large because the carbon resistors reached 20,000 ohms, and a large resistance could not be measured accurately if a shorting resistance of comparable magnitude existed. Usually this was greater than 10 Meg ohms, and was accomplished by having the Evenohm wire doubly Formvar insulated. The resistors were ground flat on both sides to aid making good thermal contact with the sample and reduce the heat capacity. This allowed them to follow temperature changes rapidly.

The a-c bridge and supporting electronics is represented schematically in figure 41. Essentially, an off-balance d.c. signal of the wheatstone bridge is caused by a temperature variation of the carbon resistors. This amplitude modulates the a.c. carrier signal from the

Figure 13



oscillator. The modulated signal is amplified outside the helium bath by an amplifier tuned to the carrier frequency. A second output from the oscillator, in phase with the carrier, is mixed with the modulated carrier. The mixer functions as a double-pole double-throw switch being driven at the oscillator frequency. The output from the mixer is the amplified d.c. off-balance signal from the bridge. This is further amplified by a conventional d.c. amplifier. The tuned amplifier, oscillator, mixer and d.c. amplifier are contained in a single "lock-in amplifier" manufactured by the Princeton Applied Research Corporation and designed for variable frequency operation from 15 cps to 1500 cps.

It was found that at low temperatures where carbon resistance values were large, and at higher frequencies, the capacitive reactance was significant. This distorted the true resistive output. For this reason the bridge was operated at 23 or 17 cycles per second. A new bridge was designed having variable capacitors in the bridge arms. (See Appendix) In practice it was difficult and time consuming to find the optimum capacitance to introduce, so low frequencies and low initial value carbon resistors were used.

Known resistances of .1, 1, 10, and 100 ohms were introduced into one side of the bridge. Thus a recorded differential variation in resistance was calibrated. The absolute value of temperature gradients was thus known, once each carbon resistor was calibrated.

The resistors were calibrated against the vapor pressure of the helium bath using mercury and oil manometers, and a McLeod gauge.

The carbon resistors follow an empirical formula quite well: (65)

$$\log_{10} R + \frac{K}{\log_{10} R} = A + \frac{B}{T} \quad (116)$$

This is usually approximated by

$$\log_{10} R = A + \frac{B}{T} \quad (117)$$

So

$$\frac{dR}{R} = \frac{-B}{T^2} dT \quad (118)$$

and for small changes, dR is proportional to dT .

Temperature gradients were sometimes too large to justify using (118). Each carbon resistor was therefore calibrated using (117), and temperature gradients measured knowing the resistance of each resistor.

The output of the lock-in-amplifier could be made proportional to the resistance of either of the carbon resistors. It could also be made proportional to ΔR , the difference in resistance between the two resistors. (See Appendix). When changes in the resistance were small (118) was valid, and the lock-in-amplifier output was proportional to ΔT . This was always true when looking at quantum oscillations.

As discussed earlier⁽⁸³⁾, ΔT is proportional to the y component of W_{ik} , where W_{ik} is the thermal resistivity tensor. The output of the lock-in-amplifier was therefore proportional to the thermal-magnetoresistance. It could be plotted continuously as a function of angle or field strength.

Since at low temperatures the thermal conductivity by electrons dominates over the conductivity by the lattice, the magnetic field dependence of the resistivity is completely analogous to the field dependence of the electrical resistivity. The thermal method has the very significant advantage of being free from field pickup in probe loops, and other noise problems inherent in d.c. electrical systems. The very narrow band pass amplifier of the a.c. method allows recovery of signals buried as low as 40 db in noise.⁽⁶⁶⁾

There are two main disadvantages of the thermal method. The first is that the system must be under a vacuum. Vacuum leaks are very troublesome. The second disadvantage is that the carbon resistors respond slowly. Rotations at fixed field and field sweeps had to be done slowly to insure that details were recorded.

F. Recording the Measurements

Three transport properties were measured. These were: the thermal magnetoresistance, the thermoelectric emf, and

the electrical magnetoresistance. Section V,C described the geometry for voltage measurements. Section V,E described the method of temperature gradient measurement.

The thermoelectric emf was measured between the twisted leads described in section C and resulted from a temperature gradient across the sample. A heater wound on the end of the sample as described in C, provided the temperature gradient. Thermoelectric measurements were made with a constant heat input.

The thermoelectric emf was measured by a Keithley 149 nanovoltmeter and recorded on a Mosley x-y recorder or a strip chart recorder.

Electrical magnetoresistance voltages were measured in the same way. In this case a constant d.c. current was provided by a Princeton Applied Research constant current supply. This maintained a constant current independent of load changes.

The magnetic field was swept linearly in time by an apparatus designed by J. LePage and a schematic is shown in the appendix. At times it got out of control because it was difficult to keep the output of the regulator zeroed. It would be worthwhile taking the output of the regulator, amplifying it and applying this to the input of the integrator. This would make regulation semi-automatic and relieve the operator to take care of writing numbers on graphs, etc.

A schematic of the measuring apparatus is shown in figure 13.

The thermal resistance and the thermoelectric emf were recorded simultaneously using the dual pen strip chart recorder. Field values were read directly from the Rawson gauss meter and recorded on the chart paper. Recording the thermal resistance oscillations and the thermoelectric oscillations simultaneously permitted a determination of their relative phase.

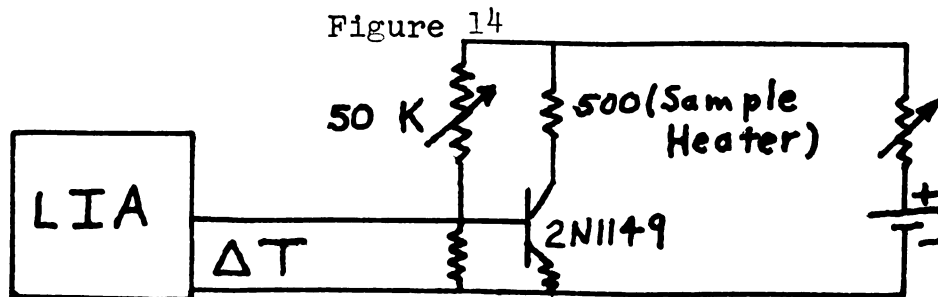
The Moseley x-y recorder was useful for observing the fine structure in data because its y axis is much larger than the y axis of the strip chart recorder. It was very useful for recording the oscillations occurring when the field was rotated at constant magnitude. However, the x-y recorder was not used for field sweeps when looking at oscillations because the oscillations needed to be spread out to be resolved.

The x-y recorder was used when looking at the thermal and electrical magnetoresistance in rotation at fixed field. It was also used at fixed angle to determine the gross field dependence of these transport properties. In this case the x axis was driven by the output of the Rawson gauss meter.

In rotation, angles were read off a pointer on the magnet and recorded by hand on the graph. Much of the labor of this method was later eliminated by recording the angles automatically every degree on one pen of the strip

chart recorder. The problem with this method was mentioned earlier; the strip chart was not wide enough to reveal all the desired details. A schematic of the automatic angle recording apparatus is shown in figure 42 .(67)

A method for measuring themopower directly was tried. The output of the lock-in-amplifier was used to control the bias on a power amplifier containing the heater current as shown in figure 14.



When the temperature difference across the sample tried to change, a voltage was applied to the transistor bias which increased or decreased the heater current. This did not work in earlier experiments because the sample temperature responded too slowly to the heater current changes. The response was fastest at 1° Kelvin when the emf leads were close together. With a bit of effort this could be made to work. Changes in \bar{H} would have to be quite slow . With ΔT a constant, $S = \frac{d \text{ emf}}{dT}$ is proportional to the emf output.

For looking at higher frequency oscillations, a differentiator was made. If the signal was

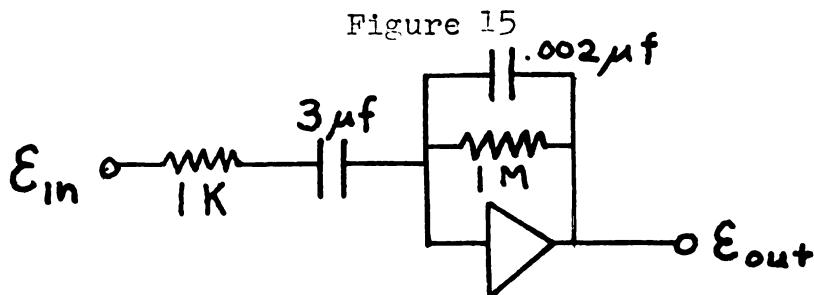
$$\delta = A_1 \cos \frac{2\pi F_1}{H} + A_2 \cos \frac{2\pi F_2}{H} \quad (119)$$

and δ was electronically differentiated then

$$\frac{d\delta}{dt} = \frac{\partial\delta}{\partial H} \frac{\partial H}{\partial t} = \text{constant} \times \frac{\partial\delta}{\partial H} \quad (120)$$

$$= A_1 \frac{2\pi F_1}{H^2} \sin \frac{2\pi F_1}{H} + A_2 \frac{2\pi F_2}{H^2} \sin \frac{2\pi F_2}{H}$$

If $F_1 \gg F_2$ the F_1 oscillation amplitude would be enhanced by the ratio of F_1 to F_2 . Higher frequencies would thus be emphasized. The circuit for this was:



The $1k\Omega$ resistor and $.002 \mu f$ eliminate the differentiation of very high frequency or pulse type signals.

$$e_{out} \simeq RC \frac{d E_{in}}{dt} = 3 \text{ sec} \times \frac{d E_{in}}{dt} \quad (121)$$

(121) gave an output signal large enough to drive the chart recorder when sweep rates were about 200 gauss per minute.

Because other experiments occupied most of the available time, differentiation was tried only once. The signal was rather noisy but one should be able to increase the

signal to noise ratio by increasing the value of the 1K resistor.

G. Field Modulation

The thermoelectric emfs in tin turned out to be very large. In fact, on one field sweep it was necessary to use the 100 volt scale on the Keithley voltmeter. Had these voltages not been so large, field modulation would have been used to observe them. Field modulation makes use of lock-in-amplifier (LIA) techniques to extract signals much below the noise level. Considerable preparation was made towards using this method, and this progress will be described.

The LIA output in field modulation thermoelectric experiments is proportional to the derivative of the emf with respect to field and is therefore ideally suited for studying quantum oscillations. These oscillations are nearly sinusoidal in H and the derivative is also sinusoidal with the same frequency.

The modulation coils used in preliminary experiments were designed in the Helmholtz configuration and mounted against the coils in the Harvey-Wells electromagnet. The a-c impedance when mounted in the magnet at 20 k gauss was 16 ohms. This value was found to be rather independent of field, as expected. Modulation was achieved using the oscillator output of the LIA amplified by a MacIntosh 30 watt power amplifier. The 16 ohm coil impedance was

matched by using the 16 ohm MacIntosh output terminals. Modulation amplitudes were measured using a pickup coil and oscilloscope. The peak to peak amplitude at zero d.c. field was 115 gauss. The amplitude was 125 gauss at 3 kgauss and decreased slowly as the field went up, reaching 100 gauss at 14 kgauss. Modulation was most effective below the saturation field of the magnet core.

The oscillating field creates a fluctuating thermoelectric emf in phase with the field. This emf is then mixed with the pure oscillator frequency and the LIA output is $\frac{d \text{ emf}}{dH}$. In addition, the oscillating field induces a.c. voltages of the same frequency in the emf leads. These $\frac{d\phi}{dt}$ oscillations would appear in the LIA output if it were not for the fact they were 90 degrees out of phase with the modulating field. If the field oscillated as

$$H_0 \cos \omega t \quad (122)$$

then

$$\frac{d\phi}{dt} = A \frac{dB}{dt} = H_0 \omega A \sin \omega t \quad (123)$$

and the cosine and sine are 90° out of phase. A is the cross sectional area and can be kept small by twisting the emf leads as described in section C.

Stark⁽⁶⁸⁾ showed that large amplitude field modulation was useful in separating de Haas - van Alphen

frequencies. Quantum oscillations vary as

$$\sin \frac{2\pi F}{H} \quad (124)$$

and with a modulating field this is

$$\sin \left(\frac{2\pi F}{H+H_0 \cos \omega t} \right) \quad (125)$$

H_0 is the amplitude of the modulation field. This can be written as

$$\simeq \sin \left[\frac{2\pi F}{H} \left(1 - \frac{H_0}{H} \cos \omega t \right) \right] \quad (126)$$

Seely⁽⁶⁹⁾ shows that this is

$$\begin{aligned} J_0 \sin \frac{2\pi F}{H} + 2 \sin \left(\frac{2\pi F}{H} \right) \sum_{h=1}^{\infty} (-1)^n J_{2n}(\delta) \cos 2n\omega t \\ - 2 \cos \left(\frac{2\pi F}{H} \right) \sum_{h=0}^{\infty} (-1)^n J_{2n+1}(\delta) \cos(2n+1)\omega t \end{aligned} \quad (127)$$

where

$$\delta = \frac{2\pi H_0 F}{H^2} \quad (128)$$

If detection on the LIA is done at the frequency ω , then all the remains of (127) is

$$- 2 \cos \left(\frac{2\pi F}{H} \right) J_1 \left(\frac{2\pi H_0 F}{H^2} \right) \cos \omega t \quad (129)$$

Seely⁽⁶⁹⁾ shows the zeros of the n^{th} Bessel functions J_n . The first zero of the $n = 1$ Bessel function is for $\delta = 3.882$. Therefore

$$H_0 = \frac{H^2 3.882}{2\pi F} \quad (130)$$

will make (129) equal to zero! For example, if H_0 is 60 gauss at 13 k gauss there will be no LIA output from the 3 δ section of the F-S. However, oscillation frequencies from other parts of the F-S will still be present and can be studied without interference from the large amplitude 3 δ oscillations.

Field modulation therefore has two distinct advantages over d.c. measurements. The use of LIA technique greatly improves signal to noise ratios. By picking modulation amplitudes, certain frequencies can be eliminated in order to study others.

Figure 16

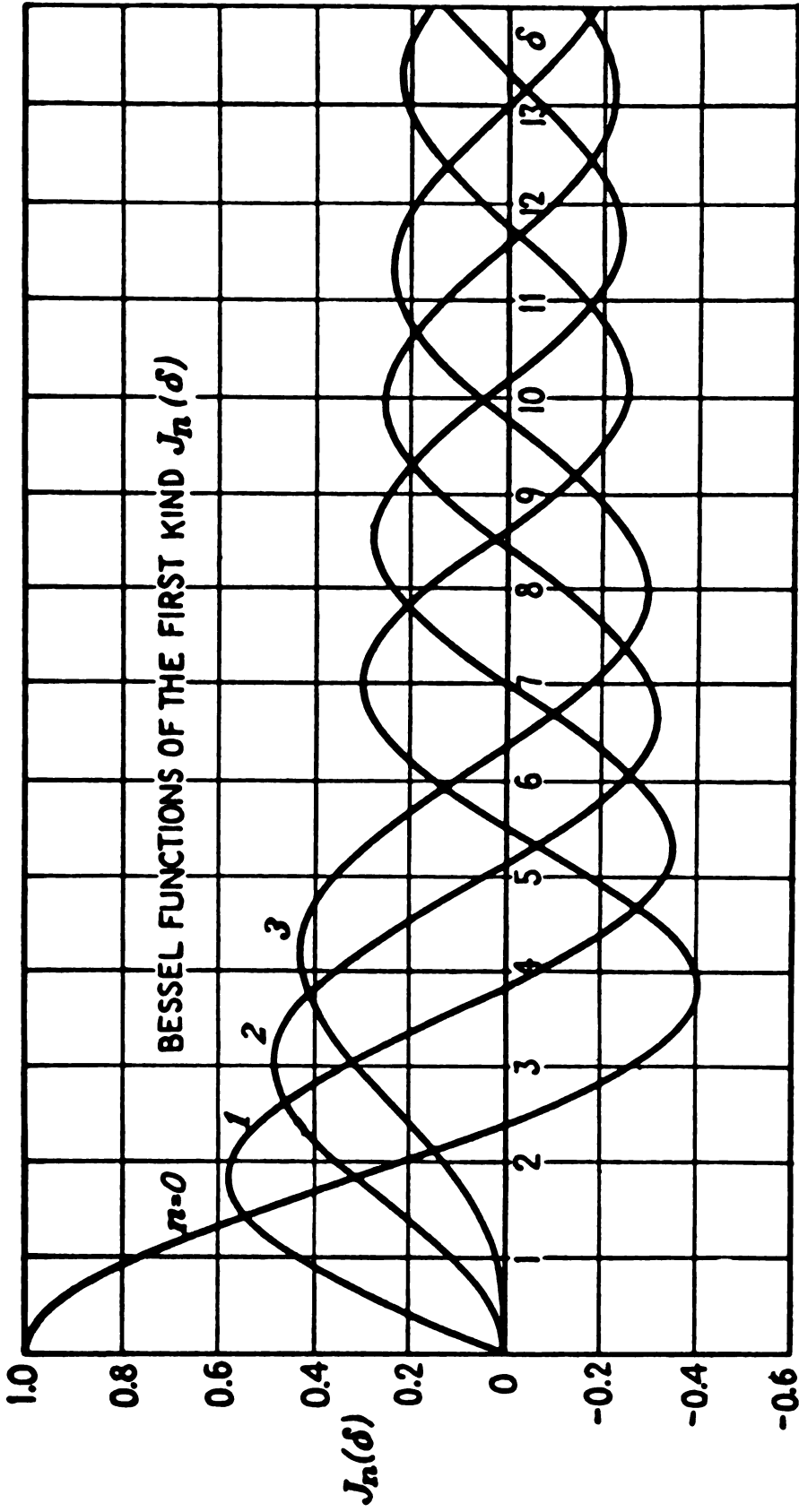


FIG. 19-3. Bessel functions of the first kind.

Reference 69

Figure 17

TABLE 19-1

ROOTS OF $J_n(\delta)$

$n = 0$	1	2	3	4	5
2.4048	3.882	5.135	6.379	7.586	8.780
5.520	7.016	8.417	9.760	11.064	12.339
8.654	10.173	11.620	13.017	14.373	15.700
11.792	13.323	14.796	16.224	17.616	18.982
14.931	16.470	17.960	19.410	20.827	22.220
18.071	19.616	21.117	22.583	24.018	25.431
21.212	22.760	24.270	25.749	27.200	28.628

Reference 69

1

VI Experimental Results ⁷⁴

A. Quantum Oscillations in the Thermoelectric Emf and Thermal Magnetoresistance

The tin single crystal referred to earlier as SnII was mounted with two different orientations with respect to the plane of rotation of the magnetic field as shown in figure 3. In position I the [001] axis was 11° , and [110] axis 4° out of the plane of \bar{H} . In position II, [001] was 16° , and [110] 7° out of the plane of rotation of \bar{H} . The crystal was in position I from August through October 7, and in II from then on.

A field sweep in position I is shown in figure 18. The magnetic field was swept slowly from 14.5 k gauss to 19.5 k gauss while a constant heat flow was maintained in the sample. The oscillations are in the thermoelectric emf, and recorded on an x-y recorder. The sweep was made with the field fixed at 22° from the closest approach to the [001] axis. The oscillations are periodic in $\frac{1}{H}$ as shown in figure 19. n is an integer corresponding to a peak position at field H .

$$\text{emf amplitude} \sim \sin \frac{2\pi}{PH} \quad (131)$$

which is a maximum when

$$\frac{2\pi}{PH} = 2\pi n \quad (132)$$

The measured period was found from:

$$P = \frac{d\left(\frac{1}{H}\right)}{dn} = 5.4 \times 10^{-7} \text{ gauss}^{-1} \quad (133)$$

Figure 18

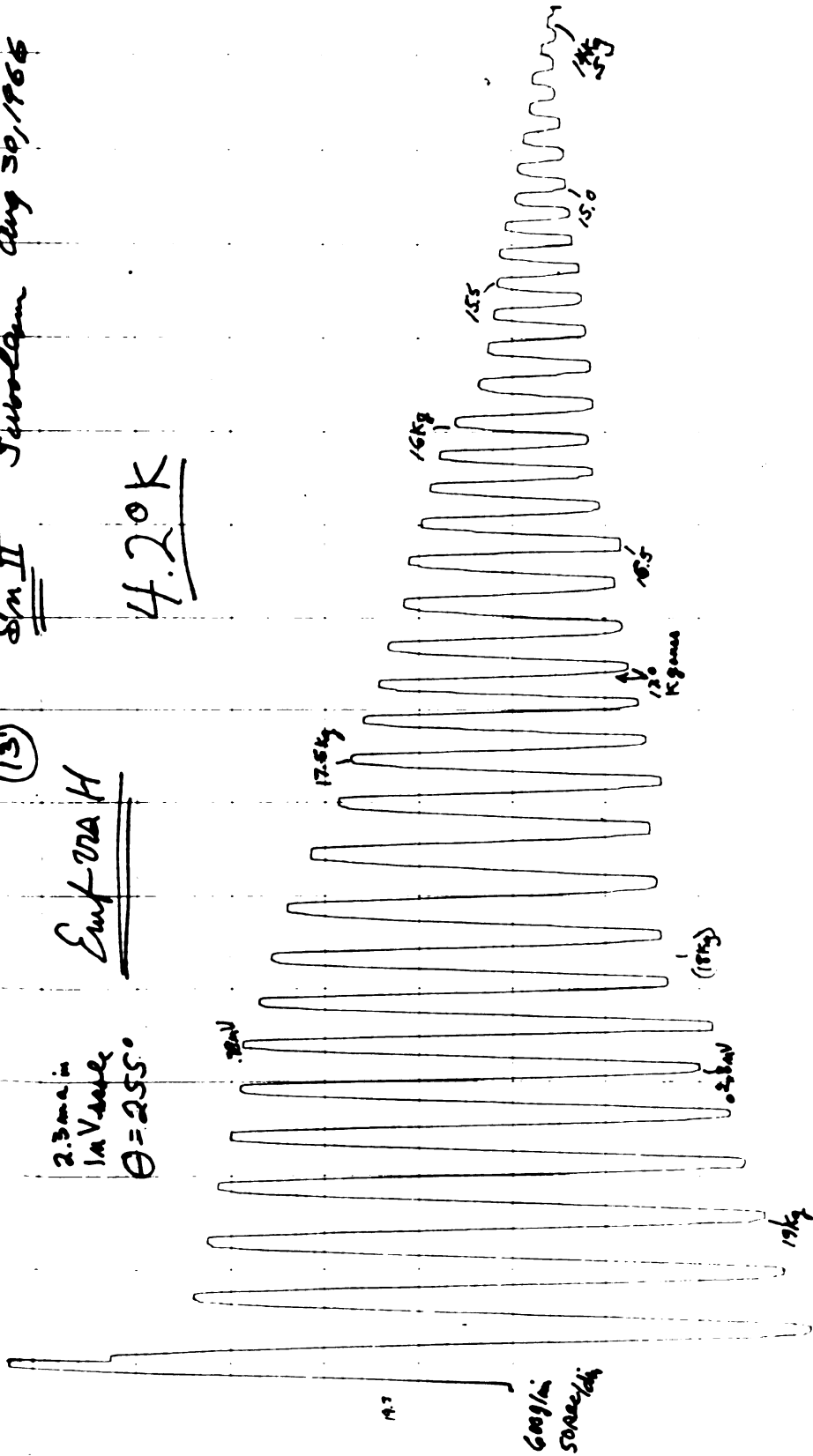
Sn II Subolgan Aug 30, 1966

4.20K

(13)

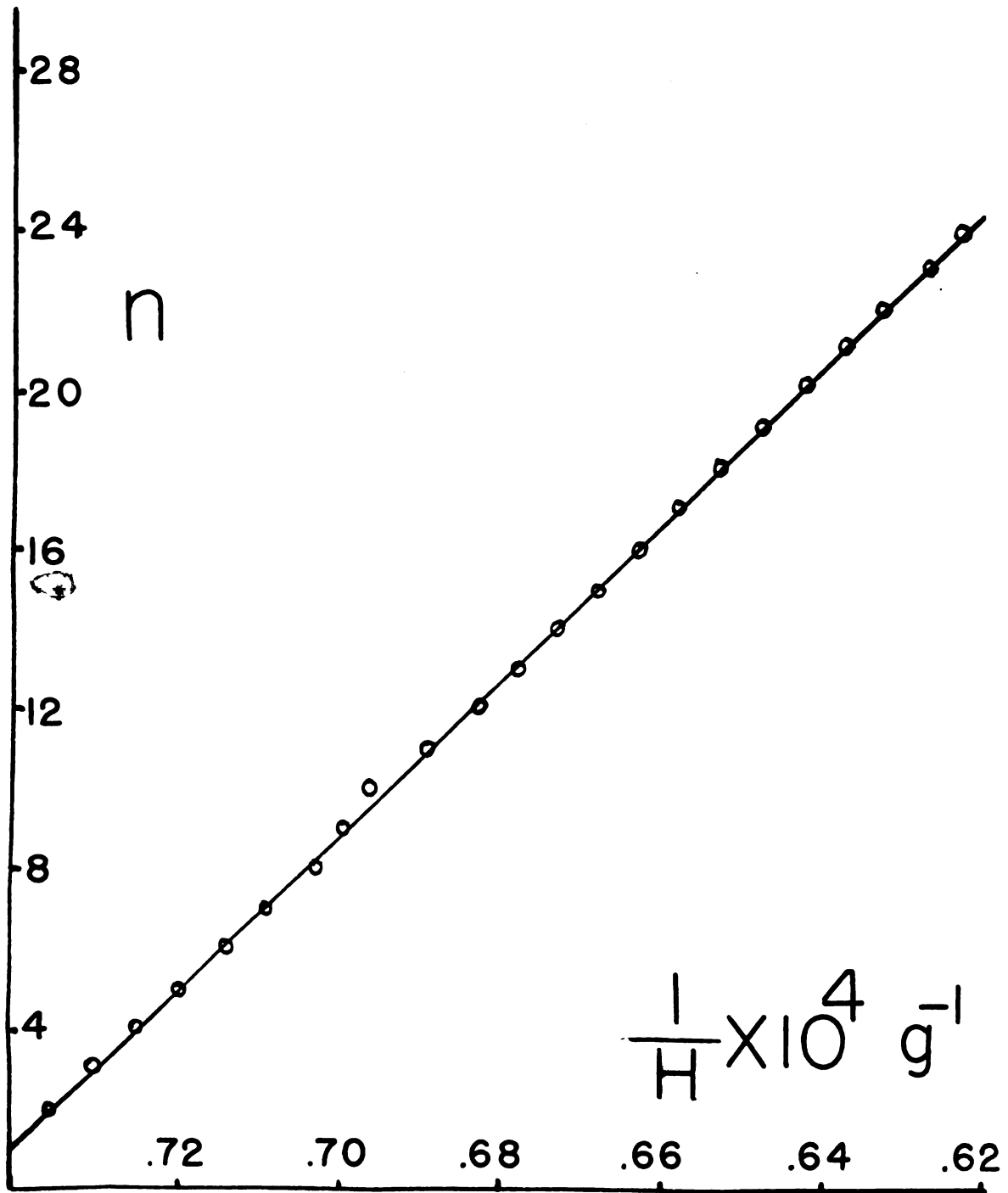
Emf-02A H

2.3 mA in
1M V scale
 $\theta = 255^\circ$



scat 18K = 0.42 mV

Figure 19



Using (132) this means that at 19 k gauss:

$$n = \frac{1}{5.4 \times 10^{-7} \times 19,000} \sim 100 \quad (134)$$

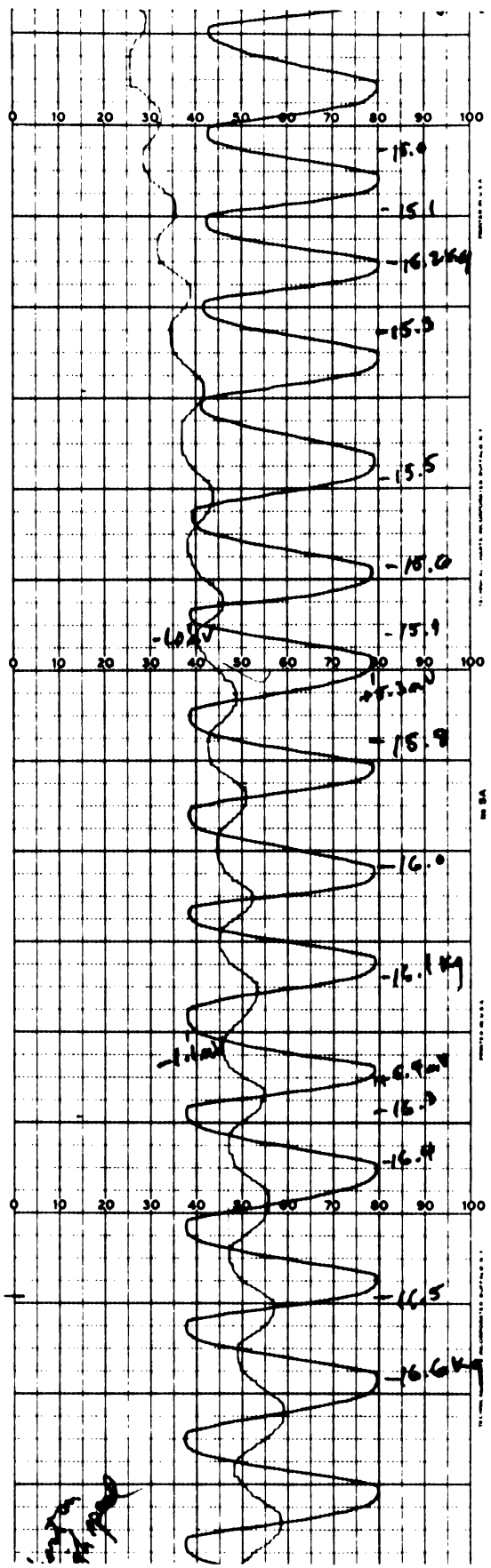
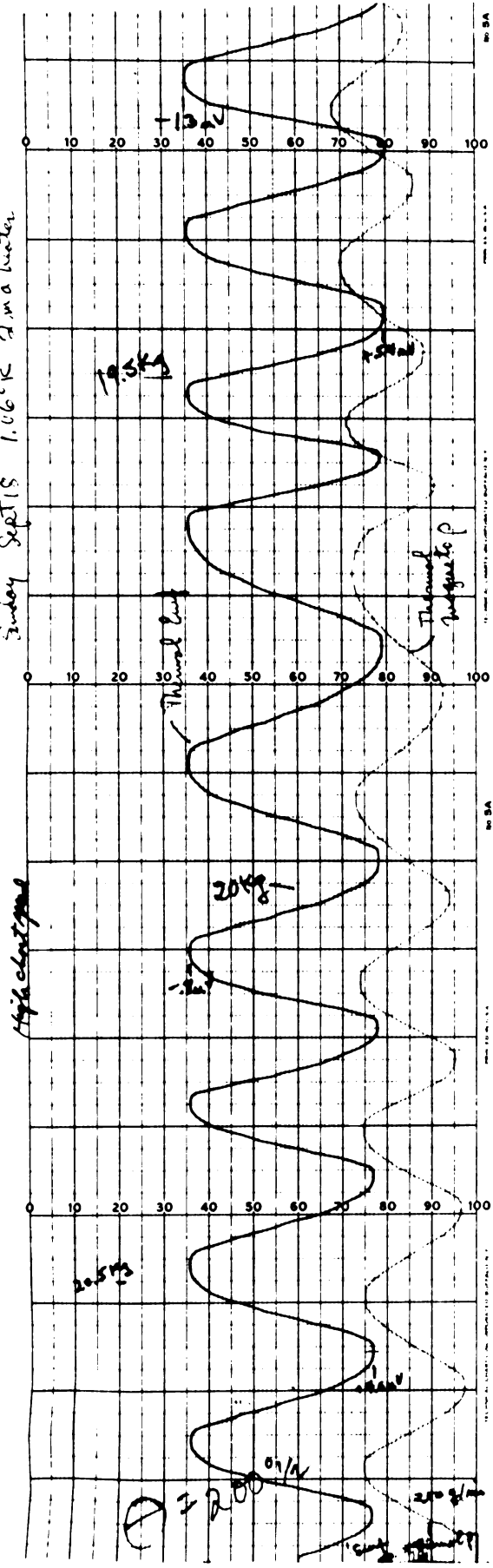
Therefore, 100 quantum levels remain below the Fermi energy at 19 k gauss, and the approximations of $n \gg 1$ used earlier are justified. Notice that the oscillations are very large even at a temperature of 4.2°K . At 19 k gauss the thermoelectric power oscillations have an amplitude of about $1 \mu\text{V}$ per $^\circ\text{K}$.

Many sweeps were made at various angles. Usually the thermoelectric emf and the thermal magnetoresistance were plotted simultaneously on a strip chart recorder. Figure 20 shows a typical field sweep for crystal position I. The upper half is at higher fields than the lower, and shows that the oscillations are not quite sinusoidal, indicating that higher harmonics of the fundamental are present. The oscillations are not spaced evenly because it was difficult to keep the sweep rate constant and to monitor both oscillations simultaneously. The bottom half shows the thermal magnetoresistance oscillations diminishing in amplitude more rapidly than the thermoelectric oscillations.

The thermal magnetoresistance oscillations are superimposed on a large slowly varying field dependent term as is apparent in lower half of figure 20. The thermoelectric oscillations, however, have little monotonic

Figure 20

July Sept 15 1.06°C 2.1 m water



field dependence and the oscillations are positive and negative. In this particular sweep the oscillations in thermoemf were seen from 20 k gauss to 4.5 k gauss and a total of 370 oscillations observed. In figure 20 the thermal magnetoresistance oscillations were not observable below 7 k gauss. For field directions where the thermoelectric oscillations were very weak, oscillations in the thermal magnetoresistance could not be seen.

Most oscillatory quantities are superimposed on large monotonic field dependent backgrounds. Such is the case for the thermal magnetoresistance oscillations. The thermoelectric emf oscillations are unique in being alternately positive and negative. This factor makes period and amplitude determination relatively easy, and is an advantage of this technique.

Figure 21 (b) shows emf vs. H for H 18° from the closest approach to the [001] axis. For this direction a higher frequency oscillation is clearly visible. Higher frequency oscillations were seen in a range of ± 16 degrees from the closest approach to [001]. The reason for this will be explained later. Only one frequency was seen in the thermal magnetoresistance.

Figure 22 shows how the oscillation periods varied as a function of the distance from the closest approach to the [001] direction for crystal position II. Both the low and high frequency oscillations agree with the data

Figure 21



(b)

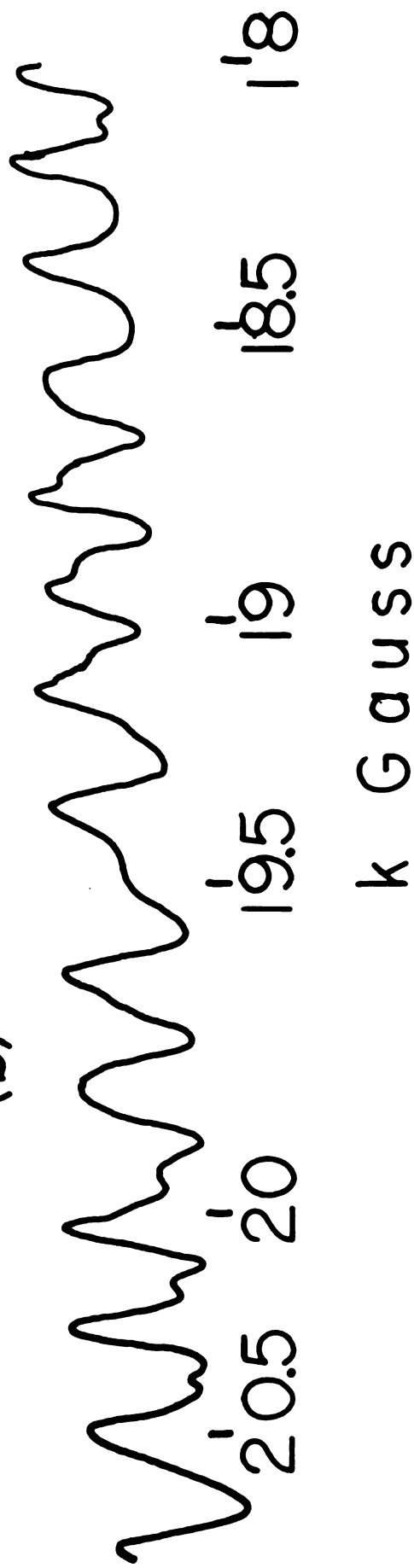
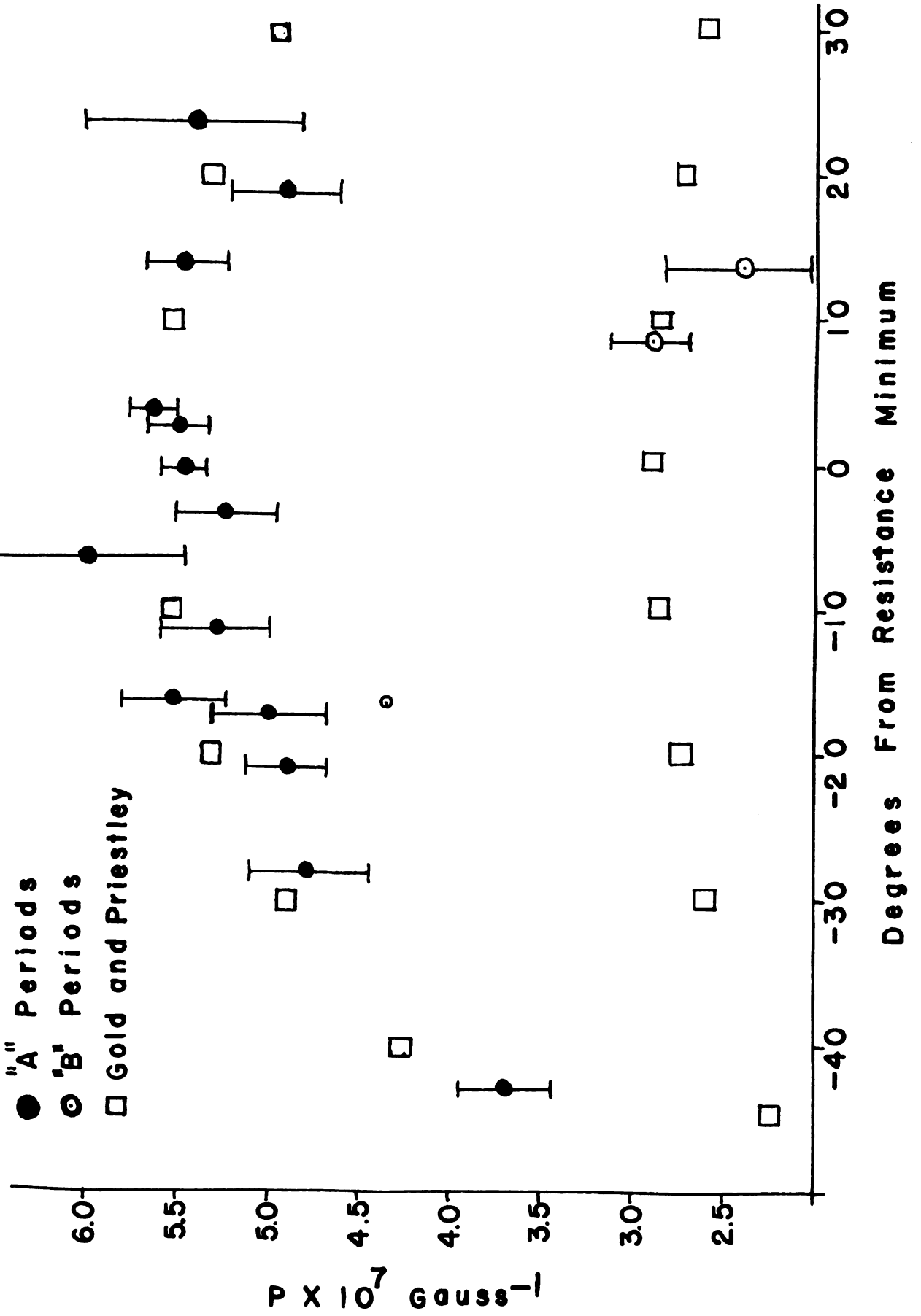


Figure 22



found in pulsed field de Haas - van Alphen effect by Gold and Priestley⁽⁷⁰⁾, and the field modulation experiments of Stafleu and de Vroomen⁽⁷¹⁾. The origin of these oscillations will be discussed in a later section.

B. Quantum Oscillations in the Thermoelectric Emf when Rotating at Constant Field Strength

Figure 23 shows quantum oscillations when the field is rotated through 180° at 21 k gauss. The direction marked 0 on the graph corresponds approximately with the direction of closest approach to the [001] direction.

Figure 24 shows the same rotation oscillations at a slower speed and over less than one half of the angle of figure 23. At $\theta = 240$ degrees a higher frequency oscillation is clearly visible. Details of this part of the rotation are displayed in figure 21 (a).

Oscillations occur in rotation because the cross sectional area of the F-S perpendicular to the field is dependent on field direction. At certain orientations there are more cylinders occupied by quantized electrons than at others. In rotating from one direction to another cylinders pass through the F-S causing oscillations.

$$\text{amplitude} \sim \sin \frac{2\pi f(\theta)}{PH} \quad (135)$$

is a maximum when

$$\frac{f(\theta)}{PH} = n \quad (136)$$

Figure 23

Emf

⑤ 10K Sept 18, 1966

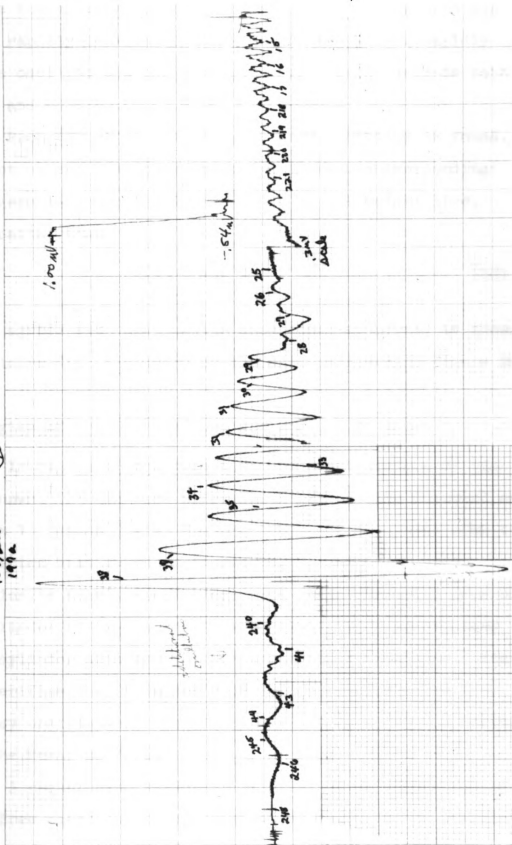
Sept 18

2000
1000
500
250
125
62.5
31.25
15.625
7.8125
3.90625
1.953125
0.9765625
0.48828125
0.244140625
0.1220703125
0.06103515625
0.030517578125
0.0152587890625
0.00762939453125
0.003814697265625
0.0019073486328125
0.00095367431640625
0.000476837158203125
0.0002384185791015625
0.00011920928955078125
0.000059604644775390625
0.0000298023223876953125
0.00001490116119384765625
0.000007450580596923828125
0.0000037252902984619140625
0.00000186264514923095703125
0.000000931322574615478515625
0.0000004656612873077392578125
0.00000023283064365386962890625
0.000000116415321826934814453125
0.0000005820766091294674072265625
0.00000029103830456473370361328125
0.000000145519152282366851806640625
0.0000000727595761411834259033203125
0.00000003637978807059171295166015625
0.000000018189894035295856475830078125
0.0000000090949470176479282379150390625
0.00000000454747350882396411895751953125
0.000000002273736754411982059478759765625
0.0000000011368683772059910297393798828125
0.00000000056843418860299551486968994140625
0.000000000284217094301497757434844970703125
0.0000000001421085471507488787172224853515625
0.0000000000710542735753744393586112426778125
0.00000000003552713678768721967930562133890625
0.000000000017763568393843609839652810669453125
0.0000000000088817841969218049198264053347265625
0.0000000000044408920984609024599132026673828125
0.00000000000222044604923045122995660133369140625
0.000000000001110223024615225614978300666845703125
0.0000000000005551115123076128074891503333428515625
0.000000000000277555756153806403744575166671428125
0.0000000000001387778780769032018722875833357140625
0.0000000000000693889390384516009361437916678515625
0.000000000000034694469519225800468071895833428125
0.00000000000001734723475961290023403594791667140625
0.00000000000000867361737980645011701797395833428125
0.0000000000000043368086899032250585089869791667140625
0.0000000000000021684043449516125292544934895833428125
0.000000000000001084202172475806264627246744791667140625
0.000000000000000542101086237903132313623372395833428125
0.0000000000000002710505431189515611561168619791667140625
0.0000000000000001355252715594757805780584309895833428125
0.000000000000000067762635779737890289029215494791667140625
0.000000000000000033881317889868945144514607747395833428125
0.0000000000000000169406589449344725722573038719791667140625
0.0000000000000000084703294724672362861365168895833428125
0.00000000000000000423516473623361814306825944791667140625
0.00000000000000000211758236811680907150342972395833428125
0.0000000000000000010587911840584045357517148619791667140625
0.0000000000000000005293955920292022678758574309895833428125
0.000000000000000000264697796014601133937928719791667140625
0.000000000000000000132348898007300566968964359895833428125
0.00000000000000000006617444900365028348448217994791667140625
0.00000000000000000003308722450182514174224108997395833428125
0.0000000000000000000165436122509125708711205449969791667140625
0.00000000000000000000827180612545628543556027249934791667140625
0.000000000000000000004135903062728142717780136249969791667140625
0.0000000000000000000020679515313640713588900681249934791667140625
0.00000000000000000000103397576568203567944503406249969791667140625
0.000000000000000000000516987882841017839722517031249934791667140625
0.000000000000000000000258493941420508919861125156249969791667140625
0.0000000000000000000001292469707102544599305625781249934791667140625
0.0000000000000000000000646234853551272299652812895833428125
0.0000000000000000000000323117426775636149827640644791667140625
0.0000000000000000000000161558713387818074913820322395833428125
0.000000000000000000000008077935669390903745691016119791667140625
0.000000000000000000000004038967834695451872845508059895833428125
0.00000000000000000000000201948391734772593642275402994791667140625
0.0000000000000000000000010097419586738629682113770149934791667140625
0.00000000000000000000000050487097933693148410568850749969791667140625
0.000000000000000000000000252435489668465742052844253749934791667140625
0.0000000000000000000000001262177448342328710264221268749969791667140625
0.000000000000000000000000063108872417116435513211063439934791667140625
0.000000000000000000000000031554436208558217756605531719969791667140625
0.000000000000000000000000015777218104279108878302765859934791667140625
0.0000000000000000000000000078886090521395544391513829279969791667140625
0.0000000000000000000000000039443045260697772195756914639934791667140625
0.0000000000000000000000000019721522630348886097887847319969791667140625
0.0000000000000000000000000009860761315174443048943923659934791667140625
0.0000000000000000000000000004930380657587221524471961829969791667140625
0.00000000000000000000000000024651903287936107622359809149934791667140625
0.000000000000000000000000000123259516439680538111799045749969791667140625
0.0000000000000000000000000000616297582198402690558995228749934791667140625
0.000000000000000000000000000030814879109920134527949761439969791667140625
0.000000000000000000000000000015407439554960067263974880719934791667140625
0.000000000000000000000000000007703719777480033631987440359969791667140625
0.000000000000000000000000000003851859888740016815993720179934791667140625
0.000000000000000000000000000001925929944370008407996860089969791667140625
0.0000000000000000000000000000009629649721850004203998300449934791667140625
0.00000000000000000000000000000048148248609250021019991502249969791667140625
0.000000000000000000000000000000240741243046250105099957511249934791667140625
0.00000000000000000000000000000012037062152312500525499787556249969791667140625
0.0000000000000000000000000000000601853107615625002627498937781249934791667140625
0.00000000000000000000000000000003009265538078125001313749468891249969791667140625
0.000000000000000000000000000000015046327690390625000656874734445749934791667140625
0.00000000000000000000000000000000752316384519531250003284373672228749969791667140625
0.0000000000000000000000000000000037615819225976562500016421868361149934791667140625
0.00000000000000000000000000000000188079096129878125000082109341805749969791667140625
0.0000000000000000000000000000000009403954806493906250000410546709028749934791667140625
0.000000000000000000000000000000000470197740324695312500002052733545139969791667140625
0.0000000000000000000000000000000002350988701623476562500001026366772559849934791667140625
0.00000000000000000000000000000000011754943508117382812500000513183386279969791667140625
0.000000000000000000000000000000000058774717540586914062500000256591693139934791667140625
0.0000000000000000000000000000000000293873587702934572812500000128295846569969791667140625
0.000000000000000000000000000000000014693679385146728640625000000641479232849934791667140625
0.00000000000000000000000000000000000734683969257336432031250000003207396164249969791667140625
0.00000000000000000000000000000000000367341984628668216101562500000016036980821249934791667140625
0.0000000000000000000000000000000000018367099231433410805078125000000080184904106249969791667140625
0.000000000000000000000000000000000000918354961571670540253906250000000400924520531249934791667140625
0.00000000000000000000000000000000000045917748078583527012695312500000002004622602656249969791667140625
0.0000000000000000000000000000000000002295887403929176350634765625000000010023113013281249934791667140625
0.0000000000000000000000000000000000001147943701964588175316738281250000000050115565066406249969791667140625
0.000000000000000000000000000000000000057397185098229408765836914062500000000250577825332031249934791667140625
0.0000000000000000000000000000000000000286985925491147043829174572812500000000125288912666106249969791667140625
0.000000000000000000000000000000000000014349296274557352191458738640625000000000626444563330531249934791667140625
0.00000000000000000000000000000000000000717464813727867609572436932031250000000003132222816652656249969791667140625
0.0000000000000000000000000000000000000035873240686393380478621846610625000000000156611140832781249934791667140625
0.000000000000000000000000000000000000001793662034319669023931092330531250000000000783055704163906249969791667140625
0.00000000000000000000000000000000000000089683101715983451196554616526562500000000003915278520819531249934791667140625
0.000000000000000000000000000000000000000448415508579917255982780827630625000000000019576392604097656249969791667140625
0.0000000000000000000000000000000000000002242077542899586279913904138153125000000000009788196302048781249934791667140625
0.00000000000000000000000000000000000000011210387714497931399569520690765625000000000004894098151024386406249969791667140625
0.00560519385724896569978476034537812500000000000244704907551219281249934791667140625
0.002802596928624482849892380172689062500000000001223524537756096406249969791667140625
0.0014012984643122414249461900863445312500000000006117622688780482031249934791667140625
0.000700649232156120712473095043172265625000000000305881134439024106249969791667140625
0.0003503246160780603562365475215861281250000000001529405672195120531249934791667140625
0.000175162308039030178118273760793062500000000007647028360975602656249969791667140625
0.00875811540195150890591368803965312500000000038235141804878013281249934791667140625
0.004379057700975754452956844019791667140625000000000191175709024390066406249969791667140625
0.002189528850487877226478422009895833428125000000000955878545121950332031249934791667140625
0.00109476442524393861323921100494791667140625000000000477939272560975166106249969791667140625
0.00054738221262196930661960550247395833428125000000002389696362804875830531249934791667140625
0.00027369110631098465330980275123697916671406250000000011948481814024379166714062500000000059742409070121895833428125
0.00013684555315549232665490137561848958334281250000000059742409070121895833428125000000002987120453506094791667140625
0.006842277657774616332745068780924791667140625000000002987120453506094791667140625000000001493560226753047395833428125
0.00342113882888730816637253439046197916671406250000000014935602267530473958334281250000000074678011337652369791667140625
0.001710569414443654083186267195230989583342812500000000746780113376523697916671406250000000037339005668826184895833428125
0.000855284707221827041593133597615494791667140625000000003733900566882618489583342812500000000186695028344130924791667140625
0.00042764235361091352299656798807749934791667140625000000001866950283441309247916671406250000000093347514172064895833428125
0.0002138211768054567614982839940387499697916671406250000000093347514172064895833428125000000004667375708603244791667140625
0.0001069105884027283807499141997019499347916671406250000000046673757086032447916671406250000000023336878543016224791667140625
0.00534552942013641903749570998509749969791667140625000000002333687854301622479166714062500000000116684392715081124791667140625
0.002672764710068209518747854994254899347916671406250000000011668439271508112479166714062500000000583421963575405624791667140625
0.0001336382355034104758939274997127499697916671406250000000058342196357540562479166714062500000000291710981787702

Figure 24

⑨ Oct 10 1.240K

(m.a) (4V scale)
5V/div
1979



Since the argument of the sin is a large number, the sin is a rapidly oscillating function of $f(\theta)$. How rapidly these oscillations occur at any given field, depends both on P and on $f(\theta)$.

From figure 24 the angle of peak positions is found. A plot of $\sec \theta$ at peak positions against corresponding integers is shown in figure 25, to be a straight line, indicating that

$$f(\theta) = \sec \theta \quad (137)$$

This agrees with the angular dependence of period as shown in figure 22. A summary of the data is given in figure 26.

C. Origins of the Oscillations and the F-S of Tin

In figure 27 the free electron Fermi surface of tin is shown. (70) In zone three the δ orbits have a period of $5.7 \times 10^{-7} \text{ gauss}^{-1}$ with H along $[001]$. This agrees with the corrected best curve in figure 22. In addition, this section is nearly a cylinder. The cross sectional area of a cylinder varies as $\sec \theta$, where θ is the angle between the cylinder axis and the perpendicular to the area. Figure 25 verifies that this $\sec \theta$ is followed and the low frequency oscillations therefore originate from the 3δ section of the Fermi surface.

A recent band structure calculation by Weisz changes the free electron picture drastically, but the 3δ section

Figure 25

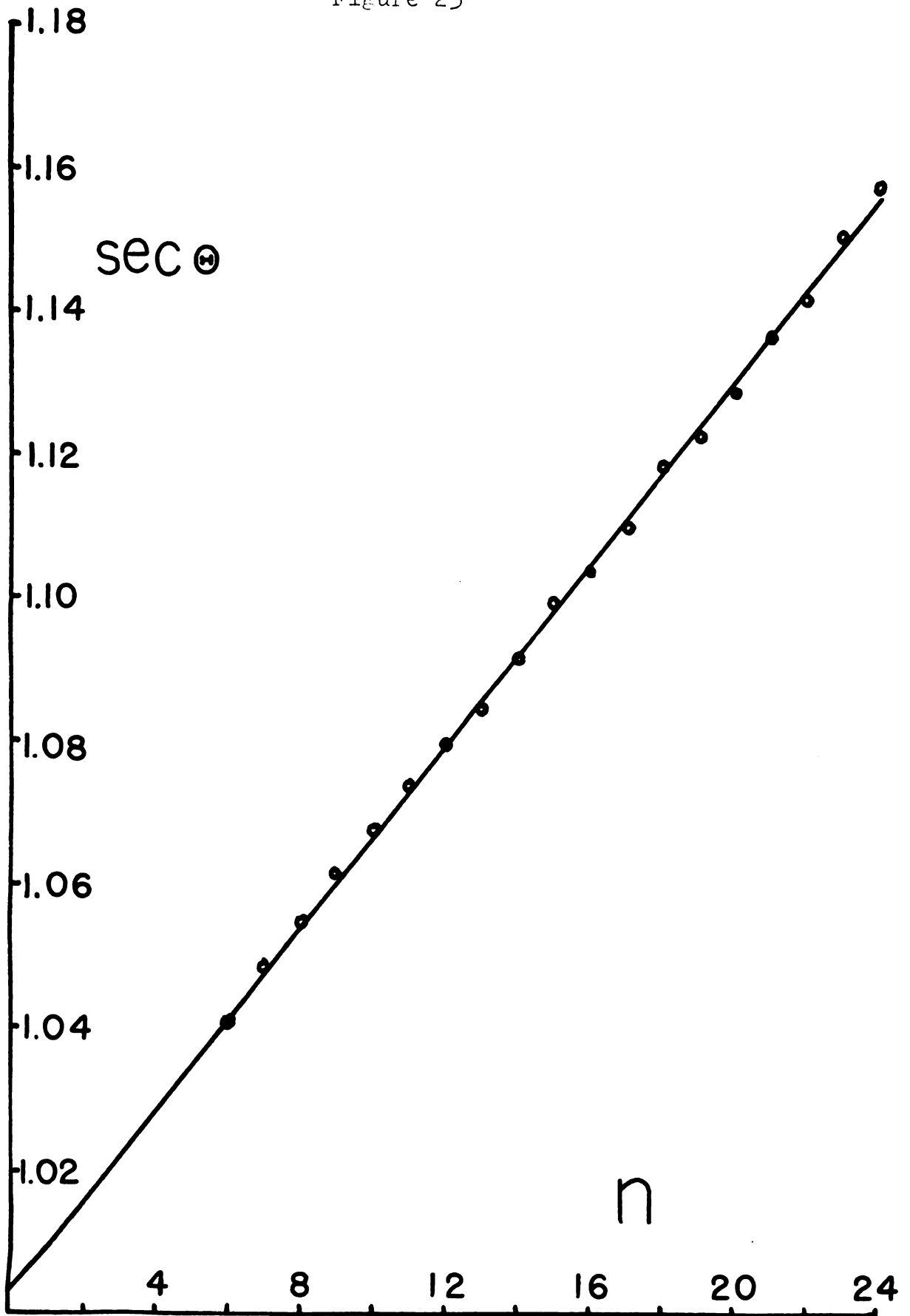


Figure 26

Summary of Frequency DataAugust 30 ([110] axis 4° , and [001] 11° , out of plane of \bar{H})

<u>θ</u>	<u>degrees from resistance minimum</u>	<u>Measured Period X 10^7 g$^{-1}$</u>	<u>Comments</u>
255 $^\circ$	up 22 $^\circ$	5.3 \pm .3	used x-y recorder
255	up 22 $^\circ$	5.3 \pm .3	"
76 $^\circ$	up 23 $^\circ$	5.1 \pm .2	"
76 $^\circ$	up 23 $^\circ$	5.1 \pm .2	"

September 15 ([110] axis 4° , and [001] 11° , out of plane of \bar{H})

340 $^\circ$	down 18 $^\circ$	4.4 \pm .2	oscillation in thermal magne- toresistance
340 $^\circ$	down 18 $^\circ$	4.9 \pm .4	thermo emf

September 18 ([110] axis 4° , and [001] 11° , out of plane of \bar{H})

200.5 $^\circ$	up 24.5 $^\circ$	5.2 \pm .1	
----------------	------------------	--------------	--

September 25 ([110] axis 4° , and [001] 11° , out of plane of \bar{H})

249	- 55 $^\circ$	4.8 \pm .1	
-----	---------------	--------------	--

October 10 ([110] is 7° and [001] is 16° out of plane of \bar{H})

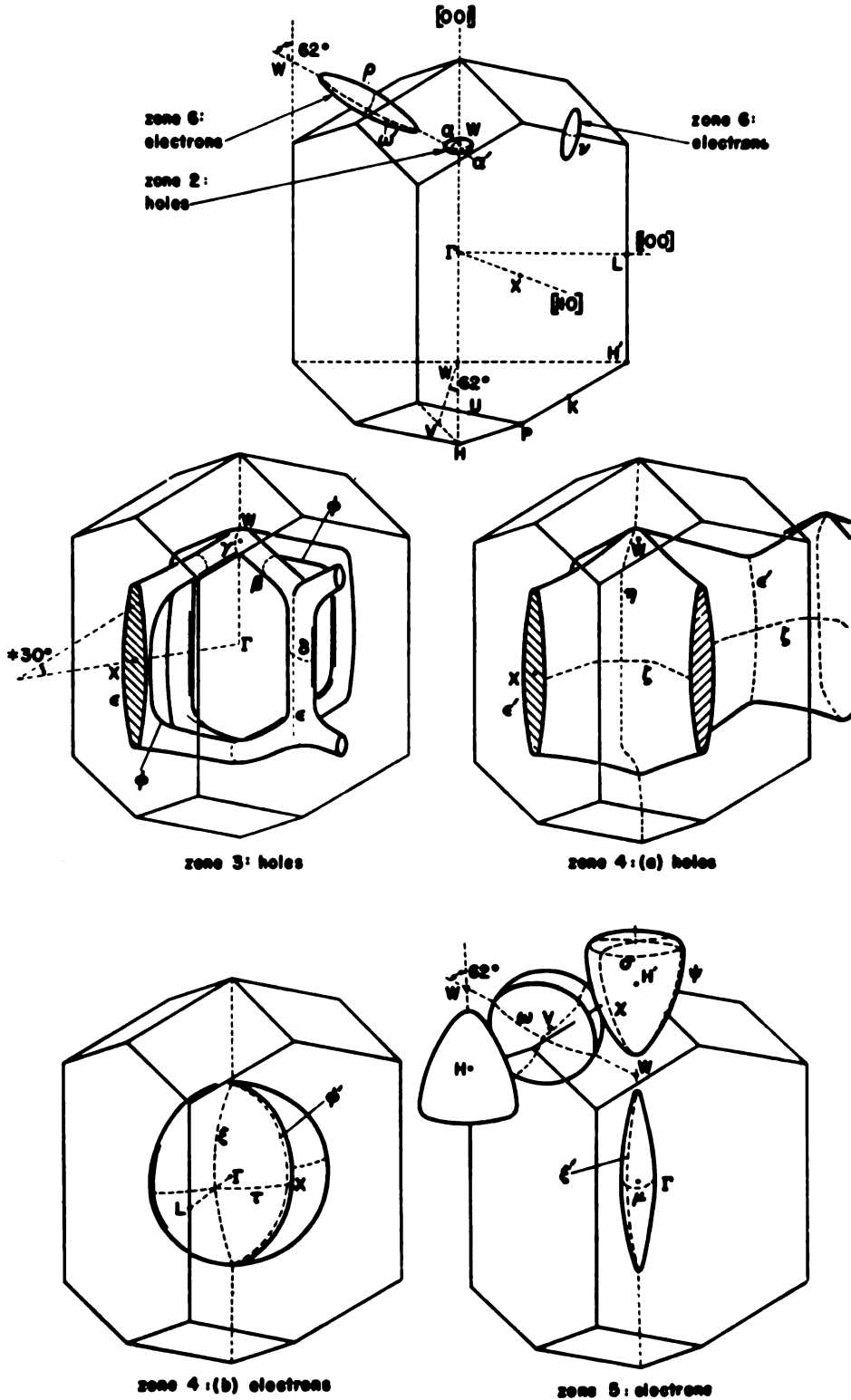
<u>θ</u>	<u>degrees from resistance minimum</u>	<u>measured period X 10^7</u>	<u>Comments</u>
237 $\frac{1}{2}$	down 20.5	$4.9 \pm .2$	strong oscillation is thermal resis- tance
241	down 17	$5.0 \pm .3$	two frequencies present, no resis- tance oscillations
255	down 3°	$5.3 \pm .1$	no resistance oscillations
261	up 3°	$5.5 \pm .1$	no resistance oscillations
215	down 43°	$3.7 \pm .3$	no resistance oscillations
230	down 28°	$4.8 \pm .3$	

October 26 ([110] axis is 7° and [001] is 16° out of plane
of \bar{H})

240	down 16°	$5.66 \pm .05$	no thermal resis- tance oscillations
240	down 16°	$4.4 \pm .4$	
245	down 11°	$5.3 \pm .3$	two frequencies, no thermal resis- tance oscillations
250	down 6°	$6.0 \pm .5$	"
256	zero	$5.45 \pm .03$	large thermal resistance oscillations
260	up 4°	$5.64 \pm .04$	large thermal resistance oscillations

265	up 9°	2.9 ± .2	two frequencies, no thermal resistance oscillations
270	up 14°	5.48 ± .08	two frequencies, no thermal resistance oscillations
270	up 14°	2.4 ± .2	strong mixing of frequencies
275	up 19°	4.9 ± .2	no thermal resistance oscillations
280	up 24	5.4 ± .6	strong thermal resistance oscillations

Figure 27



The free-electron Fermi surface in the reduced-zone scheme. The principal dimensions of the zone are:

$$\Gamma L = \frac{2\pi}{a}, \quad \Gamma X = \frac{1}{2} \left(\frac{2\pi}{a} \right), \quad \Gamma W = LH = \frac{1}{2} \left(\frac{a}{c} - \frac{c}{a} \right) \left(\frac{2\pi}{a} \right), \quad WH = \left(\frac{c}{a} \right) \left(\frac{2\pi}{a} \right),$$

where $a = 5.82 \text{ \AA}$ and $c = 3.18 \text{ \AA}$.

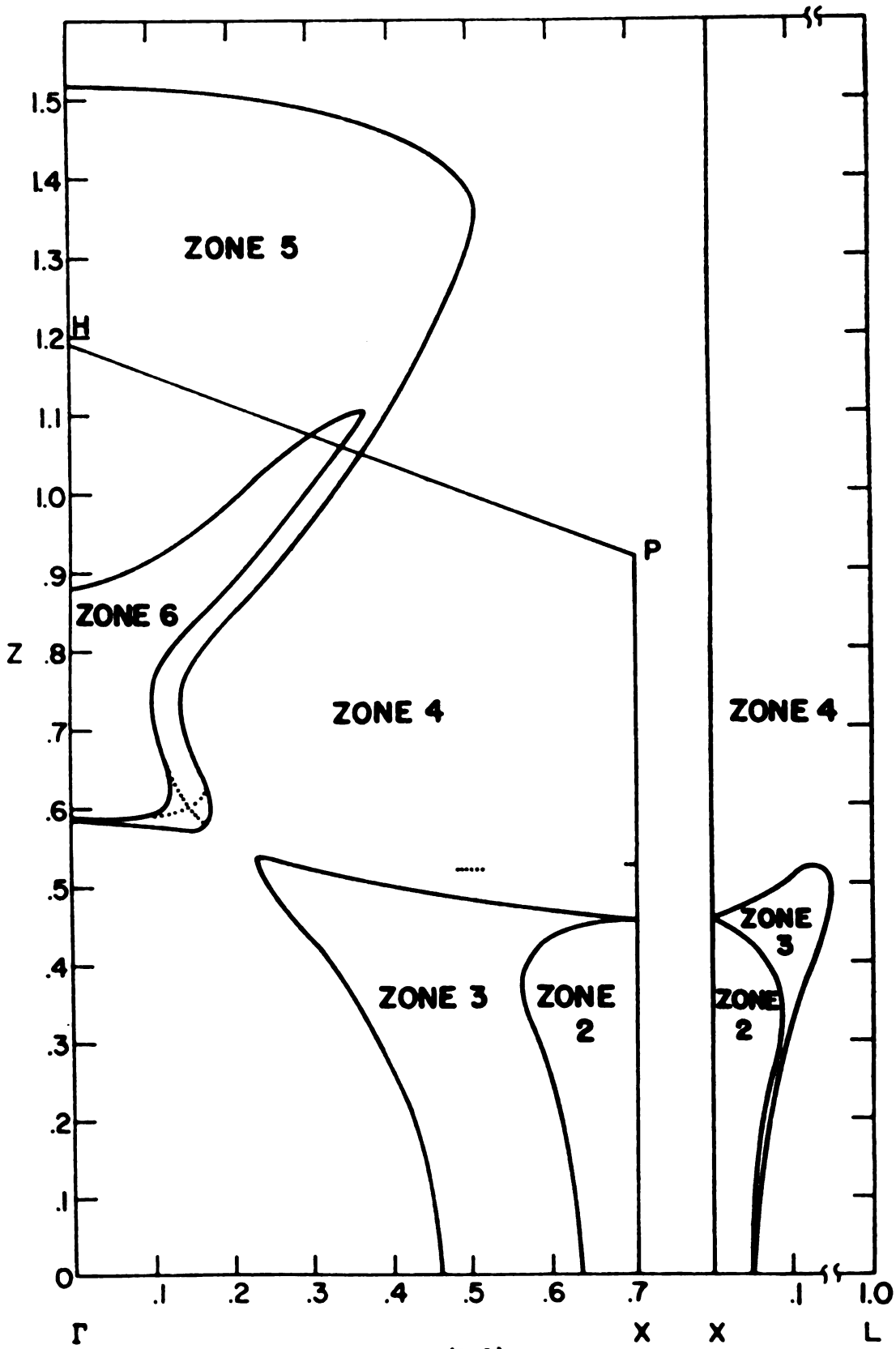
is virtually unaltered. However, the higher frequency oscillations of period $2.9 \times 10^{-7} \text{ g}^{-1}$ were designated by Gold and Priestley as originating from the 5^{th} orbits. The Weisz calculation shows these orbits no longer exist, and that this period originates at the upper end of the 3δ section. A cross section of this piece of the F-S is shown in figure 28, ⁽⁷²⁾ and in three dimensions will appear like a dog's bone. The diagram is properly interpreted by removing zone 2 from within the zone 3 section, for both the ΓX and the XL planes.

The higher frequency oscillations seen in rotation in figure 24 and in figure 21 (a) cannot be assigned to the upper end of the dog's bone, because the frequency in rotation is too rapid. If the $f(\theta)$ for this section is $\sec \theta$ then the corresponding period P is $.9 \times 10^{-7} \text{ gauss}^{-1}$. This roughly agrees with the "D" periods seen by Gold and Priestley. Not enough data was available to make a definite assignment.

D. Thermal Magnetoresistance in Rotation

Quantum oscillations in the thermal magnetoresistance were not seen in rotation since the monotonic field dependence was so large. A 360° rotation is shown in figure 29. Notice that each maxima and minima is reproducible every 180° , which is consistent with the existence of a 2 fold axis of symmetry close to the crystal axis. The signal to noise ratio is very large and drift is nearly absent. The

Figure 20



(110) Reference 72

Figure 29

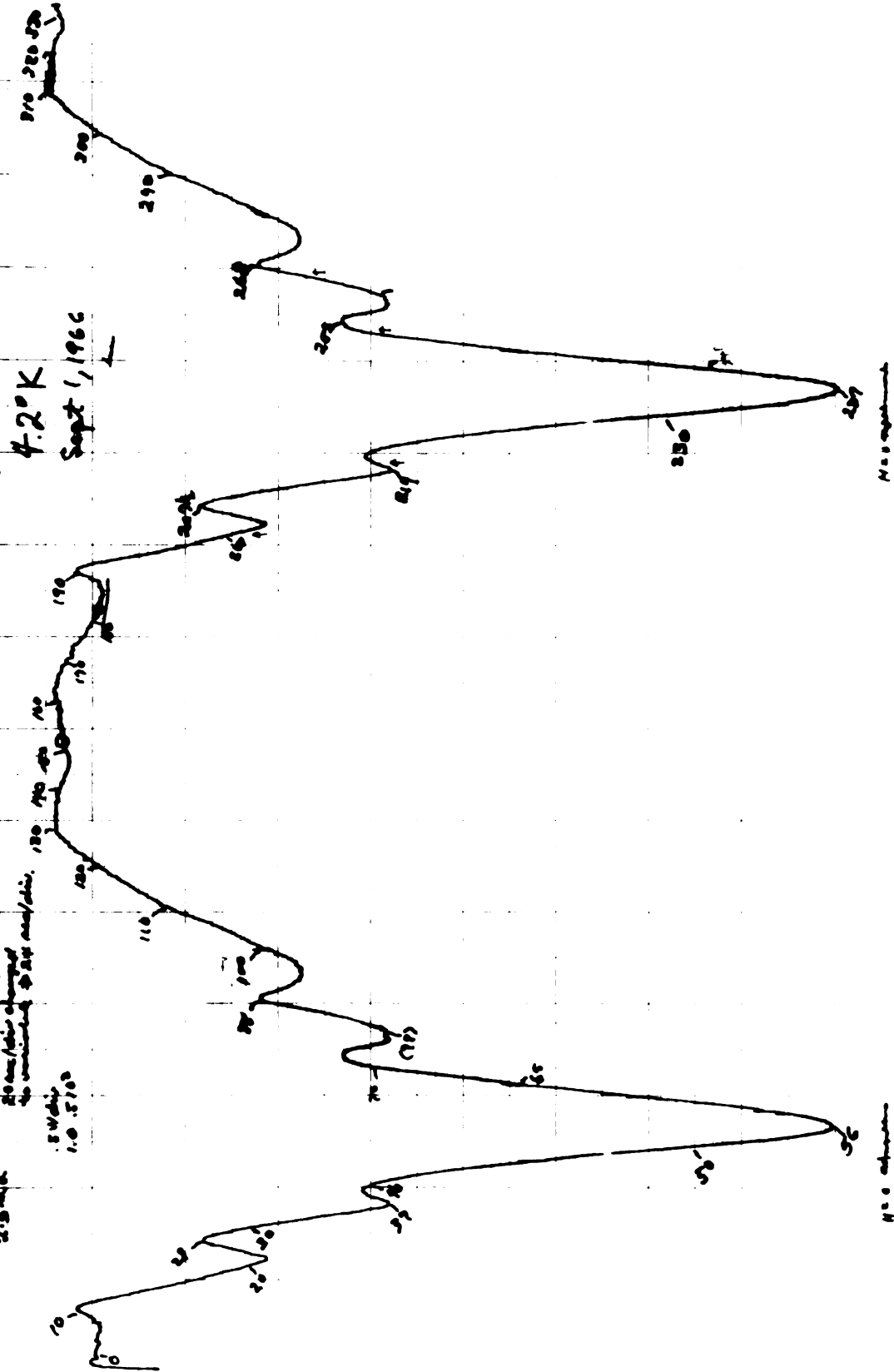
② Thermal Magneto Resistance SnII

110 amp (50% H)

2.3 m/sec

50 amp/ohm change of
the current of 2.5% amp/ohm.

5 W/ohm
1.0 5.103



4.2°K
Sept 1, 1966

Resistance

Resistance

electrical magnetoresistance will later be shown to have a much lower signal to noise ratio and drift is present. The advantages of lock-in-amplifier techniques are evident.

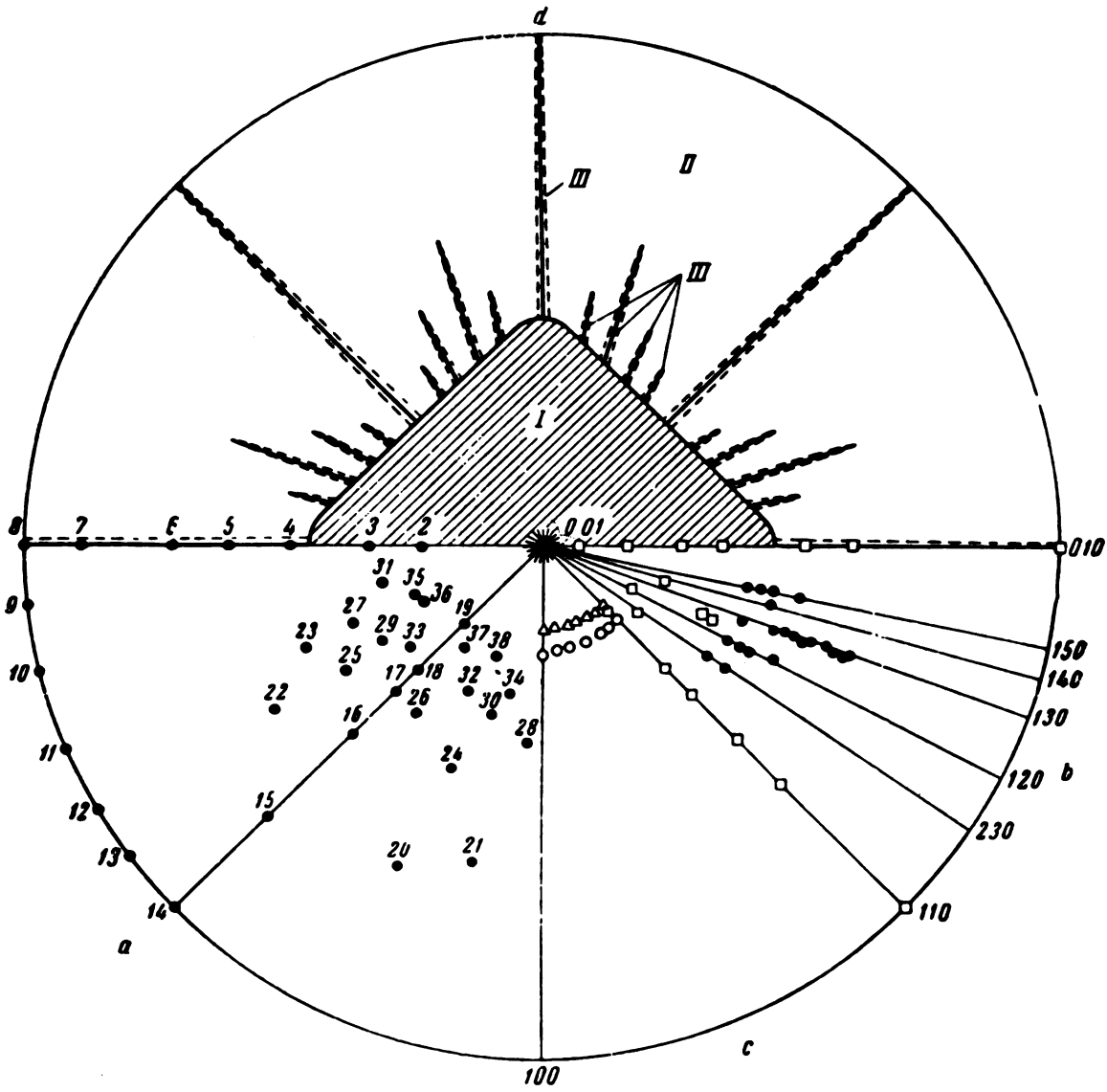
Tin is a compensated metal and the magnetoresistance has an H^2 dependence for field directions perpendicular to closed electron orbits (refer to the table of figure 4). This behavior is exhibited generally in the region between 100° and 200° in figure 29. For field directions perpendicular to orbits open in one direction, the magnetoresistance is

$$\rho \sim a + bH^2 \cos^2 \alpha \quad (13c)$$

α is the angle between the current vector \vec{J} and the open orbit direction, In our experiments \vec{J} is 4° from $[110]$ and aperiodic open orbits occur for field directions in a two dimensional region around $[001]$, as shown in the stereogram in figure 30. As the field moves into the two dimensional region α increases and is 90° at the angle of closest approach to $[001]$, giving a resistance minimum.

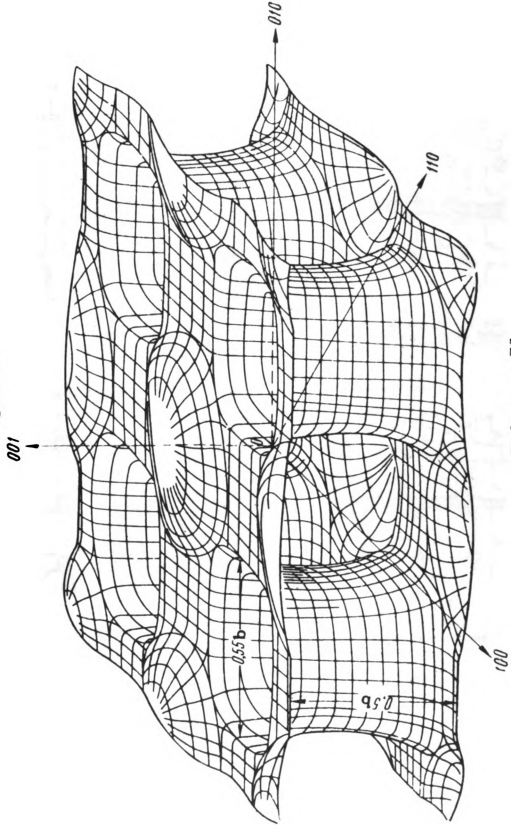
All open orbits in tin are on the 4(a) hole section of the F-S. This is shown in figure 27, and a topologically equivalent surface is shown in figure 31. As is evident, the surface is very complicated, and the open orbits on it are "aperiodic" in nature. An electron on an aperiodic open orbit does not repeat the same path in succeeding zones, as shown in figure 32.

Figure 30



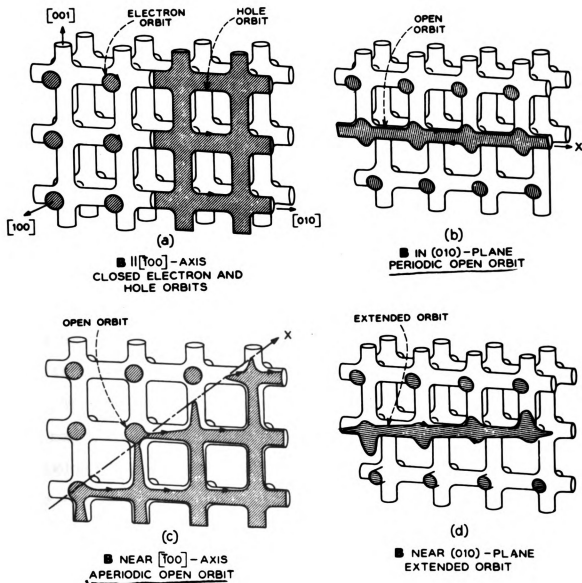
Reference 73

Figure 31



Reference 73

Figure 32



Reference 44

E. Field Dependent Structure in Magnetoresistance

The most unusual feature of both the thermal and electrical magnetoresistances is the appearance of two pairs of peaks within the two dimensional region of aperiodic open orbits. For crystal position I, the first pair is at -15° and $+19^\circ$, the second at $\pm 32^\circ$. These peaks are shown in figures 33 and 34 for various field strengths. Figure 33 is for crystal position I, and figure 34 for position II. Figure 35 shows the electrical magnetoresistance for position II.

The inner pair of peaks occur for angles where α is large and $\cos^2 \alpha$ small, characteristic of open orbits. Notice the inner pair of peaks for both crystal positions rise up at higher fields. This would occur if the open orbits of this region became closed at higher fields.

This behavior was seen by Young⁽⁷⁴⁾ in the electrical magnetoresistance and attributed by him to magnetic breakdown between the 4(a) and zone 3 sections of the F-S. (See figure 36) These sections would be connected if it weren't for spin orbit coupling which introduces a small energy gap of ~ 0.003 Rydbergs as calculated by Weisz⁽⁷²⁾. The concept of magnetic breakdown was discussed in section IV. The 0.003 Rydberg energy gap corresponds with $H_0 \cong 4,000$ gauss.

Young's interpretation is not easy to visualize, but is related to the angle θ shown in figure 37. Magnetic breakdown peaks occur at the angle θ , where orbits pass near the point x. The range of θ 's permitted in his

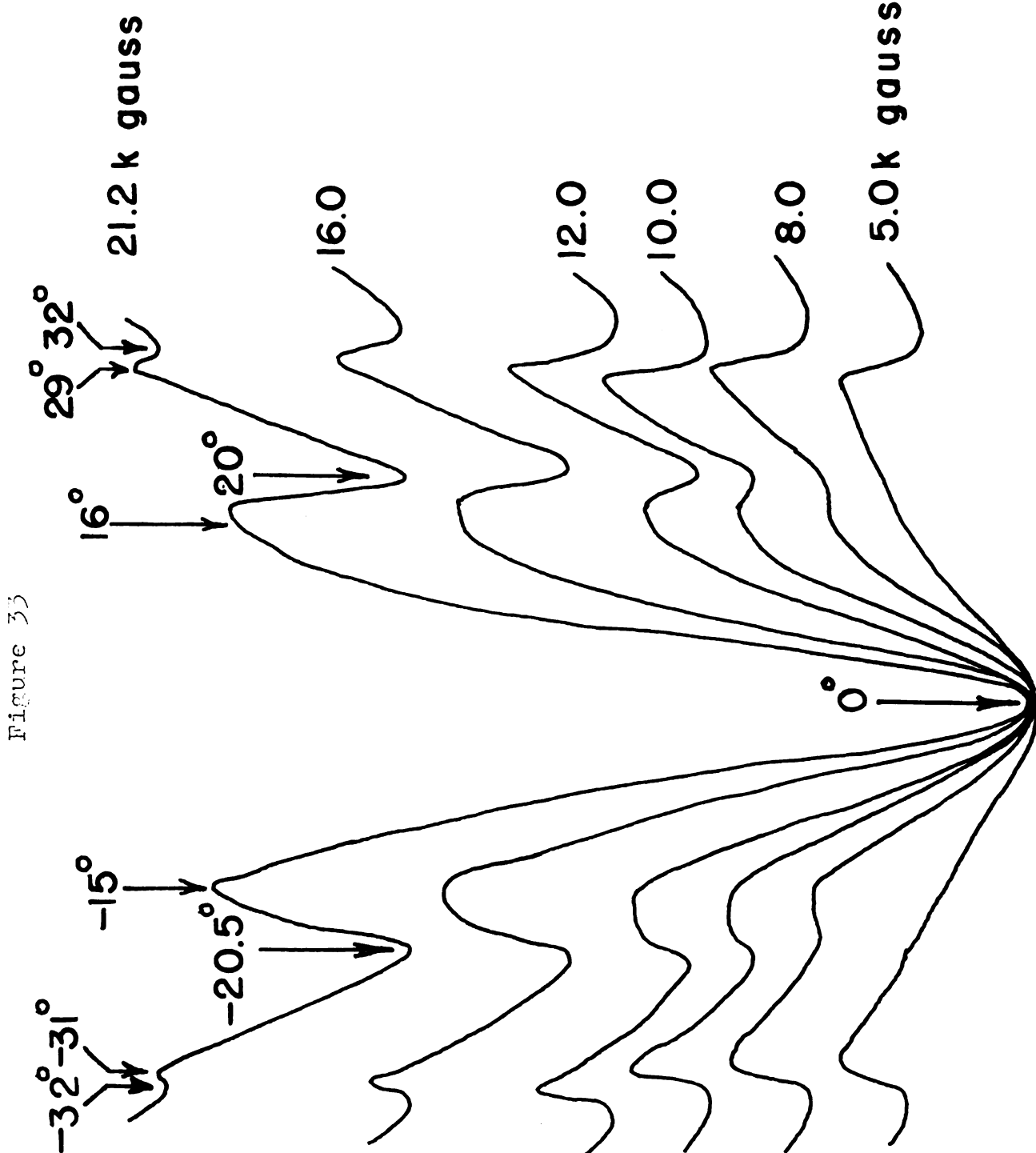
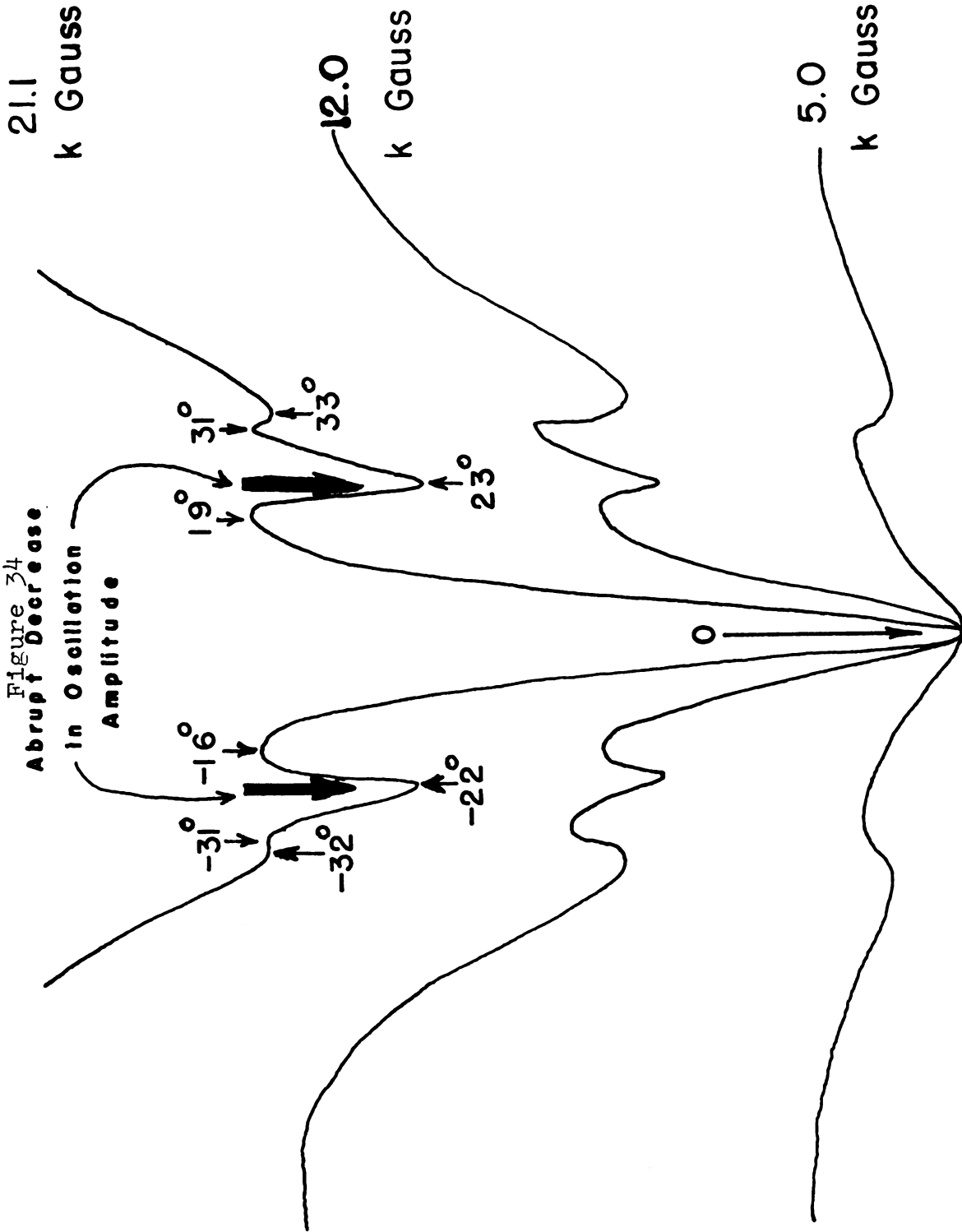


Figure 35

Thermal Magnetoresistance

25 Sept. Data



Thermal Magnetoresistance

10 October Data

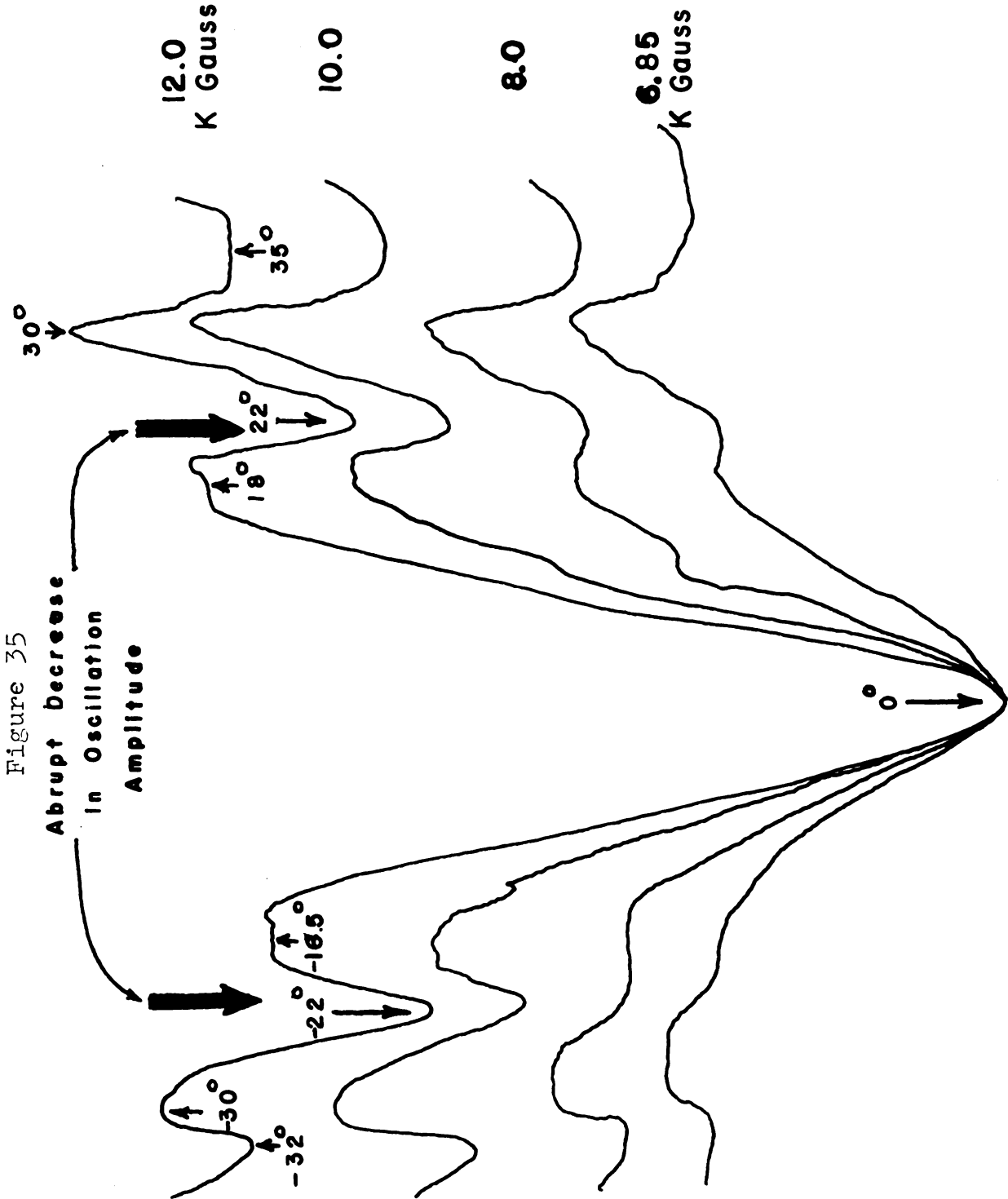


Figure 35

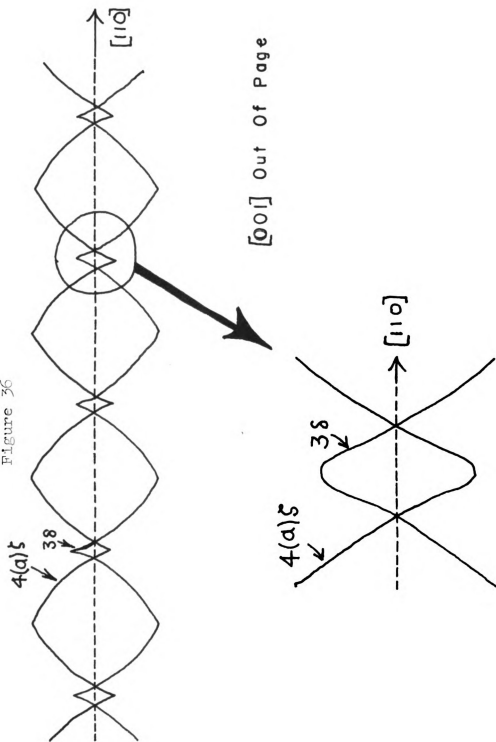
Abrupt Decrease
in Oscillation
Amplitude

Electrical

Magnetoresistance

2 January Data

Figure 36

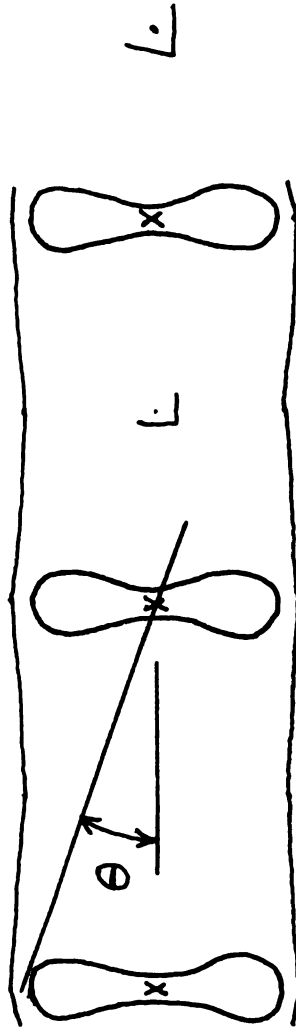


Reference 74

Figure 37

(110) Plane Through The 4th Zone Face At X

Weisz Band Structure Calculation



θ Can Range From $\sim 10^\circ$ To $\sim 20^\circ$

Reference 72

argument is

$$10^{\circ} < \theta < 20^{\circ} \quad (159)$$

and the peaks observed in our experiments fall within this range.

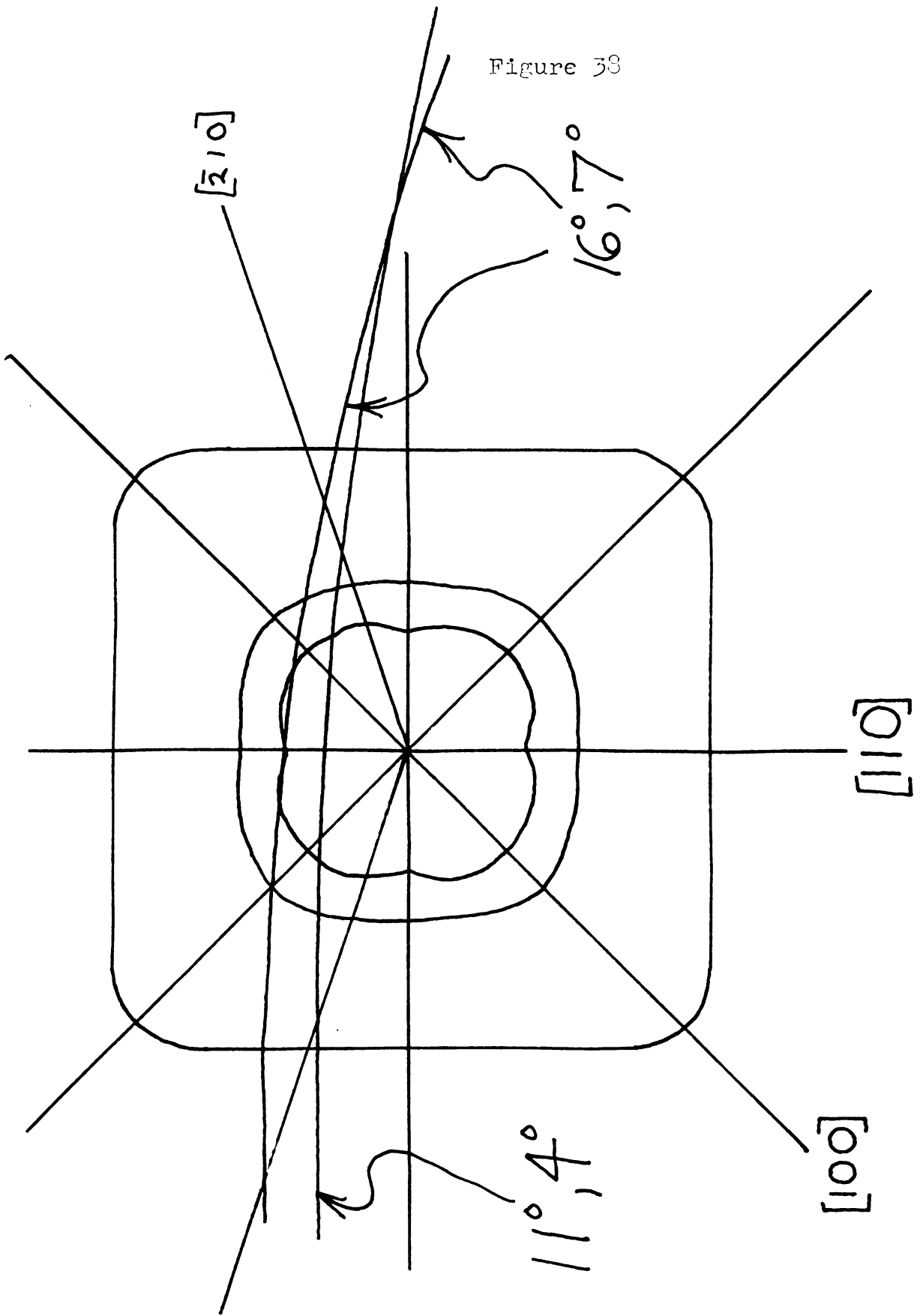
An extensive study of magnetoresistance in tin was made by Alekseevskii, et al, so we attempted to correlate our work with theirs. The stereogram of their work is shown in figure 30. The portion of interest is within the two dimensional region of open orbit field directions shown in figure 38. The inner pair of squares with rounded edges mark maxima and minima field positions found by Alekseevskii, et al. The great circles corresponding to our field sweeps are marked by the angles of [001] and [110] out of the plane of rotation of H for the two different crystal tilt positions.

The 11° , 4° curve predicts peaks at -14° and $+16^{\circ}$ and minima at $\pm 22^{\circ}$. Peaks were observed at -15° and $+16^{\circ}$ and minima at -20.5° and $+20^{\circ}$.

The crystal position II curve (16° , 7°) predicts peaks at -7° and $+10^{\circ}$ and measured to be -16° and $+19^{\circ}$. The measured angles are extremely dependent on crystal tilt angle in this region, so an error of $\pm 2^{\circ}$ in x ray orientation could greatly change this agreement. Minima are predicted at -19° , $+21^{\circ}$ and observed at $\pm 22^{\circ}$.

The outer peaks shown in figures 34 and 35 occur very roughly for field directions along [210] directions but this could not be definitely established. The unusual

Figure 38



feature of these peaks is that they disappear at higher fields and suggests that magnetic breakdown might be involved here, also. Their disappearance at higher fields would correspond with closed orbits (H^2 behavior) changing to open orbits ($H^2 \cos^2 \alpha$ behavior). The 4(a) section of the F-S of tin is very complicated and aperiodic orbits on it are even more difficult to picture.

F. Correlation of Oscillation Amplitudes with the Field Dependent Peaks in Magnetoresistance

The most striking feature of the thermoelectric power quantum oscillations is that they nearly disappear inside of $\pm 22^\circ$ and reappear within $\pm 4^\circ$ of the angle of closest approach to [001], as shown in figure 39. This is the region of the inner magnetoresistance peaks which become more pronounced at higher fields.

The oscillation amplitude reduction is consistent with the presence of magnetic breakdown between zones 3 and 4(a) since at breakdown fields not all electrons would complete cyclotron orbits on the 3δ section of the F-S. It is the completed cyclotron orbits which contribute to quantum oscillations.

Young's description of which orbits are involved in breakdown does not explain the oscillation amplitude reduction. Young's and our data are consistent with each other but not with his interpretation. All of the data agree

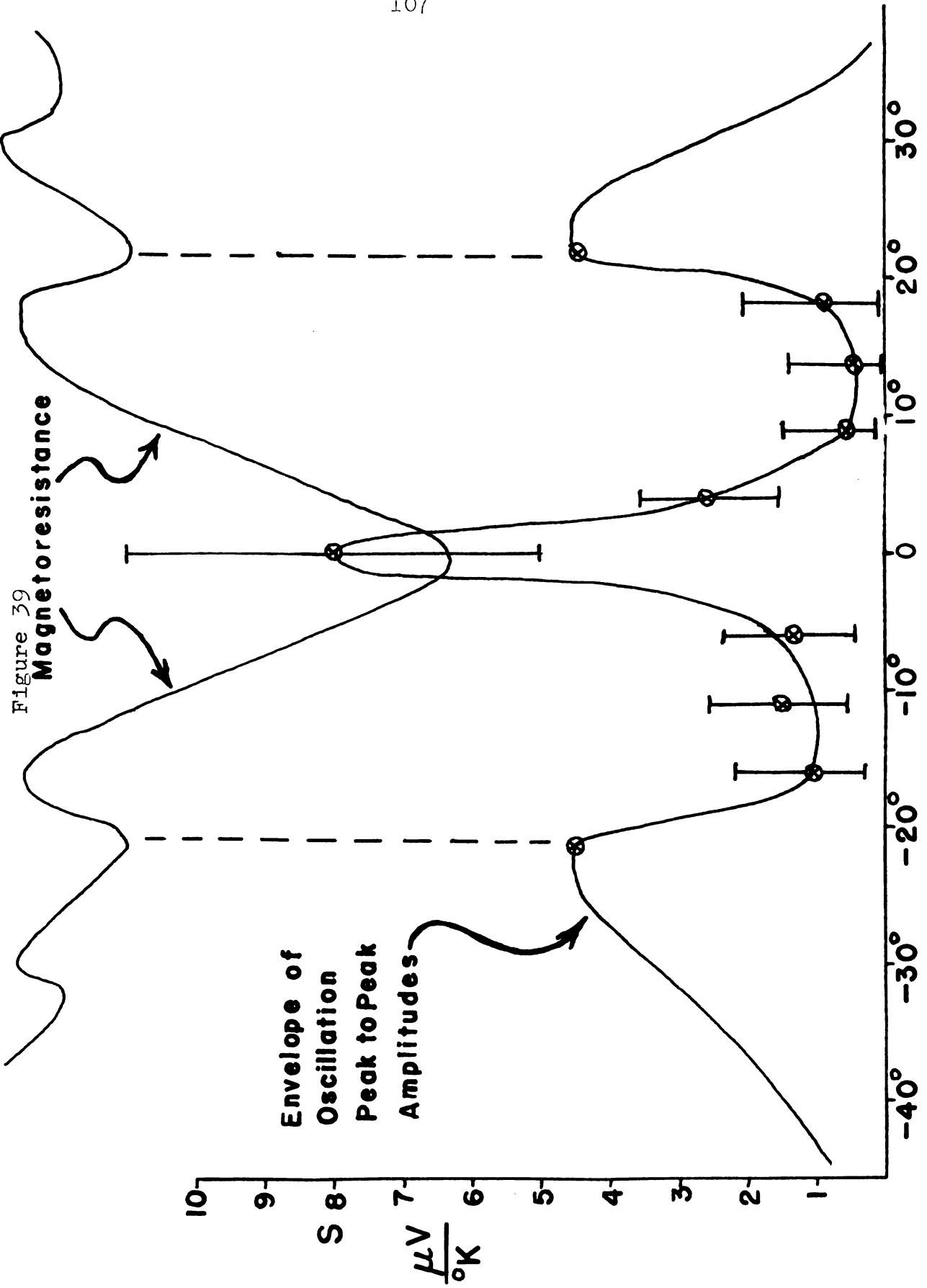


Figure 39

Magnetoresistance

Envelope of Oscillation
Peak to Peak Amplitudes

$\frac{\mu V}{^\circ K}$

with the concept that the rounded squares in the stereogram of figure 38 are due to magnetic breakdown. This idea was not suggested by Young and could be further studied by repeating the present experiments for various tilt angles.

We have demonstrated that the combination of thermal magnetoresistance and thermoelectric emf quantum oscillations is an effective tool for F-S studies. Being able to measure both quantities simultaneously is a distinct advantage. The thermoelectric emf is shown to be very sensitive to the quantization of energy levels.

References

1. W. J. de Haas and P. M. van Alphen, Proc. Amsterdam 33, 1106 (1930).
2. R. Peierls, Z. Phys. 91 186 (1933).
3. See appendix to: D. Shoenberg, Proc. Roy. Soc. A 170, 341 (1939).
4. D. Shoenberg, Proc. Roy. Soc. A 175, 49 (1940).
5. J. A. Marcus, Phys. Rev. 71, 539 (1947).
6. L. Onsager, Phil. Mag. 43, 1006 (1952).
7. I. M. Lifshitz and A. M. Kosevich, JETP 29, 730 (1955).
8. I. M. Lifshitz, M. Azbel, and M. I. Kaganov, JETP 3, 143 (1956).
9. Y. M. Azbel, E. A. Kaner, JETP 3, 772 (1956).
10. M. H. Cohen, M. M. Harrison, W. A. Harrison, Phys. Rev. 117, 937 (1960).
11. The Fermi Surface, W. A. Harrison, M. B. Webb, eds. John Wiley and Sons, Inc., N.Y. 1960.
12. Low Temperature Physics LT9, J. G. Daunt, D. O. Edwards, F. J. Milford, M. Yaquub eds., Plenum Press, N.Y. 1965.
13. C. G. Grenier, J. M. Reynolds, N. H. Zebouni, Phys. Rev. 98, 359 (1955).
14. C. G. Bergeron, C. G. Grenier, J. M. Reynolds, Phys. Rev. 119, 925 (1960).
15. C. N. Rao, N. H. Zebouni, C. G. Grenier, J. M. Reynolds, Phys. Rev. 133, 141 (1964).
16. J. R. Long, C. G. Grenier, J. M. Reynolds, Phys. Rev. 140, 187 (1965).
17. See: J.P. Jan, Solid State Physics 5, Academic Press, N. Y. 1957, p. 1.
18. M. C. Steele and J. Babiskin, Phys. Rev. 98, 359 (1955).

19. G. E. Zil'berman, JETP 2, 650 (1956).
20. V. P. Kalashnikov, Fiz. Metal. Metalloved 17, 651 (1964).
21. P. B. Horton, Ph.D. Thesis, Louisiana State University (1964). Unpublished. University Microfilm #64-8804.
22. E. N. Adams, T. D. Holstein, J. Phys. Chem. Solids 10, 254 (1959).
23. R. B. Thomas Jr., Phys. Rev. received 28 April 1966. To be published.
24. A. B. Pippard, The Dynamics of Conduction Electrons, Gordon and Breach, N. Y. 1965.
25. C. Kittel, Quantum Theory of Solids, John Wiley and Sons, Inc. 1963, Chapter 11.
26. R. M. Eisberg, Modern Physics, John Wiley and Sons, Inc. 1961 p. 256.
27. H. M. Rosenberg, Low Temperature Solid State Physics, Clarendon Press, 1963 p. 352.
28. R. B. Dingle, Proc. Roy. Soc. 211, 500 (1952).
29. Kohler, Ann. Phys. 5, 99 (1949).
30. R. G. Chambers, Proc. Roy. Soc. A 238, 344 (1956).
31. I. M. Lifshitz, Y. M. Azbel, and M. I. Kaganov, JETP 3, 143 (1956).
I. M. Lifshitz and V. G. Peschanskii, JETP 8, 875 (1958) and JETP 11, 137 (1960).
32. E. Fawcett, Adv. Phys. 13, 139 (1964).
33. C. G. Grenier, J. M. Reynolds, J. R. Sybert. Phys. Rev. 132, 58 (1963).
34. M. I. Azbel, M. I. Kaganov and I. M. Lifshitz. JETP 5, 967 (1957).
35. S. Shalyt, J. Phys. (U.S.S.R.) 8, 315 (1944).
36. J. K. Hulm, Proc. Roy. Soc. 204, 98 (1950).

37. K. Mendelssohn and H. M. Rosenberg, Proc. Roy. Soc. 218, 190 (1953).
38. P. B. Alers, Phys. Rev. 101, 41 (1956).
39. L. J. Challis, J. D. N. Cheeke, P. Wyder, Reference 12.
40. J. Longo, D. Sellmyer, P. A. Schroeder, To be published.
41. J. M. Ziman, Principles of the Theory of Solids, Cambridge University Press, 1964. p. 258.
42. R. G. Chambers, reference 11.
43. D. J. Sellmyer, Galvanomagnetic Investigation of the Fermi Surface of AuSn. Ph.D. Thesis 1965, Michigan State University.
44. E. Fawcett, reference 32.
45. E. I. Blount, Phys. Rev. 126, 1636 (1962).
46. M. H. Cohen, L. M. Falicov, Phys. Rev. Letters 7, 231 (1961).
47. A. B. Pippard, Proc. Roy. Soc. A 270, 1 (1962).
48. L. M. Falicov, P. R. Sievert, Phys. Rev. 138, 88 (1965).
49. A. B. Pippard, Proc. Roy. Soc. A 1072, 39 (1964).
50. M. G. Priestley, L. M. Falicov, G. Weisz, Phys. Rev. 131, 617 (1963).
51. R. W. Stark, T. G. Eck, W. L. Gordon, F. Moozed, Phys. Rev. Letters 9, 360 (1962).
52. R. W. Stark, Phys. Rev. Letters 9, 482 (1962).
53. A. R. Mackintosh, L. E. Spanel, R. C. Young, Phys. Rev. Letters 10, 434 (1963).
54. A. S. Joseph, A. C. Thorsen, Phys. Rev. Letters 11, 67 (1963).
55. Lawson, Gordon, reference 12, p. 854.
56. Higgs, Marcus, Whitmore, reference 12, p. 857.

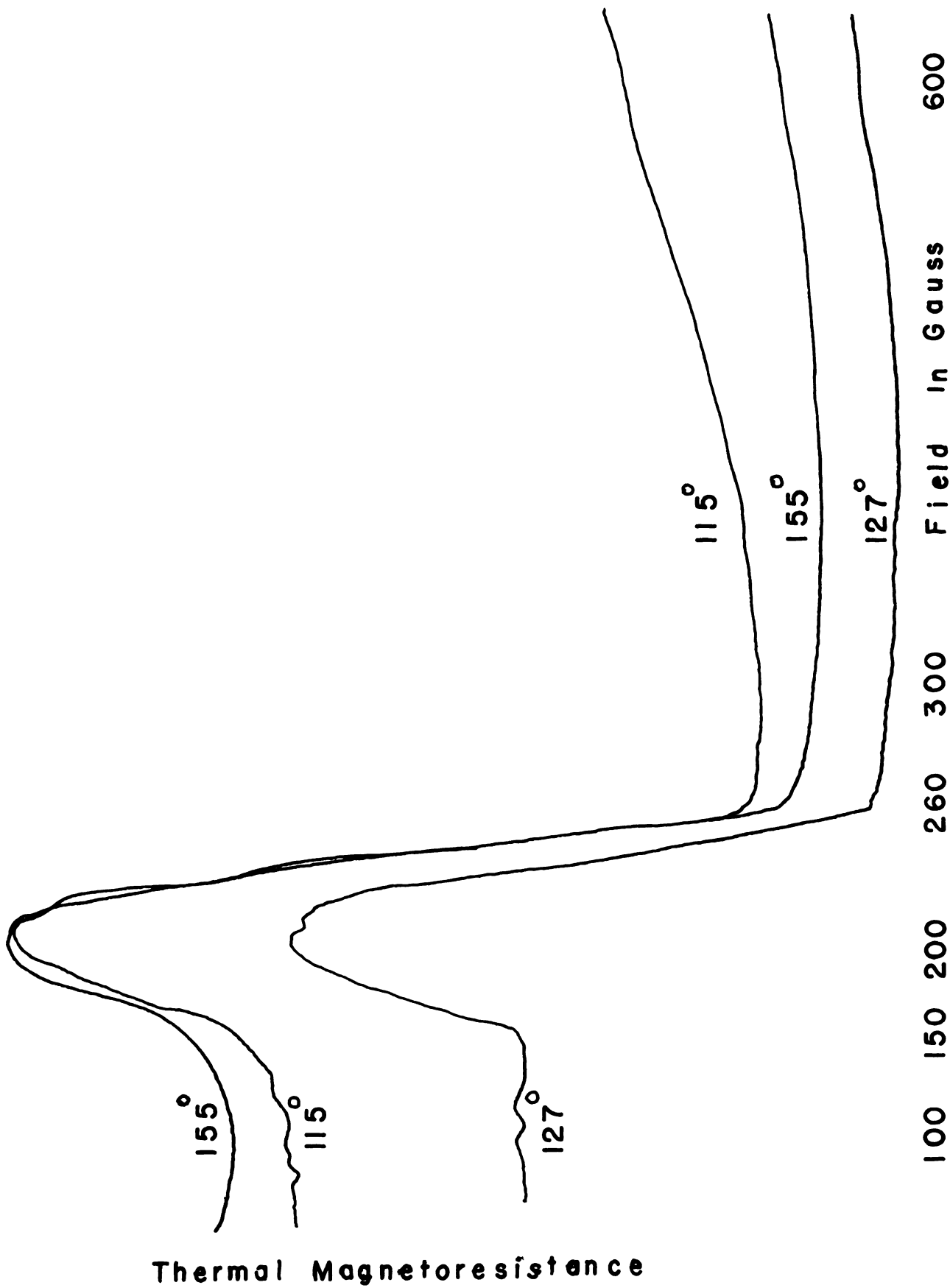
57. R. W. Stark, reference 12, p. 712.
58. R. C. Young, Phys. Rev. Letters 15, 262 (1965), also Phys. Rev. To be published.
59. Y. A. Bychkov, L. E. Gurevich, G. M. Nedlin 10, 377 (1960).
60. Kohler, Ann. Phys. 40, 196 (1941).
61. Bridgeman furnace temperature controller designed by D. J. Sellmyer.
62. M. C. Steele and J. de Launay, Phys. Rev. 82, 276 (1951).
63. D. Shoenberg, Trans. Roy. Soc. A 255, 12 (1962).
64. J. J. Lepage, Ph.D. Thesis 1965, Michigan State University.
66. R. D. Moore, O. C. Chaykowsky, Modern Signal Processing Technique for Optimal Signal to Noise Ratios. Princeton Applied Research Corporation Technical Bulletin 109 (1963).
67. I want to thank Andrew Davidson for designing and constructing this.
68. R. W. Stark, private communication.
69. Seeley, Electron Tube Circuits, McGraw-Hill Book Co, Inc. New York 1960. p. 603.
J. B. Ketterson, Y. Eckstein, Rev. Sci. Ins. 37, 44 (1966).
70. A. V. Gold, M. G. Priestley, Phil. Mag. 5, 1089 (1960).
71. M. D. Stableu, A. R. de Vroomen, Physics Letters 22, 179 (1966).
72. G. Weisz, Phys. Rev. 149, 504 (1966).
73. N. E. Alekseevskii, Y. P. Gaidukov JETP 10, 481 (1960) and JETP 14, 770 (1962).
N. E. Alekseevskii, Y. P. Gaidukov, I. M. Lifshitz, V. G. Peschanskii, JETP 12, 837 (1961).
74. R. C. Young, Phys. Rev. Letters 15, 262 (1965) and Phys. Rev. to be published.
See also R. J. Kearney, A.R. Mackintosh, R. C. Young Phys. Rev. 140, 1671 (1965).

75. E. A. Lynton, Superconductivity, Methuen and Co. LTD. London 1962, p. 58.
76. F. H. J. Cornish, J. L. Olsen, Helv. Phys. Acta 26, 369 (1953).

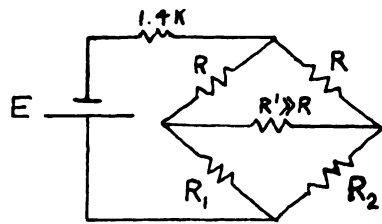
AppendixIntermediate Magnetic State

Figure 40 shows a plot of the thermal magnetoresistance against fields below 600 gauss. The sample is at 1.4°K . Below 150 gauss the entire sample is superconducting with complete Meissner effect. Between 130 gauss and 260 gauss there appear "tubes" of alternate normal and superconducting regions (75). The bump appearing in the resistivity was satisfactorily explained by Cornish and Olsen using a model of conductivity by the alternate tubes. The sharp corner at 260 gauss is at the critical field H_c for tin at this temperature. In very pure materials, the thermal conductivity below $H_c/2$ is purely from the lattice so the experiment presents an interesting way of studying pure lattice conductivity, involving almost no phonon-electron collisions.

Figure 40



Thermal Magnetoresistance

Bridge Correction

$$E = i_1 \left[1.4K + \frac{(R+R_1)(R+R_2)}{2R+R_1+R_2} \right] \quad i_1 = i_2 + i_3$$

$$i_2(R+R_1) = i_3(R+R_2) \quad \Delta V = V_1 - V_2 = R(i_2 - i_3)$$

$$\Delta V = R i_2 - i_2 \frac{R+R_1}{R+R_2} = R i_2 - \frac{R+R_1}{R+R_2} i_2$$

$$\Delta V = \frac{R}{R+R_2} (R_2 - R_1) i_2$$

$$E = i_2 + i_2 \frac{R+R_1}{R+R_2} \left[1.4K + \frac{(R+R_1)(R+R_2)}{2R+R_1+R_2} \right]$$

$$\Delta V = \frac{R}{R+R_2} \frac{(R_2 - R_1) E}{1 + \frac{R+R_1}{R+R_2} \left[1.4 + \frac{(R+R_1)(R+R_2)}{2R+R_1+R_2} \right]} \quad \delta \equiv R_2 - R_1$$

$$\Delta V = \frac{RE \delta}{(2R + 2R_1 + \delta) \left[1.4 + \frac{(R+R_1)(R+R_1+\Delta)}{2R+R_1+R_1+\Delta} \right]}$$

K is a constant

$\delta \simeq 0$ to $6K$ maximum

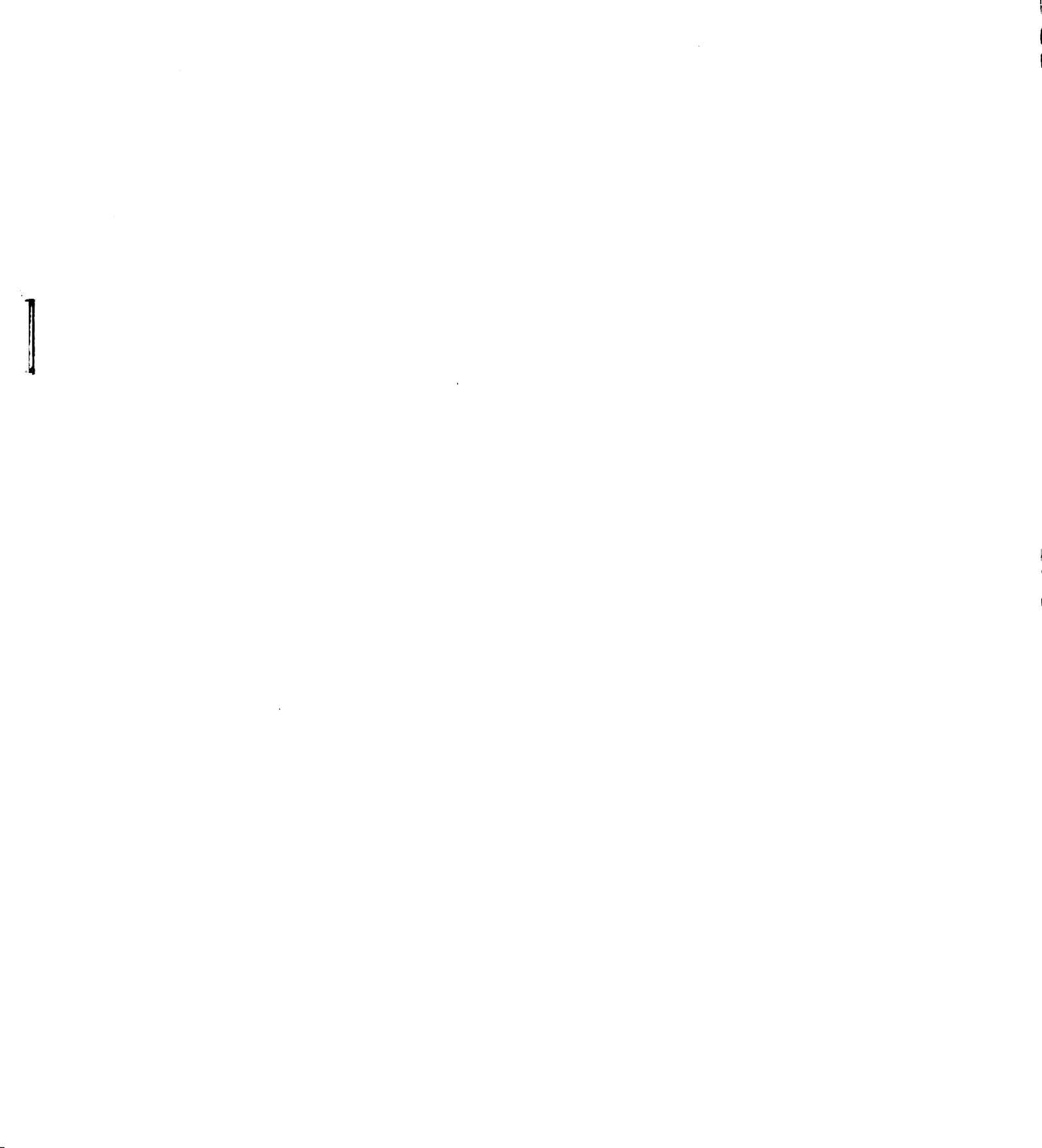
$R \sim 5K$ $R_1 \sim 3K$

$$\Delta V = \frac{K\delta}{(2R + 2R_1 + \delta)}$$

Bridge Correction Table

<u>$\delta = (R_1 - R_2)$ k ohms</u>	<u>amount to be added to bridge output to get true linear output</u>
1	6%
2	11%
3	17%
4	22%
5	25%
6	33%

above percentages calculated for $R = 5K$ ohms
and $R_1 = 3K$ ohms.



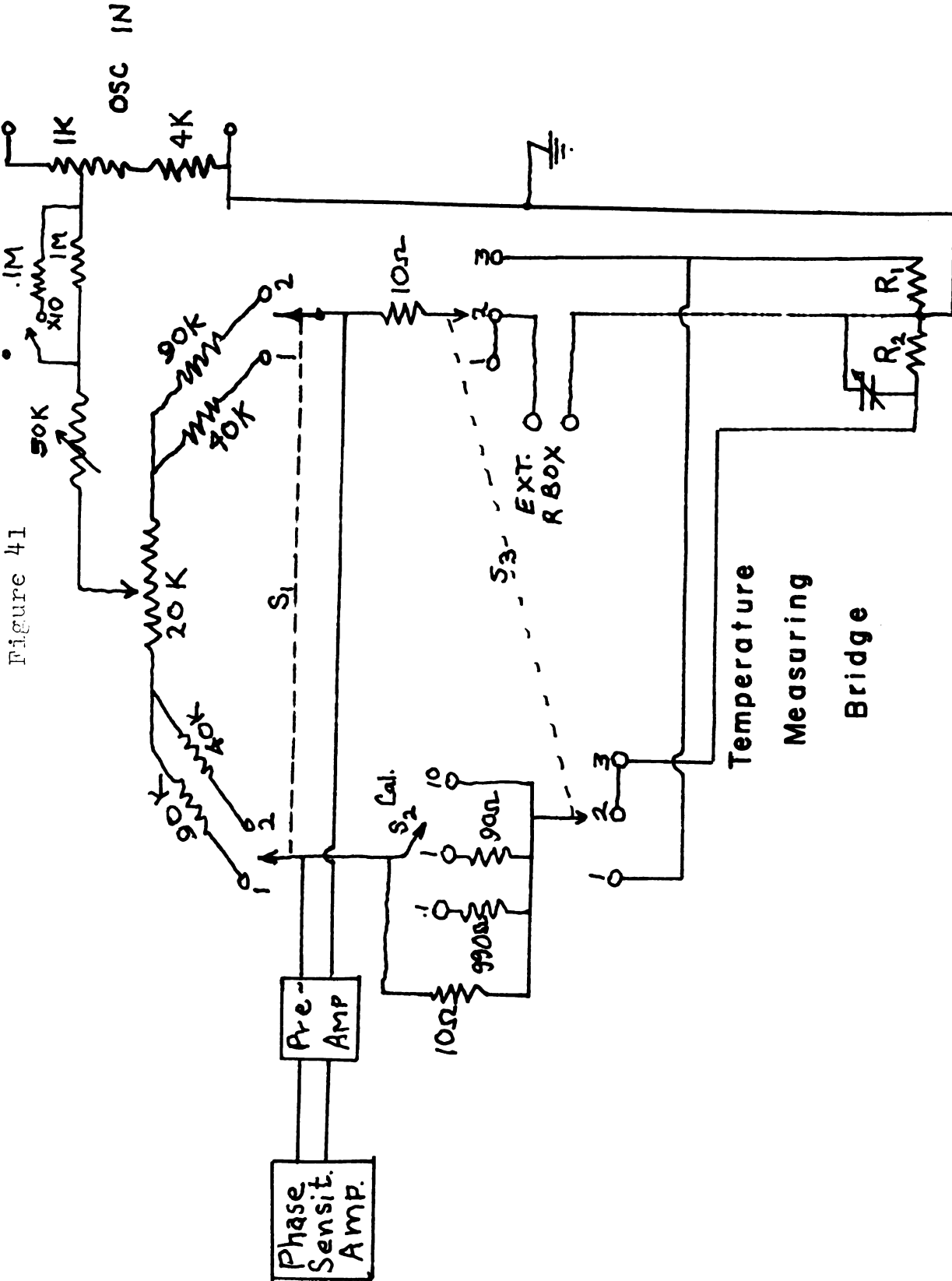


Figure 42

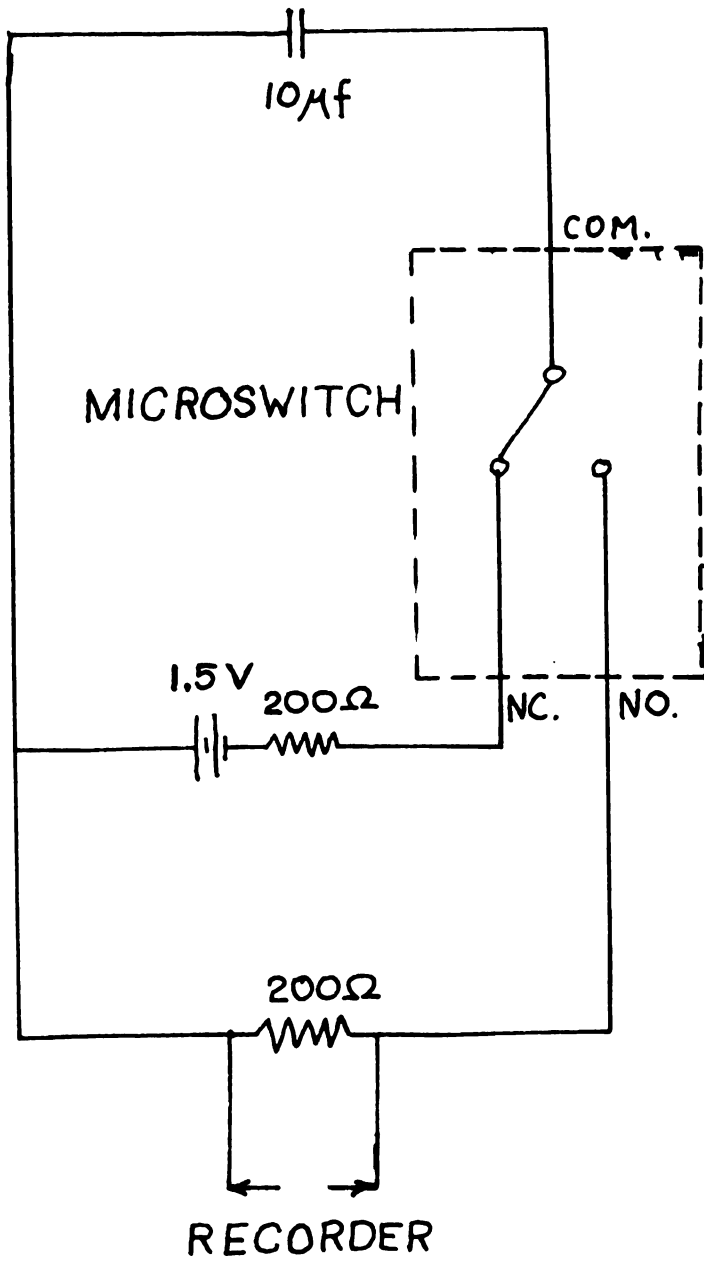
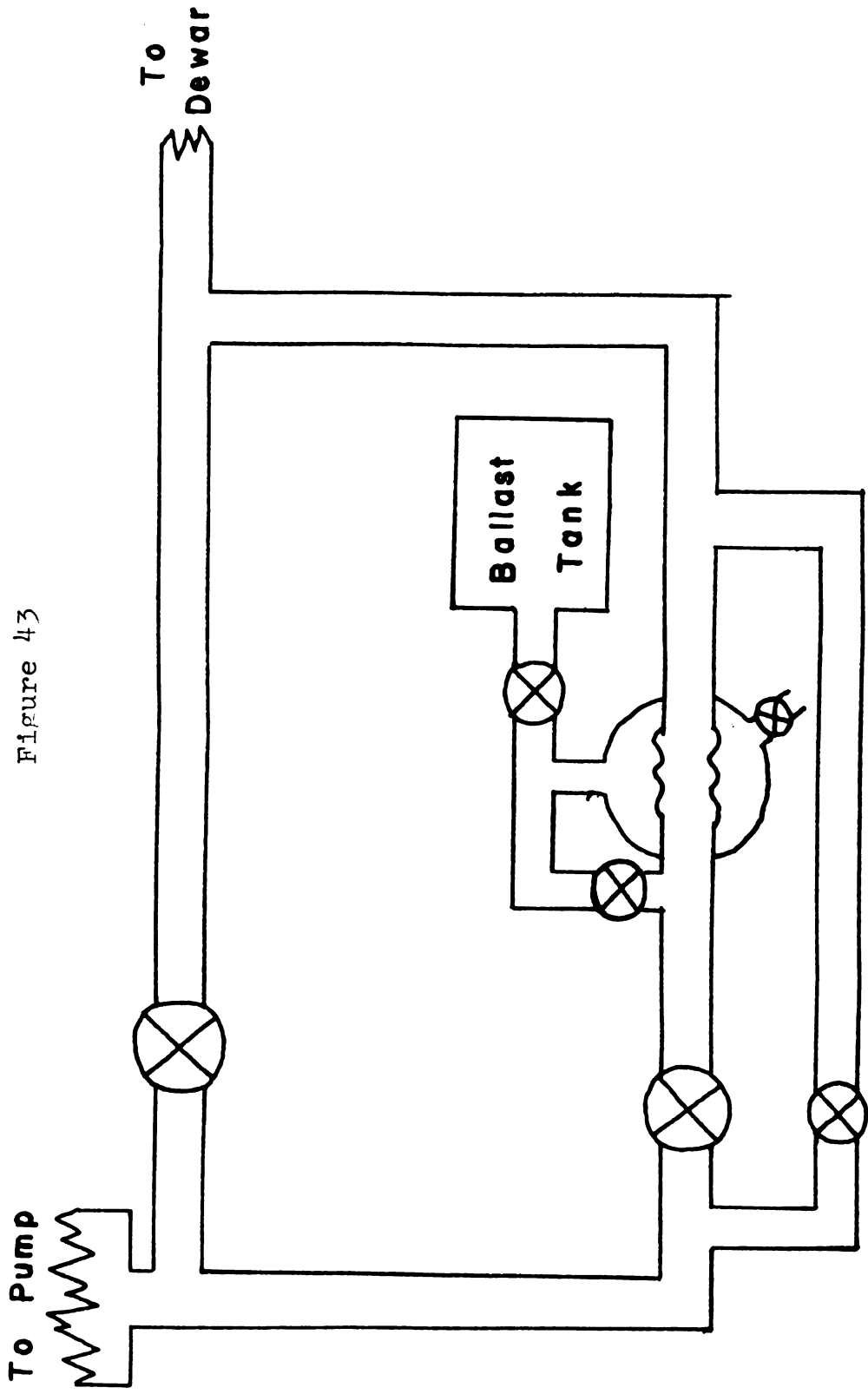
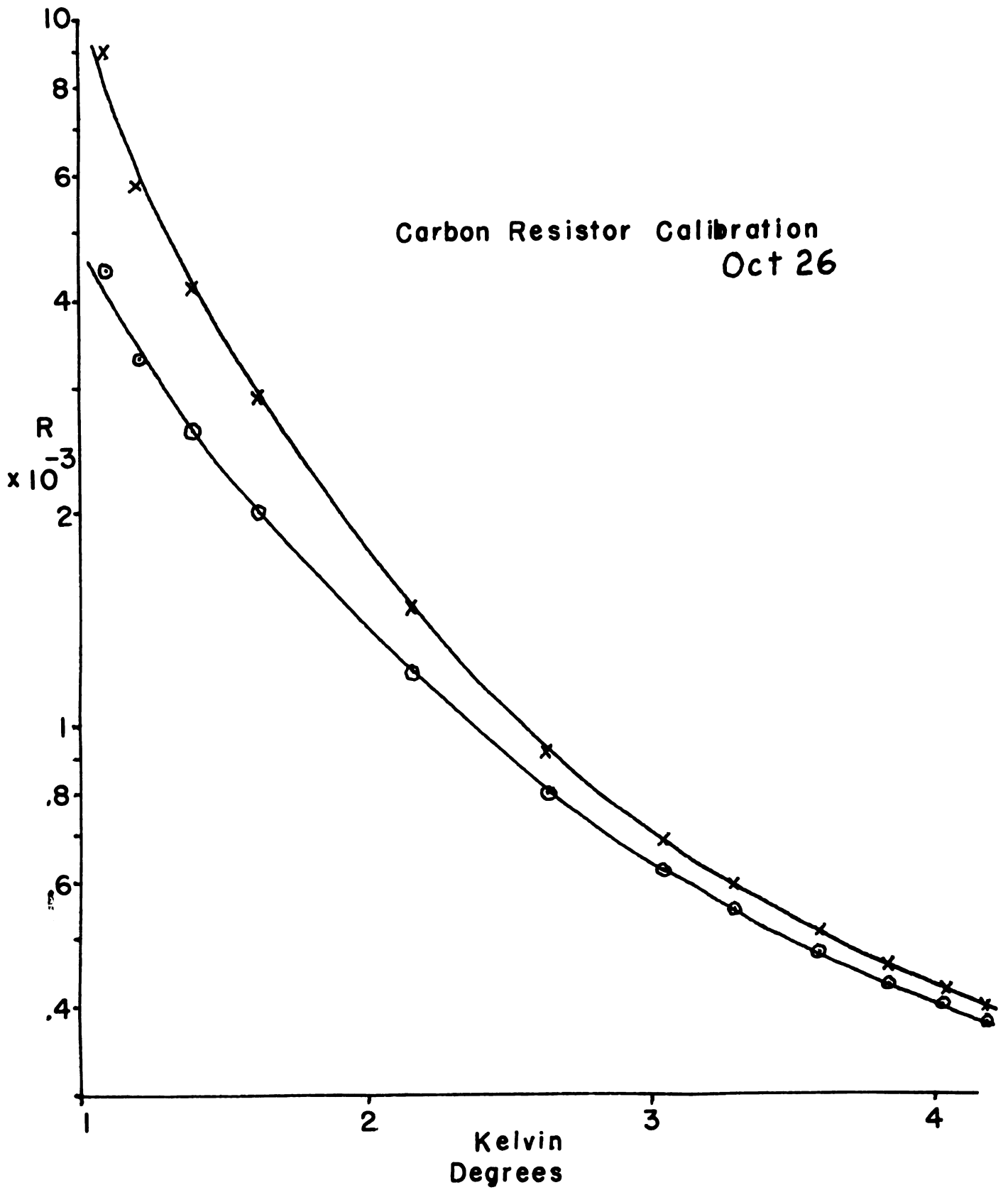


Figure 43



Pressure Regulator

Figure 44



MICHIGAN STATE UNIVERSITY LIBRARIES



3 1293 03178 5359